Stony Brook University

Novel Catalytic Nanoparticles and Nanostructures for Environmental and Energy Applications

A Dissertation Presentation

By

Shen Zhao

to

The graduate School

in Partial Fulfillment of the

Requirements

for the Degree of

Doctor of Philosophy

in

Materials Science and Engineering

Stony Brook University

December 2013

Stony Brook University

The Graduate School

Shen Zhao

We, the dissertation committee for the above candidate for the

Doctor of Philosophy degree, hereby recommend

acceptance of this dissertation.

Alexander Orlov – Dissertation Advisor
Professor, Materials Science and Engineering
Stony Brook University

Clive Clayton - Chairperson of Defense
Professor, Materials Science and Engineering
Stony Brook University

Taejin Kim – Committee Member
Professor, Materials Science and Engineering
Stony Brook University

Dong Su – Committee Member
Staff Scientist, Center for Functional Nanomaterials
Brookhaven National Laboratory

This dissertation is accepted by the Graduate School

Charles Taber
Dean of the Graduate School

Abstract of the Dissertation

Novel Catalytic Nanoparticles and Nanostructures for Environmental and Energy Applications

by

Shen Zhao

Doctor of Philosophy

in

Materials Science and Engineering

Stony Brook University

2013

Semiconductor photocatalysis is a dynamic field at the forefront of environmental and energy research. This dissertation has focused on the development of novel nanomaterials to exceed performance for environmental and energy related applications in both liquid and gas phases as compared to traditional materials.

This project investigated the impact of size of noble metal clusters on photocatalytic activity induced by UV and visible light. Compared to larger particles, sub-nanometer particles have shown much better activity for catalytic reactions in both liquid and gas phases. These nanoclusters supported on various semiconductors, such as TiO_2 and CdS showed outstanding catalytic properties for oxidation of phenol in gas phase, removal of NO_2 from gas phase via both oxidation and reduction routes and hydrogen production from water. The catalytic activities of sub-nanometer particles were much higher than those of known commercially available catalysts. Overall, this project has provided the first ever demonstration of the unique properties of ultra-small nanoparticles in sub-nanometer range for photocatalytic applications.

Additionally, this project has focused on utilization of novel nanostructures to provide a high surface area support for photocatalysts and to achieve better

dispersion of nanoparticles. More specifically, this research has focused on a new generation of highly ordered mesoporous SBA-15 sieves, which have large pore diameter (22 nm) and short pore length (500 nm), which were subsequently templated to facilitate photooxidation reactions. In addition, this project has focused on inverse opal structures to facilitate a better light capture inside these 3D structures, which can potentially lead to enhancement of photocatalytic reactions.

All catalysts and catalysts' precursors were characterized using high-resolution electron microscopy (HR-EM), which included Scanning Electron Microscopy (SEM), Transmission Electron Microscopy (TEM) and Scanning Transmission Electron Microscopy (STEM); Matrix assisted laser desorption ionization/time of flight (MALDI-TOF), X-ray diffraction (XRD), Scanning Tunneling microscopy (STM); while catalytic activity was determined by diffuse reflectance infrared Fourier Transform Spectroscopy (DRIFTS), High Performance Liquid Chromatography (HPLC) and Gas Chromatography (GC).

Table of Contents

List of Figures

List of Abbreviations

XRD	X-Ray diffraction
SEM	Scanning electron microscopy
TEM	Transmission electron microscopy
STEM	Scanning transmission electron microscopy
GC	Gas chromatography
HPLC	High performance liquid chromatography
MALDI	Matrix assisted laser desorption ionization
NPs	Nanoparticles
UV	Ultraviolet
wt. %	Weight %

Acknowledgments

I would never have been able to finish my dissertation without the guidance of my committee members, help from my friends, and support from my family.

I want to firstly show my deepest gratitude to my thesis advisor, Prof. Alexander Orlov. I will always remember all the help and guidance you provided throughout my graduate studies.

I would also like to thank Dr. Dong Su, who contributed tremendously on the characterization part of my Ph. D. thesis. To me, he is truly a great mentor and a caring friend whom I can always look up to.

I am very grateful to Dr. Clive Clayton and Dr. Gary Halada for their endless support and constructive criticism. Many thanks go to Dr. Yan Li who did the amazing job on the TDDFT calculation for my nanoparticle structure investigation.

I would like to thank the whole research group from Prof. Orlov for their friendship and support. I could not have achieved any of these without all your help.

Finally I want to thank my parents for all their love and encouragement throughout every second of my life.

Papers arising from this work

1. **Zhao, S.**, Ramakrishnan, G., Shen, P., Su, D., Orlov, A." The first experimental demonstration of beneficial effects of sub-nanometer platinum particles for photocatalysis", Chemical Engineering Journal, submitted
2. Shen, P, **Zhao, S.**, Su, D., Li, Y., Orlov, A. "Outstanding activity of sub-nm Au clusters for photocatalytic hydrogen production", *Applied Catalysis B: Environmental*, 126, 153-160, 2012
3. **Zhao, S.**, Su, D., Che, J., Orlov, A. "Photocatalytic properties of TiO_2 supported on SBA-15 mesoporous materials with large pores and short channels", *Materials Letters*, 65, 3354–3357, 2011.
4. **Zhao, S.**, Ramakrishnan, G., Su, D., Rieger, R., Koller, A., Orlov, A. "Novel photocatalytic applications of sub-nanometer gold particles for environmental liquid and gas phase reactions", *Applied Catalysis B: Environmental*, 104, 239-244, 2011.
5. Ramakrishnan, G., **Zhao, S.**, Han, W., Orlov, A. "Simultaneous observation of gas phase and surface species in photocatalytic reactions on nanosize Au modified TiO_2: The next generation of DRIFTS systems", *Chemical Engineering Journal*, 170, 445-450, 2011.

Selected conference presentations arising from this work

1. **Zhao, S.**, Ramakrishnan, G., Shen, P., Han, W. and Orlov, A. (2010) Novel applications of sub-nanometer noble metal particles for photocatalysis. American Chemistry Society. Boston, MA.
2. **Zhao, S.**, Ramakrishnan, G., Su D., Rieger R., Antonius K. and Orlov A. (2011) Novel applications of sub-nanometer metal particles and mesoporous support in environmental photocatalysis. American Chemical Society Denver
3. **Zhao, S.**, Ramakrishnan, G., Su D. and Orlov A. (2012) Photocatalytic applications of sub-nanometer Pt particles prepared from micelle-stabilized precursors. American Chemical Society San Diego
4. **Zhao S.**, Li Y., Shen P., Su D. and Orlov A. (2012) Enhanced photocatalytic H_2 production by sub-nanometer Au nanoparticles. American Physical Society Boston

Chapter 1. Introduction: Photocatalysis on semiconductors

1.1 Photocatalysis introduction

Combining light and nano-size catalysts is a very important area of research, which has a potential to address both environmental and energy issues [1-7]. Not only can it convert dangerous pollutants in water and air to benign compounds, but also it can address energy demand in a sustainable way. Ever since 1972, when A. Fujishima and K. Honda achieved first experimental water splitting using TiO_2 under the ultraviolet light [8], the possibility of conversion solar energy to sustainable energy source by using semiconductors has been a motivation for many research efforts. During the 1980s, the work gained by Heller et al. in developing TiO_2 based photocatalysts for decomposition of organic compounds has shown great potential of using photocatalyts to address environmental pollutions [9]. Recently, this field has been expanding rapidly addressing the issues ranging from environmental remediation to sustainable energy conversion. Thousands of patents and papers about photocatalysis in either aqueous or gaseous system have been published. Given the fact that the world is now facing unprecedented crises in terms of energy supply and the quality of global environment, photocatalysis opens new opportunities for a sustainable future.

The photocatalytic process has several advantages, such as complete mineralization of organic substances, and low cost, while utilizing the free source of energy - sunlight. Semiconductors with wide bandgap, such as, for example, TiO_2 has become one of the bench marks in heterogeneous catalysis research [10-12]. However, there are a few limitations for the traditional photocatalysts, such as stability of the catalysts and the lack of activity under visible light irradiation. In order to increase the efficiency of photocatalysis, numerous studies have been conducted over the years. Among these studies, great attention has been contributed to photocatalysts' modifications to achieve activity under visible light [13]. In addition to doping, several other strategies have been developed

including synthesis of metal-semiconductor system which can reduce the electron-hole recombination rate [14], and porous or high surface area catalysts which provide more active sites for catalytic reactions [15].

This chapter concentrates on the basis of semiconductor based photocatalysts and photocatalytic reaction mechanisms. In addition this chapter discusses various known strategies of catalyst modification methods including: 1) nitrogen doping to shift the photoresponse towards visible light region; 2) introducing metal-semiconductor system to increase the photoresponse; 3) applying nano-structured titania to expand reactive surface area.

1.2 Semiconductor as Photocatalysts

Semiconductors have a void energy region in a solid where no electron states can exist. The term, bandgap or energy gap is the energy range from the top of the valance band to the bottom of the conduction band. Unlike metals or insulators, semiconductors have the energy gap which allows not only producing electron hole pairs during photoactivaton but also preventing them from recombination. The bandgap energy between valence and conduction band varies significantly for different semiconductors. Several most commonly used semiconductors and their bandgap energy have been shown on Table 1.1.

Bandgap width is one of the crucial parameters in judging semiconductor activities for reduction/oxidation (redox) reactions. Selection of suitable semiconductor photocatalysts for different redox reactions under various ranges of light radiation is considered to be another key criterion. Based on the bandgap energy, we can determine which semiconductors can be activated under visible light and which can only used under UV light. Semiconductors like TiO_2, ZnS, ZnO, and CdS have been proven to be more efficient promoting serious of catalytic reactions under visible and near UV radiation.

Photocatalyst	*Bandgap energy (eV)*
La_2O_3	5.5
ZrO2	5.0
SnO	4.2
ZnS	3.6
SnO_2	3.5
ZnO	3.2
TiO_2 (anatase)	3.2
TiO_2 (rutile)	3.0
SiC	3.0
V_2O_5	2.8
WO_3	2.7
CdS	2.4
GaP	2.25
Fe_2O_3	2.2
HgS	2.0
HgO	1.9
CuO	1.7
CdSe	1.7
Ti_2O_3	1.6
Ag_2O	1.33
Cu_2S	1.1
TiS_2	0.7
MnO_2	0.25
Fe_2O_3	0.1

Table 1.1 Band gap energy of various photocatalysts

A good photocatalyst should be (i) photoactive, (ii) able to utilize visible and/or near UV light, (iii) biologically and chemically inert, (iv) photostable (i.e.

not prone to photocorrosion), (v) inexpensive and (vi) non-toxic. Currently, most of the photocatalysts have their own limitations [16], such as lack of activity under visible radiation and the low rate of photo-oxidation of organic compounds on the surface of the catalyst [16], which makes photocatalysis very difficult to be fully commercialized.

Among all these catalysts, TiO_2 is considered to be the most suitable photocatalysts for the reasons that it is relatively inexpensive, highly chemically stable, photoactive and nontoxic. The increased interest towards TiO_2 stimulated the development of a variety of preparation methods to obtain materials with better performance than commercial titania powders. Titanium dioxide has three natural polymorphs: anatase, rutile and brookite and their crystal structures are stated in Figure 2 [11, 17].

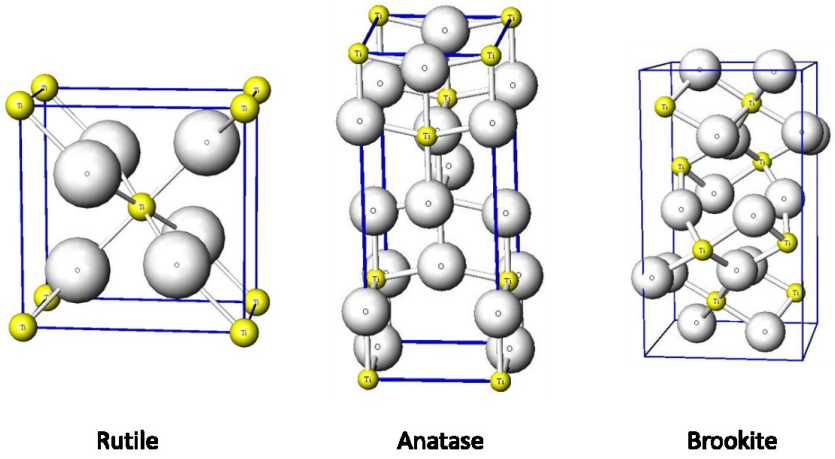

Fig. 1.1 Crystal structures of different types of TiO_2 nanoparticles

Among all the various ones available, anatase is the most active allotropic in terms of photocatalytic activity, either natural (rutile and brookite) or artificial (TiO_2–B, TiO_2–H). However, anatase is thermodynamically less stable than rutile.

Its formation is kinetically favored only at lower temperature (<600°C). This lower temperature could explain the anatase has the higher surface area and surface density of active sites which are beneficial for adsorption and catalytic processes.

1.3 Heterogeneous photocatalysts

In chemistry, heterogeneous catalysis refers to catalysis form where the phase of the catalyst differs from that of the reactants. Heterogeneous photocatalysis is a discipline which includes a large variety of reactions: selective or complete oxidation, dehydrogenation, hydrogen transfer, etc. It has many applications including industrial, energy, and also environmental, including water purification, gaseous pollutant removal, etc [18]. Heterogeneous photocatalysis can be performed in a variety of media: gas phase, liquid phase and aqueous solutions. As for classical heterogeneous catalysis, the overall process can be broke down into five independent steps:

1) Transfer of the reactants to the catalyst surface;
2) Adsorption of the reactants;
3) Catalytic reaction in the adsorbed phase;
4) Desorption of the products;
5) Removal of the products.

In terms of environmental applications, heterogeneous photocatalysis on semiconductor metal oxide is the method which has the following advantages comparing to other processes [19, 20]:

1) It can decompose the hazardous organic compound in the gaseous and aqueous phase more efficiently compared to regular homogeneous catalysts;
2) It has a potential to decompose organic compounds to CO_2, water and

mineral acids;

3) It can take place at mild experimental conditions, such as ambient temperature and atmospheric pressure;
4) It has higher efficiency especially for diluted pollutants.

The efficiency of photocatalytic degradation is determined by several factors, such as catalyst surface area, wavelength, initial concentration, temperature and radiant flux [21]. Given the low efficiency of commercialized photocatalysts at current stage, the industrial applications are still very limited.

1.4 Photocatalytic mechanism and kinetics

While designing the systems for conducting photocatalytic reactions, two principal factors must be taken account of. The first one is the efficiency of creation of electron and hole pairs when absorbing solar irradiation. The other one is the efficiency in terms of separation of the electron hole pairs before they lose their redox ability due to recombination. When catalysts based on oxides (TiO_2, ZnO, CeO_2, WO_3…), or sulfides (CdS, ZnS,…) are illuminated with photons whose energy is equal to or greater than their bandgap energy E_g ($h\nu \geqslant E_g$), there is absorption of these photons and creation of charge separation, which excite free electrons in the conduction band and leave positive charged holes in the valence band.

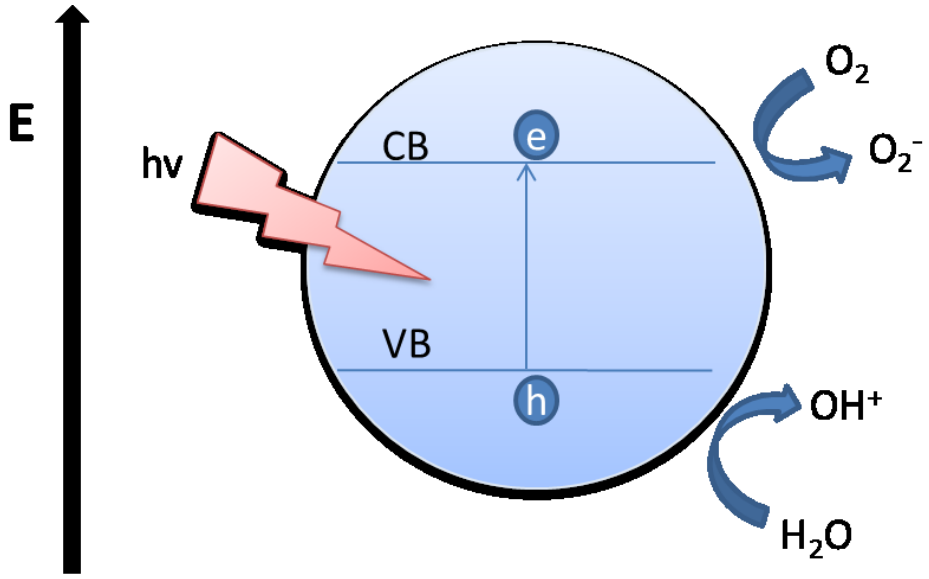

Fig. 1.2 The schematic view of photocatalytic mechanism

As mentioned earlier, the initial process for heterogeneous photocatalysis of organic and inorganic compounds by semiconductors is the generation of electron-hole pairs in the semiconductor particles. Figure 1.2 shows the excitation of an electron from the valence band to the conduction band initiated by light absorption with energy equal to or greater than the band gap of the semiconductor. Upon excitation, the fate of the separated electron and hole can follow several pathways. Then the positive holes can neutralize the OH^- surface groups and generate hydroxyl radicals which are very oxidative and non-selective. The reductive reaction is due to the activated electrons with an oxidant to produce reduced products.

As reported in the previous 20 years, the mechanism of photocatalytic oxidation is complicated and it is difficult to get the exact reaction kinetics from the elementary reaction steps. The reaction rate depends on the light irradiance and the photocatalysis [17].

An empirical power rate law including the influence of light irradiance was also proposed in equation (1.1) [22]:

$$\mathbf{r} = \mathbf{kCo}^{\boldsymbol{m}}\mathbf{I}^{\boldsymbol{n}} \qquad (1.1)$$

Where ***I*** is the light intensity, ***m*** and ***n*** are related with other experimental variables, such as the diffusion, temperature and so on. Also ***m*** and ***n*** are interrelated rather than independent, which also make the model more complicated.

The efficiency of the photocatalytic process can be experimentally measured as a quantum yield [18]. It is defined as the number of events occurring per photon absorbed. However, it is not a trivial issue to measure the actual absorbed light in heterogeneous systems due to scattering of light by the surface of the catalysts. Therefore, the assumption of all the light is absorbed is usually made and the efficiency can be calculated as an apparent quantum yield.

To determine the efficiency or quantum yield, a combination of all the pathway probabilities for the electron and hole must be considered [21]. The quantum yield for an ideal system (∅), given by Linsebigler et al [23] is described b a simple relationship

$$\emptyset \propto \frac{k_{CT}}{k_{CT} + K_R}$$

where quantum yield (∅) is proportional to the rate of the charge transfer processes (k_{CT}) and inversely proportional to the sum of the charge transfer rate (k_{CT}) and the electron-hole recombination rate (k_R).

In general, experimental conditions can also affect the efficiency of

the photocatalytic pathway. They can be categorized as following points:

1) Light source. Higher the intensity of the light can lead to better charge separation of the electron-hole pairs;
2) Ratio between catalysts and solution. Normally 1 g/L is considered an optimum ratio for liquid photocatalytic reactions;
3) pH of the solution. pH can affect the adsorption properties of the catalysts due to the different charge of the semiconductor surface influencing adsorption and homogeneous chemistry of the reactants;
4) Temperature. The effect of the temperature on photocatalytic reactions varies based on different reactants, affecting both the reaction rate and distribution between aqueous and gas phases.

1.5 Modification of TiO_2

Modification of TiO_2 can largely increase the efficiency of the photocatalysis and can be achieved by several approaches in, including: 1) increasing the light utilization spectral range; 2) inhibiting electron–hole pair recombination rate; 3) increasing reactive surface area.

1.5.1 Doping of semiconductors

As mentioned above, one of the major drawbacks of TiO_2 is its limited photoresponse to visible light area of the spectrum, as only 5 % of the solar energy lies in the UV region where TiO_2 is active. Therefore, it is desirable to develop a semiconductor system capable of utilizing visible light region. The doping of semiconductors leads to creating energy levels in bandgap and/or narrowing a bandgap, thus requiring smaller energy to excite electrons to conduction band [24]. An initial approach to achieve such doping of TiO_2 is to use

transition-metal elements. However, metal doping has several drawbacks. The doped materials have been shown to suffer from thermal instability, and the metal centers act as electron traps, which reduces the photocatalytic efficiency [25]. The activity of the doped semiconductors can be determined by the concentration of dopants, their energy level within the bandgap and homogeneity of dispersion of the dopants [13, 26, 27].

Recent studies have demonstrated nitrogen doping in TiO_2 lattice results in shifting the optical response to the visible spectral range. Some reports suggest this redshift effect is mainly due to formation of the oxygen vacancies rather than narrowing the bandgap of the TiO_2.

1.5.2 Metal – semiconductor system

Modification of semiconductor with noble metals (precious metals) is another effective way of improving the activity of the photocatalysts. It is known that metals and semiconductors have different Fermi level positions. When mixing with one metal and one semiconductor, electrons from Schottky barrier of this metal can interact with the surface of the semiconductor, therefore, causing electron migration from the semiconductor surface to the metal until the Fermi levels of the two materials become equal.

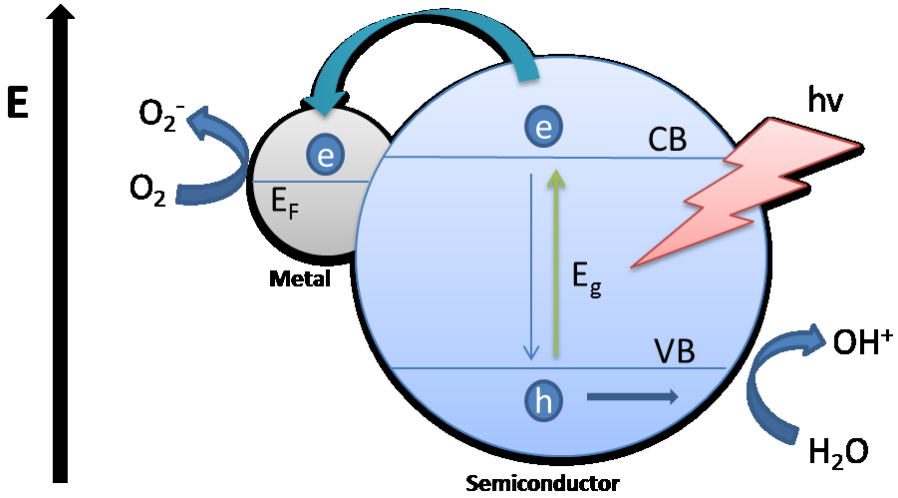

Fig. 1.3 Proposed mechanism of electron-hole separation in metal-semiconductor system during photocatalysis

Catalytic applications of metal nanoparticles have been an exciting area of chemistry research, leading to many promising applications. These studies showed that catalytic behavior of metal nanoparticles exhibits a strong size and shape dependency, which can be used to tune these reactive interfaces to achieve high activity and selectivity for various types of reactions. One of exciting area of research is how to achieve a high degree of control over the cluster size, shape, and dispersion on the support. These adjustments of nanoparticles size and shape can be accomplished by several new synthetic procedures described in the recent literature. Some examples are shown in Figure 1.4. The shape and size control can be accomplished by using various methods of synthesis including synthesis of metal nanoparticles protected by organic ligands or by combining metal precursors with polymer micelles surfactants to tune metal nanoparticles within predefined size and shape range [29-31].

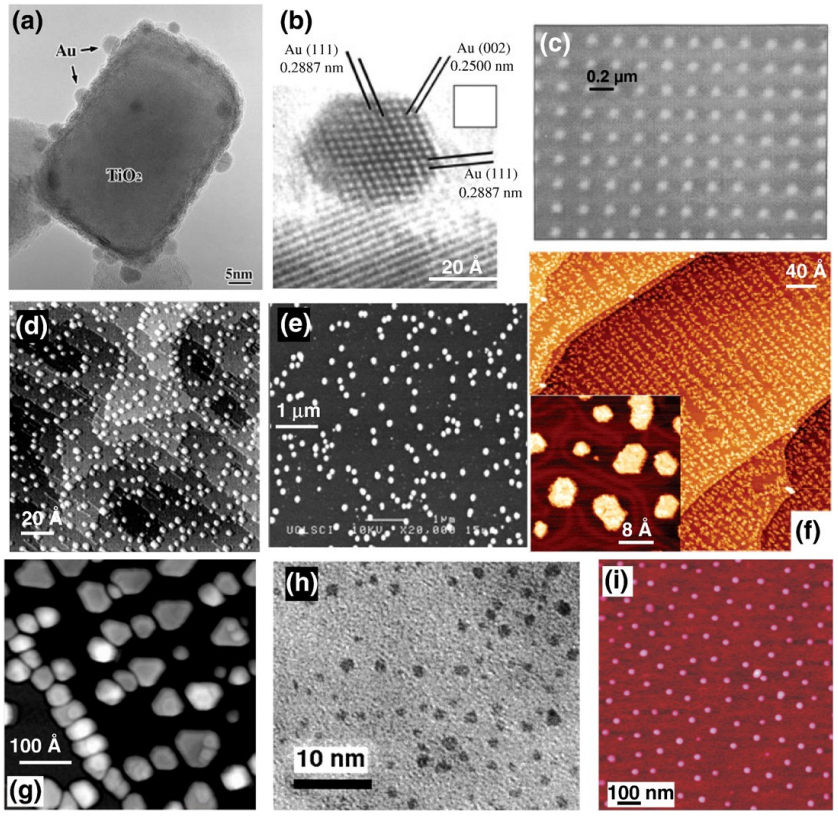

Fig. 1.4 Microscopy images of noble metal nanoparticles with different sizes prepared by various methods [32-41]

This mechanism of increase in activity is due to the enhanced charge separation due to formation metal-semiconductor interface. Gold, for example, has been regarded as an inactive catalyst on its own. However, when it deposited on certain metal oxides as ultra-fine particles, its chemistry dramatically changes [42, 43]. It exhibits an extraordinarily high activity for low-temperature catalytic reaction such as hydrogenation of hydrocarbons and reduction of nitrogen oxides [44]. For example, the experimental observations by Haruta et al. on the dramatic enhancement of the catalytic activity and selectivity of highly dispersed gold particles (<5 nm) supported on metal oxides [34] reveal the influence of the nanoparticle size on reaction rate.

It was suggested that the catalytic activity of gold NPs for CO oxidation depends strongly on the contact area between nanoparticles and the support [45]. It is important to highlight that the key element to control this parameter is the shape of the nanoparticles. However, a very limited number of papers have studied the relationship between the particle shape and catalytic activity. Important contributions to the understanding of the shape–reactivity relationship have been made by several groups [46-48]. For example, Cuenya et al focused on using block copolymers to synthesize well-defined two-dimensional metal clusters (Au, Pt). She found that metal clusters with lower geometry dimensions (2D, flat geometry) have higher catalytic performances than 3D, round shaped clusters [41, 49]. However, none of the studies mentioned above have looked into photcatalytic reactions, which are the focus of this dissertation.

1.5.3 Nanostructured semiconductors

It is well known that, the efficiency of the photocatalyst can be tuned by manipulating its structural characteristic and surface area. The fabrication of complex nanostructures with controlled morphology, orientation, and dimensionality have attracted significant attention over the past decade since

such control is critical for the determination of catalytic properties in many processes [50-53]. Ordered nanostructures like nanoparticles, nanorods, nanobelts, and nanosheets were achieved by various methods [54-56]. A lot of work has been done for determination of structure – catalytic property relationships over the years. Zeng et al. reported using facile route to synthesize porous nanoflower structures hematite and achieved promising photocatalytic activity [57]. Zhang et al. published Self-Assembled 3-D Architectures of BiOBr which can be applied as visible light driven photocatalysts [58].

Nanostructured semiconductors can also be achieved by introducing inverse opal structure to fabricate photonic crystals to increase the utility ratio of the light [59-61]. By making such three-dimensional periodic semiconductors can enhance the light-trapping inside of the semiconductors which leads to better efficiency of catalytic performance [62].

The strategies of maximizing the active sites by dispersing conventional catalysts over the high surface area materials can further enhance the catalytic performances. For example, various types of porous molecular sieves including zeolite and mesoporous silica can be used as inert supports for photocatalysts.

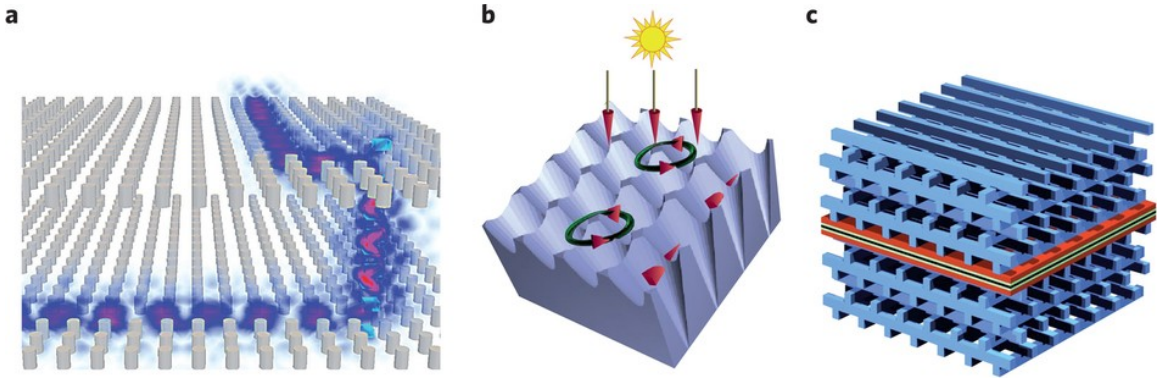

Fig. 1.5 Different forms of light-trapping photonic crystals [62]

1.6 Photocatalytic reaction described in this dissertation

1.6.1 Phenol degradation

Contamination of water supplies with various organics is becoming an increasing concern which can lead to serious of environmental and health problems. Phenols and phenolic compounds are common pollutants of aquatic system. Billions of pounds of phenol are produced and used annually in the United States. Oxidation of phenols often produces a number of reaction products, primarily of lower molecular weight although there are some products which are polymeric in nature [63]. Both parent compound and its byproducts are hazardous and harmful to the environment. Therefore, it is crucial to find an effective way to fully mineralize them into CO_2 and water.

Many conventional water treatment processes can only transfer the contaminants from one medium to another or generate waste that requires further treatment and disposal [64]. Heterogeneous photocatalysis, a relatively new wastewater treatment and water purification technique, is a fast growing research area in the past decade [65, 66]. The advantages of this technique over the traditional wastewater treatment include complete mineralization of the organic compounds and high degradation efficiency in treating nearly any organic compounds at low concentrations [67].

The reaction mechanism of photocatalytic phenol degradation is a very complicated process and the initial steps of the oxidation were shown as follows:

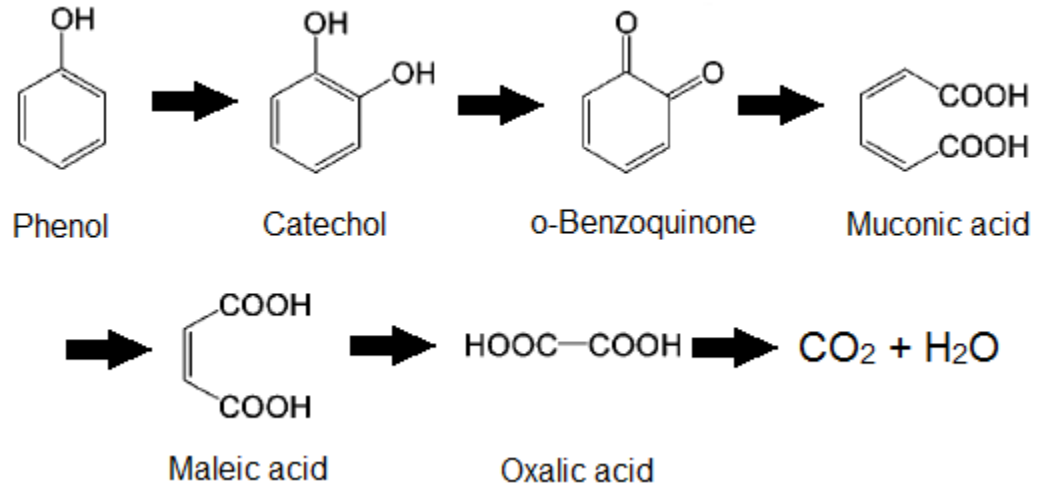

Fig 1.6 Phenol degradation reaction pathway

The final product of the phenol oxidation would be CO_2 and H_2O. One of the many reaction pathways of phenol oxidation was presented above to demonstrate a possible route for its complete mineralization. The intermediate product (catechol) has been selected here in this dissertation to monitor the reaction production due to the detection limitation of the final products.

The aim of this study is to examine the decomposition of phenol by photodegradation. Photocatalytic degradation rates of phenol have been examined in the presence of different photocatalysts under UV illumination.

1.6.2 NO_2 oxidation

Addressing the air quality issues by using photocatalysts has been a focal point of research for many groups in the previous years. One of the criteria pollutants, which can be removed by this approach, is NO_2. The NO_2 emissions can contribute to formation of acid rain, atmospheric particles and various other toxic substances resulting in health problems, visibility reduction and global

warming. One of the most prevalent problems associated with these emissions is the formation of ground level ozone, which is produced by NO_2 reacting with volatile organic compounds (VOCs) in the presence of sunlight. The ground level ozone can damage lung tissues and reduce lung function. It is a significant problem worldwide as millions of people live in areas that do not meet the health standards for ozone [68].

The majority of the studies related to photocatalytic removal of NO_X ($NO + NO_2$) have concentrated on the gas phase analysis of the reaction products, without a simultaneous analysis of the surface composition [69-73]. This project describes the next generation of DRIFTS system. The feasibility of this approach has been demonstrated for NO_2 conversion on TiO_2 based modified novel photocatalysts, which is the first ever application of such system for study of photocatalytic NO_2 conversion.

1.6.3 Water splitting

In order to reduce our dependence on fossil fuels it is vital to explore various sustainable energy options. For example, one possible strategy is to develop a hydrogen based energy, which can potentially offer numerous environmental and energy efficiency benefits [74]. However, the sustainable advantages of using hydrogen are limited given the fact that currently hydrogen is primarily produced from fossil fuels, such as natural gas, via steam reforming. Therefore, it will be tremendously beneficial to find alternative ways to produce hydrogen in efficient and sustainable manner. A potentially viable way forward is to make H_2 from water by combining solar energy and heterogeneous catalysts. Photocatalytic water splitting has the potential to dissociate water into it constituent parts, H_2 and O_2 without producing greenhouse gases or other harmful effects on the atmosphere. In recent years, many studies focusing on the visible light photocatalytic water splitting are aiming to utilize direct solar light to produce renewable hydrogen

fuels instead of artificial light source.

In order to explore the photocatalysts in H_2 production under visible light region, we have chosen a standard catalyst (CdS), which is known to be active in water splitting, and modified it with noble metal clusters. Given the CdS bandgap of 2.4 eV and the positions of its valence and conductions bands, it has a modest activity for water splitting under visible light. We then modified the CdS with noble metal nanoparticles to achieve much higher hydrogen evolution than the conventional catalysts.

Reference:

[1] H. Yang, G.Y. Li, T.C. An, Y.P. Gao, J.M. Fu, Photocatalytic degradation kinetics and mechanism of environmental pharmaceuticals in aqueous suspension of TiO2: A case of sulfa drugs, Catal Today, 153 (2010) 200-207.

[2] J. Colina-Marquez, F. Machuca-Martinez, G.L. Puma, Radiation Absorption and Optimization of Solar Photocatalytic Reactors for Environmental Applications, Environ Sci Technol, 44 (2010) 5112-5120.

[3] A. Di Paola, E. Garcia-Lopez, G. Marci, L. Palmisano, A survey of photocatalytic materials for environmental remediation, J Hazard Mater, 211 (2012) 3-29.

[4] H. Yang, T.C. An, G.Y. Li, W.H. Song, W.J. Cooper, H.Y. Luo, X.D. Guo, Photocatalytic degradation kinetics and mechanism of environmental pharmaceuticals in aqueous suspension of TiO2: A case of beta-blockers, J Hazard Mater, 179 (2010) 834-839.

[5] M. Matsuoka, M. Kitano, M. Takeuchi, K. Tsujimaru, M. Anpo, J.M. Thomas, Photocatalysis for new energy production - Recent advances in photocatalytic water splitting reactions for hydrogen production, Catal Today, 122 (2007) 51-61.

[6] K. Rangan, S.M. Arachchige, J.R. Brown, K.J. Brewer, Solar energy conversion using photochemical molecular devices: photocatalytic hydrogen production from water using mixed-metal supramolecular complexes, Energ Environ Sci, 2 (2009) 410-419.

[7] D. Katakis, C. Mitsopoulou, E. Vrachnou, Photocatalytic Splitting of Water - Increase in Conversion and Energy-Storage Efficiency, J Photoch Photobio A, 81 (1994) 103-106.

[8] A. Hagfeldt, M. Gratzel, Light-Induced Redox Reactions in Nanocrystalline Systems, Chem Rev, 95 (1995) 49-68.

[9] A. Heller, Conversion of Sunlight into Electrical-Power and Photoassisted Electrolysis of Water in Photoelectrochemical Cells, Accounts Chem Res, 14

(1981) 154-162.

[10] U. Diebold, The surface science of titanium dioxide, Surf Sci Rep, 48 (2003) 53-229.

[11] X. Chen, S.S. Mao, Titanium dioxide nanomaterials: Synthesis, properties, modifications, and applications, Chem Rev, 107 (2007) 2891-2959.

[12] I.K. Konstantinou, T.A. Albanis, TiO2-assisted photocatalytic degradation of azo dyes in aqueous solution: kinetic and mechanistic investigations - A review, Appl Catal B-Environ, 49 (2004) 1-14.

[13] R. Asahi, T. Morikawa, T. Ohwaki, K. Aoki, Y. Taga, Visible-light photocatalysis in nitrogen-doped titanium oxides, Science, 293 (2001) 269-271.

[14] M.I. Litter, Heterogeneous photocatalysis - Transition metal ions in photocatalytic systems, Appl Catal B-Environ, 23 (1999) 89-114.

[15] M. Anpo, M. Takeuchi, The design and development of highly reactive titanium oxide photocatalysts operating under visible light irradiation, J Catal, 216 (2003) 505-516.

[16] D. Friedmann, C. Mendive, D. Bahnemann, TiO2 for water treatment: Parameters affecting the kinetics and mechanisms of photocatalysis, Appl Catal B-Environ, 99 (2010) 398-406.

[17] A.J. Bard, Photoelectrochemistry and Heterogeneous Photocatalysis at Semiconductors, J Photochem, 10 (1979) 59-75.

[18] J.M. Herrmann, Heterogeneous photocatalysis: fundamentals and applications to the removal of various types of aqueous pollutants, Catal Today, 53 (1999) 115-129.

[19] O.M. Alfano, D. Bahnemann, A.E. Cassano, R. Dillert, R. Goslich, Photocatalysis in water environments using artificial and solar light, Catal Today, 58 (2000) 199-230.

[20] G. Marci, M. Addamo, V. Augugliaro, S. Coluccia, E. Garcia-Lopez, V. Loddo, G. Martra, L. Palmisano, M. Schiavello, Photocatalytic oxidation of toluene on irradiated TiO2: comparison of degradation performance in humidified air, in water and in water containing a zwitterionic surfactant, J Photoch Photobio A, 160 (2003) 105-114.

[21] S. Yamazaki, S. Tanaka, H. Tsukamoto, Kinetic studies of oxidation of ethylene over a TiO2 photocatalyst, J Photoch Photobio A, 121 (1999) 55-61.
[22] N.J. Peill, M.R. Hoffmann, Mathematical model of a photocatalytic fiber-optic cable reactor for heterogeneous photocatalysis, Environ Sci Technol, 32 (1998) 398-404.
[23] A.L. Linsebigler, G.Q. Lu, J.T. Yates, Photocatalysis on Tio2 Surfaces - Principles, Mechanisms, and Selected Results, Chem Rev, 95 (1995) 735-758.
[24] W.Y. Choi, A. Termin, M.R. Hoffmann, The Role of Metal-Ion Dopants in Quantum-Sized Tio2 - Correlation between Photoreactivity and Charge-Carrier Recombination Dynamics, J Phys Chem-Us, 98 (1994) 13669-13679.
[25] C. Burda, Y.B. Lou, X.B. Chen, A.C.S. Samia, J. Stout, J.L. Gole, Enhanced nitrogen doping in TiO2 nanoparticles, Nano Lett, 3 (2003) 1049-1051.
[26] O. Carp, C.L. Huisman, A. Reller, Photoinduced reactivity of titanium dioxide, Prog Solid State Ch, 32 (2004) 33-177.
[27] J.C. Yu, J.G. Yu, W.K. Ho, Z.T. Jiang, L.Z. Zhang, Effects of F- doping on the photocatalytic activity and microstructures of nanocrystalline TiO2 powders, Chem Mater, 14 (2002) 3808-3816.
[28] S. Ikeda, N. Sugiyama, B. Pal, G. Marci, L. Palmisano, H. Noguchi, K. Uosaki, B. Ohtani, Photocatalytic activity of transition-metal-loaded titanium(IV) oxide powders suspended in aqueous solutions: Correlation with electron-hole recombination kinetics, Phys Chem Chem Phys, 3 (2001) 267-273.
[29] L.K. Ono, D. Sudfeld, B.R. Cuenya, In situ gas-phase catalytic properties of TiC-supported size-selected gold nanoparticles synthesized by diblock copolymer encapsulation, Surf Sci, 600 (2006) 5041-5050.
[30] G. Kastle, H.G. Boyen, F. Weigl, G. Lengl, T. Herzog, P. Ziemann, S. Riethmuller, O. Mayer, C. Hartmann, J.P. Spatz, M. Moller, M. Ozawa, F. Banhart, M.G. Garnier, P. Oelhafen, Micellar nanoreactors - Preparation and characterization of hexagonally ordered arrays of metallic nanodots, Adv Funct Mater, 13 (2003) 853-861.
[31] B.R. Cuenya, S.H. Baeck, T.F. Jaramillo, E.W. McFarland, Size- and support-dependent electronic and catalytic properties of Au-0/Au3+ nanoparticles

synthesized from block copolymer micelles, J Am Chem Soc, 125 (2003) 12928-12934.

[32] D. Thompson, A golden future for catalysis, Chem Brit, 37 (2001) 43-44.

[33] G.J. Hutchings, M. Haruta, A golden age of catalysis: A perspective, Appl Catal a-Gen, 291 (2005) 2-5.

[34] M. Haruta, Size- and support-dependency in the catalysis of gold, Catal Today, 36 (1997) 153-166.

[35] A.S. Eppler, G. Rupprechter, L. Guczi, G.A. Somorjai, Model catalysts fabricated using electron beam lithography and pulsed laser deposition, J Phys Chem B, 101 (1997) 9973-9977.

[36] T.V. Choudhary, D.W. Goodman, Oxidation catalysis by supported gold nano-clusters, Top Catal, 21 (2002) 25-34.

[37] R.G. Palgrave, I.P. Parkin, Surfactant directed chemical vapour deposition of gold nanoparticles with narrow size distributions, Gold Bull, 41 (2008) 66-69.

[38] D. Song, J. Hrbek, R. Osgood, Formation of TiO2 nanoparticles by reactive-layer-assisted deposition and characterization by XPS and STM, Nano Lett, 5 (2005) 1327-1332.

[39] H.J. Freund, Model systems in heterogeneous catalysis: Selectivity studies at the atomic level, Top Catal, 48 (2008) 137-144.

[40] R.M. Crooks, M.Q. Zhao, L. Sun, V. Chechik, L.K. Yeung, Dendrimer-encapsulated metal nanoparticles: Synthesis, characterization, and applications to catalysis, Accounts Chem Res, 34 (2001) 181-190.

[41] B.R. Cuenya, Synthesis and catalytic properties of metal nanoparticles: Size, shape, support, composition, and oxidation state effects, Thin Solid Films, 518 (2010) 3127-3150.

[42] Y. Iizuka, H. Fujiki, N. Yamauchi, T. Chijiiwa, S. Arai, S. Tsubota, M. Haruta, Adsorption of CO on gold supported on TiO2, Catal Today, 36 (1997) 115-123.

[43] H. Sakurai, A. Ueda, T. Kobayashi, M. Haruta, Low-temperature water-gas shift reaction over gold deposited on TiO2, Chem Commun, (1997) 271-272.

[44] A. Ueda, T. Oshima, M. Haruta, Reduction of nitrogen monoxide with propene in the presence of oxygen and moisture over gold supported on metal

oxides, Appl Catal B-Environ, 12 (1997) 81-93.
[45] M. Haruta, Nanoparticulate gold catalysts for low-temperature CO oxidation, J New Mat Electr Sys, 7 (2004) 163-172.
[46] R. Narayanan, M.A. El-Sayed, Effect of colloidal catalysis on the nanoparticle size distribution: Dendrimer-Pd vs PVP-Pd nanoparticles catalyzing the Suzuki coupling reaction, J Phys Chem B, 108 (2004) 8572-8580.
[47] R. Narayanan, M.A. El-Sayed, Shape-dependent catalytic activity of platinum nanoparticles in colloidal solution, Nano Lett, 4 (2004) 1343-1348.
[48] V. Komanicky, H. Iddir, K.C. Chang, A. Menzel, G. Karapetrov, D. Hennessy, P. Zapol, H. You, Shape-Dependent Activity of Platinum Array Catalyst, J Am Chem Soc, 131 (2009) 5732-+.
[49] B.R. Cuenya, J.R. Croy, S. Mostafa, F. Behafarid, L. Li, Z.F. Zhang, J.C. Yang, Q. Wang, A.I. Frenkel, Solving the Structure of Size-Selected Pt Nanocatalysts Synthesized by Inverse Micelle Encapsulation, J Am Chem Soc, 132 (2010) 8747-8756.
[50] J.T. Hu, T.W. Odom, C.M. Lieber, Chemistry and physics in one dimension: Synthesis and properties of nanowires and nanotubes, Accounts Chem Res, 32 (1999) 435-445.
[51] M. Law, J. Goldberger, P.D. Yang, Semiconductor nanowires and nanotubes, Annu Rev Mater Res, 34 (2004) 83-122.
[52] J.K. Yuan, W.N. Li, S. Gomez, S.L. Suib, Shape-controlled synthesis of manganese oxide octahedral molecular sieve three-dimensional nanostructures, J Am Chem Soc, 127 (2005) 14184-14185.
[53] H. Zeng, P.M. Rice, S.X. Wang, S.H. Sun, Shape-controlled synthesis and shape-induced texture of MnFe2O4 nanoparticles, J Am Chem Soc, 126 (2004) 11458-11459.
[54] H. Colfen, M. Antonietti, Mesocrystals: Inorganic superstructures made by highly parallel crystallization and controlled alignment, Angew Chem Int Edit, 44 (2005) 5576-5591.
[55] Z.Y. Tang, N.A. Kotov, One-dimensional assemblies of nanoparticles: Preparation, properties, and promise, Adv Mater, 17 (2005) 951-962.

[56] G. Zhang, X. Lu, W. Wang, X. Li, Facile synthesis of a hierarchical PbTe flower-like nanostructure and its shape evolution process guided by a kinetically controlled regime, Chem Mater, 19 (2007) 5207-5209.
[57] S.Y. Zeng, K.B. Tang, T.W. Li, Z.H. Liang, D. Wang, Y.K. Wang, Y.X. Qi, W.W. Zhou, Facile route for the fabrication of porous hematite nanoflowers: Its synthesis, growth mechanism, application in the lithium ion battery, and magnetic and photocatalytic properties, J Phys Chem C, 112 (2008) 4836-4843.
[58] J. Zhang, F.J. Shi, J. Lin, D.F. Chen, J.M. Gao, Z.X. Huang, X.X. Ding, C.C. Tang, Self-assembled 3-D architectures of BiOBr as a visible light-driven photocatalyst, Chem Mater, 20 (2008) 2937-2941.
[59] J.Y. Chen, Improvement of photovoltaic efficiency using 3D photonic-crystal enhanced light trapping and absorption, Physica E, 44 (2011) 43-48.
[60] J. Upping, A. Bielawny, R.B. Wehrspohn, T. Beckers, R. Carius, U. Rau, S. Fahr, C. Rockstuhl, F. Lederer, M. Kroll, T. Pertsch, L. Steidl, R. Zentel, Three-Dimensional Photonic Crystal Intermediate Reflectors for Enhanced Light-Trapping in Tandem Solar Cells, Adv Mater, 23 (2011) 3896-+.
[61] D.Y. Zhou, R. Biswas, Photonic crystal enhanced light-trapping in thin film solar cells, J Appl Phys, 103 (2008).
[62] S. John, Why trap light?, Nat Mater, 11 (2012) 997-999.
[63] T.Y. Wei, C.C. Wan, Heterogeneous Photocatalytic Oxidation of Phenol with Titanium-Dioxide Powders, Ind Eng Chem Res, 30 (1991) 1293-1300.
[64] J.C. Crittenden, J.B. Liu, D.W. Hand, D.L. Perram, Photocatalytic oxidation of chlorinated hydrocarbons in water, Water Res, 31 (1997) 429-438.
[65] D. Bahnemann, A. Cassano, Special issue on TiO2 photocatalytic purification and treatment of water and air - Preface, J Adv Oxid Technol, 5 (2002) 3-3.
[66] M. Schiavello, Some Working Principles of Heterogeneous Photocatalysis by Semiconductors, Electrochim Acta, 38 (1993) 11-14.
[67] N. Serpone, R.F. Khairutdinov, Application of nanoparticles in the photocatalytic degradation of water pollutants, Semiconductor Nanoclusters-Physical, Chemical, and Catalytic Aspects, 103 (1997) 417-444.

[68] B. LubkertAlcamo, M. Krzyzanowski, Estimate of health impacts of acidifying air pollutants and tropospheric ozone in Europe, Water Air Soil Poll, 85 (1995) 167-176.

[69] C.H. Ao, S.C. Lee, C.L. Mak, L.Y. Chan, Photodegradation of volatile organic compounds (VOCs) and NO for indoor air purification using TiO2: promotion versus inhibition effect of NO, Appl Catal B-Environ, 42 (2003) 119-129.

[70] S. Devahasdin, C. Fan, K.Y. Li, D.H. Chen, TiO2 photocatalytic oxidation of nitric oxide: transient behavior and reaction kinetics, J Photoch Photobio A, 156 (2003) 161-170.

[71] J. Jeong, J. Jurng, S. Jin, Y. Kim, Optimization of the removal efficiency of nitrogen oxides in the air using a low-pressure Hg lamp, J Photoch Photobio A, 197 (2008) 50-54.

[72] Y.M. Lin, Y.H. Tseng, J.H. Huang, C.C. Chao, C.C. Chen, I. Wang, Photocatalytic activity for degradation of nitrogen oxides over visible light responsive titania-based photocatalysts, Environ Sci Technol, 40 (2006) 1616-1621.

[73] T. Maggos, J.G. Bartzis, P. Leva, D. Kotzias, Application of photocatalytic technology for NOx removal, Appl Phys a-Mater, 89 (2007) 81-84.

[74] T. Bak, J. Nowotny, M. Rekas, C.C. Sorrell, Photo-electrochemical hydrogen generation from water using solar energy. Materials-related aspects, Int J Hydrogen Energ, 27 (2002) 991-1022.

Chapter 2. Design and Development of highly active novel photocatalysts

2.1 Developing benchmark catalyst for photocatalysis

TiO_2 P25 has been studied extensively over the years, including its use in environmental aspects such as wastewater treatment, exhaust gases conversion, air purification as well as in energy application, such as hydrogen production, CO_2 reduction and etc. Because of its superior catalytic properties resulted from the mixing of rutile and anatase, TiO_2 P25 (Degussa) represents the benchmark among all these materials for photocatalytic applications [1-3]. It exhibits unsurpassed photocatalytic activity under ultraviolet light due to its wide bandgap of 3.2 eV [4-6]. One can see from Figure 2.1 that the conduction band energy increase in the space charge layer of anatase stops the electrons going from anatase to rutile, but the holes in anatase particles can be transferred to rutile particles. These concepts provide one possibility of P25's intrinsic charge separation resulting in high photocatalytic activity.

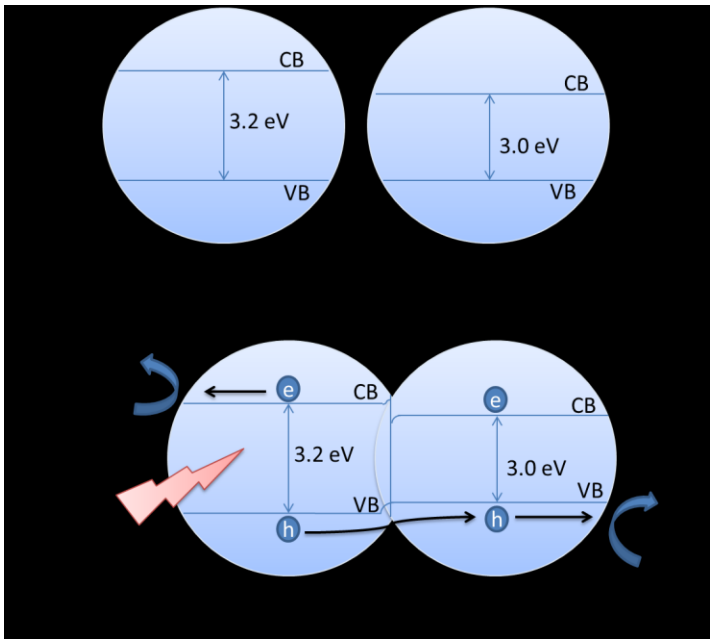

Fig. 2.1 Proposed mechanism of electron-hole separation in P25 during photocatalysis

2.2 Experimental strategy

The initial goal of my thesis study was to develop a series of catalysts using various synthesis methods to optimize the catalytic activity for reduction/oxidation (redox) reactions. One major task was to modify semiconductor system with noble metal particles in order to increase the catalytic efficiency. The project involved synthesis of noble metal modified photocatalysts, which utilized Au, Pt and Pd deposited on TiO_2. Preliminary Density Functional Theory (DFT) calculations by our collaborators (Yan Li et al) indicated that the geometry and size of the metal particles (before deposition) can have a profound effect on their optical absorption and therefore on catalytic activity. Thus, further optimization of the synthetic procedure to produce optimal size and shape of the metal particles to achieve the highest catalytic activity was conducted. Additionally, the project was also focused on application of novel nanostructured materials for environmental photocatalysis. The rationale for utilizing these materials is based on their high surface areas and unique light trapping properties, which can potentially enhance photocatalytic activity. More specifically, SBA-15 mesoporous sieves and inverse opal structured titania were employed as naostructured material supports for catalysis. All catalysts were characterized by various techniques, including spectroscopic, microscopy techniques and chromatography techniques. A comprehensive combination of these techniques was able to provide a valuable feedback for both synthesis and catalytic evaluation.

2.3 Noble metal modified titania

This project was focused on modifying semiconductor surfaces with noble metal nanoparticles by depositing synthesized metal particles on semiconductor supports. Sub-nanometer size metal nanoparticles were first synthesized in this project to explore metal-semiconductor (or metal – non-metal) transitions, which can occur in this size-range. It was expected that this strategy might produce the most significant enhancement of photocatalytic activity in both the UV and visible regions due to the appearance of the HOMO-LUMO gap in metal particles leading to a change in photocatalytic mechanism of oxidation reaction, perhaps not necessarily dissimilar to that observed in semiconductor-semiconductor systems (co-catalysts). Additionally, it may decrease electron-hole recombination rate and promote oxidation activation. In this way, one can have dramatic improvement of quantum efficiency of the catalytic reaction. By systematically varying the particle size and shape of the metals, system's performance can be further optimized. Several synthetic strategies to produce nanoparticles below 1 nm size with lower geometry and exceptional stability toward agglomeration are described in this dissertation.

It is very important to point out that the deposited noble metal nanoparticless do not process photocatalytic activity. They only work in synergy with the semiconductor. One experiment which using Au modified SiO2 to facilitate photocatalytic phenol oxidation has been conducted to prove the above mentioned point. As expected, SiO2 itself does not have any photocatalytic activity under UV light and even after modified with Au metal nanoparticles, the catalytic activity of Au-SiO2 for phenol oxidation is still negligible (< 1%).

2.3.1 Gold nanoparticles synthesis and catalytic properties

Although gold is considered to be one of the most studied metals, it has

been long considered as inert noble materials with very limited applications in catalysis [7]. Several recent developments in gold nanoparticles (AuNPs) synthesis and applications have led to discovery of highly unusual magnetic, optical and catalytic properties [2, 8-15].

Physicists predicted that nanoparticles with size ranging from 1 to 10 nm would show electronic properties which are quite different from those of bulk materials. The reason is that these nanoparticles reflect a discrete electronic band structure, as described by quantum-mechanical rules. When gold particles are above 10 nm in size, they show chemical inertness and are often regarded as a poor catalysts [16]. However, when gold particle are below 10 nm in size, they become very active for many catalytic reactions [8]. Studies of gold clusters ranging from 1-10 nm showed unusual properties in the low-temperature catalytic oxidation of carbon [17, 18]. Scanning tunnelling microscopy and elevated pressure kinetic measurements demonstrate that the structure sensitivity of this reaction on gold clusters was related to a quantum size effect with respect to the thickness of the gold islands [19]. It is suggested that supported clusters may have unusual catalytic properties as one dimension of the cluster becomes smaller. It is important to mention that the properties of sub- nm particles for photocatalytic applications are not known. This project is aimed at addressing this knowledge gap by using new methods of nanoparticle synthesis and photocatalytic testing.

The new properties of Au nanoparticels in the size range between 1-10 nm have been first discovered in 2004 [20]. This first study demonstrated that Au nanoparticles can be extremely active photocatalysts for environmental application. It was then reported a significant increase in photocatalytic efficiency for oxidation of various organic compounds can be achieved by TiO_2 modification with gold nanoparticles [21]. A possible reason for such improvement is the reduction of work function of TiO_2 surface at Au-TiO_2 interface, therefore facilitating electron transfer to O_2, which is often viewed as a rate limiting step in photocatalytic reactions. In the results obtained in this project, we have produced our own Au-TiO_2 photocatalysts and confirmed the conclusions mentioned above.

Fig. 2.2 shows a difference of TiO_2 photocatalytic efficiencies with or without gold nanoparticles deposition, showing almost doubling oh photocatalytic activity of TiO_2 decorated with the Au nanoparticles of the average size of 3.6 nm.

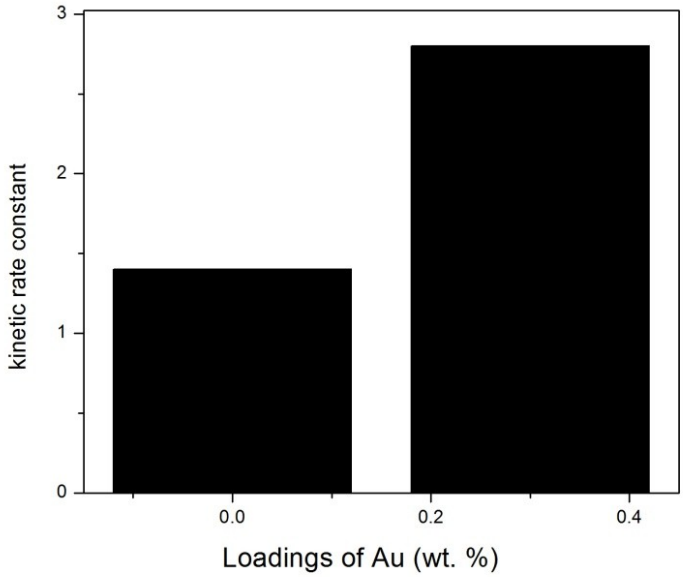

Fig. 2.2 Activity Contrast between TiO_2 with and without Au loading

Among all these conventional methods for synthesizing the Au nanoparticles by reduction of gold (III) derivatives, the most significant one is the reduction of $HAuCl_4$ in water with citrate, which was first introduced by Turkevitch in 1951 [22]. The subsequent attempts by Frens in 1973 developed a procedure of controlling the AuNPs size (between 16 and 147 nm) by combination of the reducing and stabilizing agents [23]. Another important contribution to the field of synthesis of gold nanoparticles was done by Schmidt and his co-workers. They claimed that well-defined phosphine-stabilized gold clusters showed the properties of quantum-dot particles, which were different from those of bulk gold [24-26]. More specifically, of the Schmidt's group has synthesized 55 atoms gold cluster precursor stabilized with phosphine ligand,

which has a chemical formula of $[Au_{55}(PPh_3)_{12}Cl_6]$ [27]. Despite a notable progress on synthesis part of AuNPs, only recently sub-nanometer size gold particles have been used for catalytic applications. However, no studies on photocatalytic applications of gold nanoparticles have ever been reported.

2.3.2 Platinum nanoparticles synthesis and catalytic properties

Although the mechanism of photoactivity enhancement of platinum modified TiO_2 is still open to interpretation, there are many results may suggest the platinum clusters has better catalytic efficiency than gold nanoparticles. This phenomenon cannot simply be attributed to the transfer of electrons to Pt. Other factors influencing the photocatalytic activity might be taken in to consideration such as interaction of Pt with TiO_2 surface, the effect of Pt on chemical state of Ti, energy level, and interfacial charge transfer [28, 29]. In this project, I focused on several unexplored areas of Pt modified TiO_2 catalysis. Firstly, it explores sub-nm range of Pt nanoparticles, which is a new approach to tuning the photocatalytic activity. Secondly, this work focuses on both gas phase and liquid phase oxidation reaction to assess the enhancement effect of Pt for two distinctly different photocatalytic systems. Thirdly it concentrates on Pt nanoparticles of flat geometry following the recent developments by Cuenya et al [30, 31], which is a completely unexplored approach in photocatalytic area. Fourthly, it assesses the advantages of sub-nm particles versus the larger ones for two different reactions.

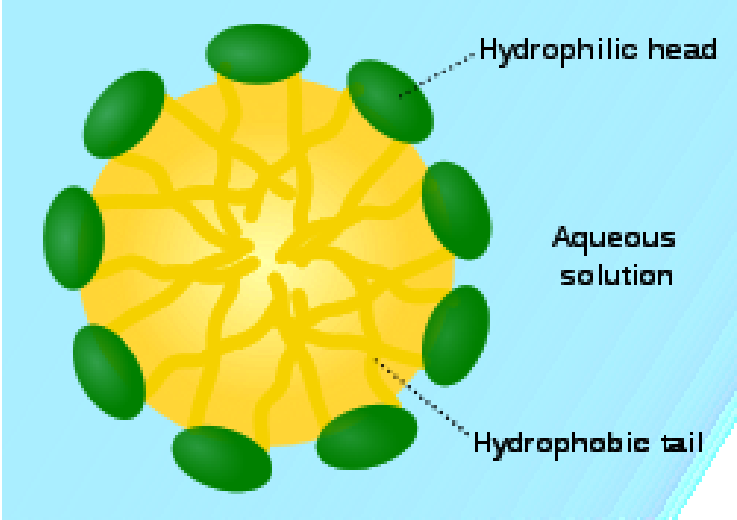

Fig. 2.3 Scheme of a micelle formed by polymer in aqueous solution

These catalysts were prepared by a heterogeneous photocatalytic deposition of platinum on semiconductor support. This unique and simple method of preparation produces finely dispersed metal nanoparticles which were further utilized in photocatalytic reaction.

2.4 Photonic crystal titania

One of the recent strategies to achieve a significant breakthrough in optical industry is to tailor the structures of porous materials to achieve brand new optical properties. A notable example of such approach is fabrication of photonic crystals. Photonic crystals are three-dimensional periodic dielectric composites with lattice parameters on the order of the wavelength of light. More specifically, photonic crystals consist of repeating internal regions of high and low dielectric constant. Wavelengths of light that are allowed to travel are called modes, and groups of allowed modes can form bands. Forbidden bands of wavelengths are named photonic band gaps (PBG) [32]. Photonic crystals are especially useful to achieve a PBG that allow the control of spontaneous emission and the localization of photons [33, 34].

The PBG can be defined as the range of frequencies in which light cannot propagate through the photonic crystal structure. Therefore, the porous structured crystal can form a kind of perfect optical “insulator,” which can confine light losslessly around sharp bends, in lower index media.

Titanium dioxide can in principal be incorporated into the photonic crystal, for the reason that it combines a high refractive index (about 2.6 at 500 nm wavelength for anatase) with large band gap energy of 3.2 eV and it can be made with high purity. With the photon energy equation,

$$E_{photon} = h * c/\lambda$$

the maximum wavelength needed is calculated as follows.

$$\lambda_{max} = h * \frac{c}{E} = \frac{6.6260 \times 10^{-34} J * S \times 3 \times 10^{8} m/s}{3.2 eV \times 1.6021 \times 10^{-19} j/eV} \times \frac{10^{9} nm}{m} = 388\ nm$$

where the λ is wavelength, c is light speed, h is the Planck's constant and E is the energy of the photon. Since the maximum wavelength is at near UV region, UV light was chosen to be the testing light region in this project.

Many methods for synthesis of three-dimensional photonic crystals which can be active under the visible light range have been proposed. 3-D inverse opal titania or Photonic Crystals (PC) are fabricated by many methods. Nanomachining, lithography, chemical vapor deposition (CVD) and 3-D holography are a few of the most commonly used however each of these methods has their own deficiencies [35, 36].

In this project, microscope slides and Si wafer were used as the templates while liquid phase chemical reaction and vapor deposition were both used to fabricate the 3D photonic crystals.

2.5 Titania modified mesoporous (SBA-15) materials

TiO_2 is widely used in the field of photocatalyst for a wide range of applications. However, increasing photocatalytic activity by increasing the illuminated surface area of TiO_2 is a viable strategy to achieve a better performance of TiO_2. The strategies of modifying such conventional catalysts with co-catalysts (Au, Pt) and the surfaces with nanostructures (photonic structure) can be further enhanced by dispersing the catalysts on high surface area materials, such as mesoporous materials. Such inorganic porous materials are the desirable supports for the heterogeneous catalysts due to their highly thermal and chemical stability [37]. In addition to stability they can also provide additional benefits resulting from: (1) very high surface area and adsorption capacity to mediate the surface reactions; (2) tailored adsorption properties which can be varied from hydrophobic to hydrophilic type materials; (3) tailored concentration of active sites, such as acid sites that can be generated in the framework; (4) tailored pore sizes of the channels (5-25 nm), in order to control the diffusion of molecules which are interested in.

These high surface area materials have already made a considerable impact on designing and testing of catalytic materials and compared them with industrial catalysis. The earlier generation of the mesoporous materials, such as MCM-41, initiated the development of similar new molecular sieves with various structures and pore diameters. The advantages of such materials, as compared to disordered amorphous silica, are relatively uniform pore sizes and high void volumes and surface areas. The pore sizes of these materials can be tailored depending on the synthesis method used, ranging from about 15 to about 100 Å [38, 39]. The surface area can be extended over 1000 m^2/g, depending on the method of preparation. In order to broaden the applications of such materials to heterogeneous catalysis, the surfaces of such structures can be functionalized with various other co-catalysts, such as Au and Pt. They can be achieved by post-synthesis procedures or by direct synthesis. SBA-15 mesoporous silica is

considered to be one of the most promising supports given their high surface area (800 m^2/g), high thermal stability and large pore sizes (4-10 nm).

Recently, the synthesis and application of silica based ordered mesoporous materials with covalently bonded organic species, either via surface modification, or direct synthesis, have attracted a significant attention. The current work addresses the issues of both synthesis and characterization of SBA-15 materials with the porous size much larger than that of conventional SBA-15 materials. This study is focused on synthesis, characterization and testing of novel SBA-15 materials modified with titania.

The sustainable energy applications of SBA-15 modified with titanium have only recently become a topic of substantial interest, especially in photocatalytic applications. A lot of preliminary work has already been done on modification of mesoporous materials with Ti and Mn [40, 41]. This project will focus on modification of the SBA-15 mesoporous molecular sieve with photocatalysts, which will be achieved by using four different methods: (1) impregnation; (2) modification with colloidal titania.

2.6 Conclusion

Photocatalytic reaction is a promising technology for pollution remediation of contaminated water and air. This project is primarily focused on the following strategies:

(1) Developing photocatalysts capable of reduction/oxidation reactions under visible/ UV light radiation;

(2) Increasing the surface area of photocatalysts by dispersing them on mesoporous supports;

(3) Reducing electron-hole recombination rate by modifying the catalyst with metal nanoparticles;

(4) Increasing the intensity of light reaching the surface of the catalyst by trapping the light in photonic crystal structures.

(5) Using comprehensive range of analytical techniques for the catalytic activity testing and materials characterization.

The previous assumptions indicate that it would be possible to transform metallic particles into particles exhibiting HOMO-LUMO separation by reducing their sizes to sub-nm dimensions. By systematically investigating the activity as a function of particle size, we can manipulate the bandgaps (or more precisely HOMO-LUMO separation) of nanoparticles to optimize the charge separation and therefore the activity in such semiconductor-semiconductor systems. Literature indicates that such metals as Au, Pt, and Pd exhibit the most promising size-dependent effects that can be utilized in photocatalytic reactions. Based on some of the latest publications, we expect that the strongest size dependence will be observed by Au and Pt followed by Pd nanoparticles.[42] Therefore this project initially concentrated on Au, Pt, Pd nanoparticles, which can not only be used as single metal but can also be combined into bi-metallic systems (Au-Pt, Au-Pd and Pt-Pd). This work also focused on how to deposit nanoparticles on the surface and subsequently remove the protecting organic ligands and surfactants. Furthermore, this project expanded the existing experimental approach by modifying the shape of the nanoparticles, given that two dimensional nanoparticles can potentially lead to a dramatic increase in activity for oxidation/reduction reactions. A manipulation of nanoparticle shape can be achieved by following the procedures described by Cuenya *et al [43].*

Increasing the photocatalytic efficiency of materials by dispersing them on high surface area supports has been also utilized in this project, achieving higher catalytic activities of the catalysts as compared to unmodified ones.

Reference:

[1] A. Hagfeldt, M. Gratzel, Light-Induced Redox Reactions in Nanocrystalline Systems, Chem Rev, 95 (1995) 49-68.

[2] M.R. Hoffmann, S.T. Martin, W.Y. Choi, D.W. Bahnemann, Environmental Applications of Semiconductor Photocatalysis, Chem Rev, 95 (1995) 69-96.

[3] M.A. Fox, M.T. Dulay, Heterogeneous Photocatalysis, Chem Rev, 93 (1993) 341-357.

[4] H. Tang, H. Berger, P.E. Schmid, F. Levy, G. Burri, Photoluminescence in Tio2 Anatase Single-Crystals, Solid State Commun, 87 (1993) 847-850.

[5] H. Tang, K. Prasad, R. Sanjines, P.E. Schmid, F. Levy, Electrical and Optical-Properties of Tio2 Anatase Thin-Films, J Appl Phys, 75 (1994) 2042-2047.

[6] D.C. Hurum, A.G. Agrios, K.A. Gray, T. Rajh, M.C. Thurnauer, Explaining the enhanced photocatalytic activity of Degussa P25 mixed-phase TiO2 using EPR, J Phys Chem B, 107 (2003) 4545-4549.

[7] M.C. Daniel, D. Astruc, Gold nanoparticles: Assembly, supramolecular chemistry, quantum-size-related properties, and applications toward biology, catalysis, and nanotechnology, Chem Rev, 104 (2004) 293-346.

[8] M. Haruta, Size- and support-dependency in the catalysis of gold, Catal Today, 36 (1997) 153-166.

[9] D. Thompson, New advances in gold catalysis part I, Gold Bull, 31 (1998) 111-118.

[10] G.C. Bond, D.T. Thompson, Gold-catalysed oxidation of carbon monoxide, Gold Bull, 33 (2000) 41-51.

[11] M. Haruta, Catalysis of gold nanoparticles deposited on metal oxides, Cattech, 6 (2002) 102-115.

[12] G.J. Hutchings, Gold catalysis in chemical processing, Catal Today, 72 (2002) 11-17.

[13] P. Mukherjee, C.R. Patra, A. Ghosh, R. Kumar, M. Sastry, Characterization and catalytic activity of gold nanoparticles synthesized by autoreduction of

aqueous chloroaurate ions with fumed silica, Chem Mater, 14 (2002) 1678-1684.
[14] Catalysts: golden opportunities, Tce-the Chem Eng, (2004) 34-36.
[15] D.T. Thompson, Catalysis by Gold/Platinum Group Metals MIXED METAL SYSTEMS DISPLAYING INCREASED ACTIVITY, Platin Met Rev, 48 (2004) 169-172.
[16] M. Brust, C.J. Kiely, Some recent advances in nanostructure preparation from gold and silver particles: a short topical review, Colloid Surface A, 202 (2002) 175-186.
[17] M. Valden, X. Lai, D.W. Goodman, Onset of catalytic activity of gold clusters on titania with the appearance of nonmetallic properties, Science, 281 (1998) 1647-1650.
[18] M. Valden, S. Pak, X. Lai, D.W. Goodman, Structure sensitivity of CO oxidation over model Au/TiO2 catalysts, Catal Lett, 56 (1998) 7-10.
[19] X. Lai, T.P. St Clair, M. Valden, D.W. Goodman, Scanning tunneling microscopy studies of metal clusters supported on TiO2 (110): Morphology and electronic structure, Prog Surf Sci, 59 (1998) 25-52.
[20] A. Orlov, D.A. Jefferson, N. Macleod, R.M. Lambert, Photocatalytic properties of TiO2 modified with gold nanoparticles in the degradation of 4-chlorophenol in aqueous solution, Catal Lett, 92 (2004) 41-47.
[21] A. Orlov, D.A. Jefferson, M. Tikhov, R.M. Lambert, Enhancement of MTBE photocatalytic degradation by modification of TiO2 with gold nanoparticles, Catal Commun, 8 (2007) 821-824.
[22] J. Turkevich, P.C. Stevenson, J. Hillier, A Study of the Nucleation and Growth Processes in the Synthesis of Colloidal Gold, Discuss Faraday Soc, (1951) 55-&.
[23] G. Frens, Controlled Nucleation for Regulation of Particle-Size in Monodisperse Gold Suspensions, Nature-Phys Sci, 241 (1973) 20-22.
[24] G. Schmid, M. Baumle, M. Geerkens, I. Helm, C. Osemann, T. Sawitowski, Current and future applications of nanoclusters, Chem Soc Rev, 28 (1999) 179-185.
[25] G. Schmid, B. Corain, Nanoparticulated gold: Syntheses, structures, electronics, and reactivities, Eur J Inorg Chem, (2003) 3081-3098.

[26] H.J. Zhang, G. Schmid, U. Hartmann, Reduced metallic properties of ligand-stabilized small metal clusters, Nano Lett, 3 (2003) 305-307.

[27] G. Schmid, N. Klein, L. Korste, U. Kreibig, D. Schonauer, Large Transition-Metal Clusters .6. Ligand-Exchange Reactions on Au55(Pph3)12cl6 - the Formation of a Water-Soluble Au55 Cluster, Polyhedron, 7 (1988) 605-608.

[28] H. Alekabi, N. Serpone, E. Pelizzetti, C. Minero, M.A. Fox, R.B. Draper, Kinetic-Studies in Heterogeneous Photocatalysis .2. Tio2-Mediated Degradation of 4-Chlorophenol Alone and in a 3-Component Mixture of 4-Chlorophenol, 2,4-Dichlorophenol, and 2,4,5-Trichlorophenol in Air-Equilibrated Aqueous-Media, Langmuir, 5 (1989) 250-255.

[29] J.C. Yang, Y.C. Kim, Y.G. Shul, C.H. Shin, T.K. Lee, Characterization of photoreduced Pt/TiO2 and decomposition of dichloroacetic acid over photoreduced Pt/TiO2 catalysts, Appl Surf Sci, 121 (1997) 525-529.

[30] S. Mostafa, F. Behafarid, J.R. Croy, L.K. Ono, L. Li, J.C. Yang, A.I. Frenkel, B.R. Cuenya, Shape-Dependent Catalytic Properties of Pt Nanoparticles, J Am Chem Soc, 132 (2010) 15714-15719.

[31] B.R. Cuenya, J.R. Croy, S. Mostafa, F. Behafarid, L. Li, Z.F. Zhang, J.C. Yang, Q. Wang, A.I. Frenkel, Solving the Structure of Size-Selected Pt Nanocatalysts Synthesized by Inverse Micelle Encapsulation, J Am Chem Soc, 132 (2010) 8747-8756.

[32] S.L. Kuai, X.F. Hu, V.V. Truong, Synthesis of thin film titania photonic crystals through a dip-infiltrating sol-gel process, J Cryst Growth, 259 (2003) 404-410.

[33] E. Yablonovitch, Inhibited Spontaneous Emission in Solid-State Physics and Electronics, Phys Rev Lett, 58 (1987) 2059-2062.

[34] S. John, Strong Localization of Photons in Certain Disordered Dielectric Superlattices, Phys Rev Lett, 58 (1987) 2486-2489.

[35] I. Sakellari, A. Gaidukeviciute, A. Giakoumaki, D. Gray, C. Fotakis, M. Farsari, M. Vamvakaki, C. Reinhardt, A. Ovsianikov, B.N. Chichkov, Two-photon polymerization of titanium-containing sol-gel composites for three-dimensional structure fabrication, Appl Phys a-Mater, 100 (2010) 359-364.

[36] J.G. Fleming, S.Y. Lin, Three-dimensional photonic crystal with a stop band

from 1.35 to 1.95 mu m, Opt Lett, 24 (1999) 49-51.

[37] L. Li, J.L. Shi, J.N. Yan, H.G. Chen, X.G. Zhao, SBA-15 supported quaternary ammonium salt: an efficient, heterogeneous phase-transfer catalyst, J Mol Catal a-Chem, 209 (2004) 227-230.

[38] B.J. Aronson, C.F. Blanford, A. Stein, Solution-phase grafting of titanium dioxide onto the pore surface of mesoporous silicates: Synthesis and structural characterization, Chem Mater, 9 (1997) 2842-2851.

[39] Y.M. Xu, C.H. Langford, Photoactivity of titanium dioxide supported on MCM41, zeolite X, and zeolite Y, J Phys Chem B, 101 (1997) 3115-3121.

[40] A. Orlov, Q.Z. Zhai, J. Klinowski, Photocatalytic properties of the SBA-15 mesoporous silica molecular sieve modified with titanium, J Mater Sci, 41 (2006) 2187-2193.

[41] A. Orlov, J. Klinowski, Oxidation of volatile organic compounds on SBA-15 mesoporous molecular sieves modified with manganese, Chemosphere, 74 (2009) 344-348.

[42] J.K. Norskov, T. Bligaard, B. Hvolbaek, F. Abild-Pedersen, I. Chorkendorff, C.H. Christensen, The nature of the active site in heterogeneous metal catalysis, Chem Soc Rev, 37 (2008) 2163-2171.

[43] B.R. Cuenya, A.I. Frenkel, S. Mostafa, F. Behafarid, J.R. Croy, L.K. Ono, Q. Wang, Anomalous lattice dynamics and thermal properties of supported size- and shape-selected Pt nanoparticles, Phys Rev B, 82 (2010).

Chapter 3. Experimental Methods for photocatalysts study

3.1 Experimental techniques

This chapter describes experimental methods used for the characterization of photocatalysts, such as Transmission Electron Microscopy (TEM), Diffuse Reflectance Infrared Fourier Transform Spectroscopy (DRIFTS), Ultraviolet-visible spectroscopy and Matrix-assisted Laser Desorption/Ionization (MALDI). These techniques were used to examine the gold modified TiO_2 samples. For Inverse opal TiO_2 project, the experimental techniques included X-ray diffraction (XRD), Scanning electron microscope (SEM), Ultraviolet-visible spectroscopy and DRIFTS. The photocatalytic testing was done for both liquid and gas phase reactions, such as oxidation of phenol and NO_2 oxidation in liquid gas and phases respectively.

3.1.1 X-ray diffraction (XRD)

W.H. Bragg was first proposed an equation in 1913 to explain the relationship between the crystal planes which appear to reflect X-ray beams and the angles of incidence (theta).

$$\mathbf{n\lambda = 2dsin\theta}$$

This phenomenon is caused by X-ray wave interference, which now known as X-ray diffraction (XRD). It has later been proved as the evidence for the periodic atomic structure of crystals [1].

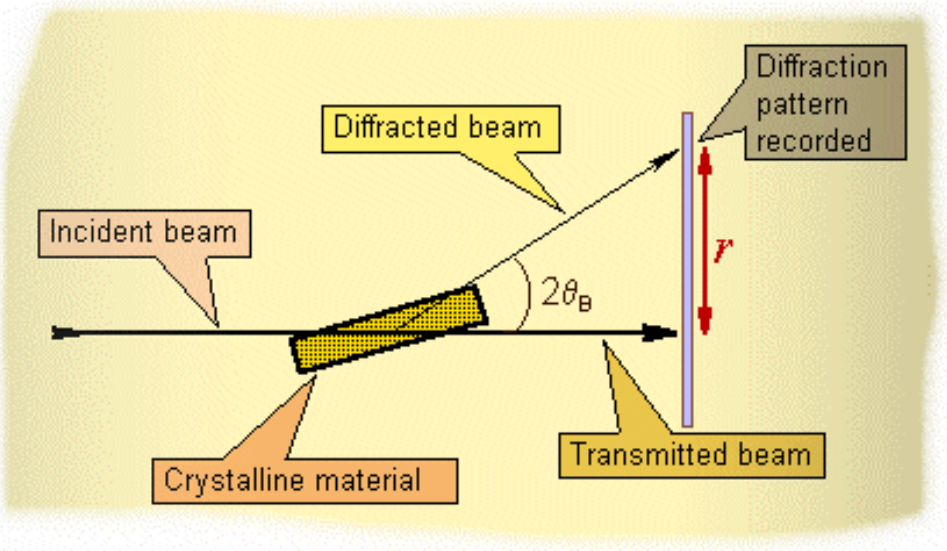

Fig. 3.1 Diagram of XRD system

A crystal has the atomic planes which can cause an incident beam of X-rays to interfere with one another when they leave the crystal. This phenomenon, which known as X-ray diffraction, can in principle:

1. measure the average spacing between layers of the atoms (d-spacing);
2. determine the orientation of a single crystal or grain;
3. discover the crystal structure for unknown materials;
4. calculate the size, shape and internal stress of a small region of the crystal

The most important use of XRD is to obtain the XRD pattern and compare data with known standards in order to identify the sample phase. It is a fast, non-destructive way for phase identification and high accuracy for d-spacing calculations. The technique can be used in single crystals and amorphous materials.

3.1.2 Scanning electron microscope (SEM)

The scanning electron microscope (SEM) is a type of electron microscope that images the sample surface by scanning it with a high-energy beam of electrons in a raster scan pattern. The electrons interact with the atoms that make up the sample producing signals that contain information about the sample's surface topography, composition and other properties such as electrical conductivity [2, 3]. Modern scanning electron microscopes (SEMs) utilize digital scan controls, digital signal acquisition and processing of grayscale digital images. When used in conjunction with the closely-related technique of energy-dispersive X-ray spectroscopy (EDS), the composition of the materials can be easily determined.

Scanning electron microscope usually operates under high vacuum. The basic principle is that the electron beam is generated by a suitable source, normally a field emission gun. The electron beam is accelerated through a high voltage (20 kV) and pass through a series of apertures and electromagnetic lenses to produce a focused beam of electrons. Then the beam scans the surface of the specimen by the scanning coils. Electrons are emitted from the specimen by the action of the scanning beam and collected by a suitably-positioned detector.

As a powerful technique, SEM has been extensively used for imaging new materials, especially at micro and nano scales. SEM is a valuable tool for probing the structure and morphology of such materials. Here we use the SEM to determine the type and orientation of the porous titania.

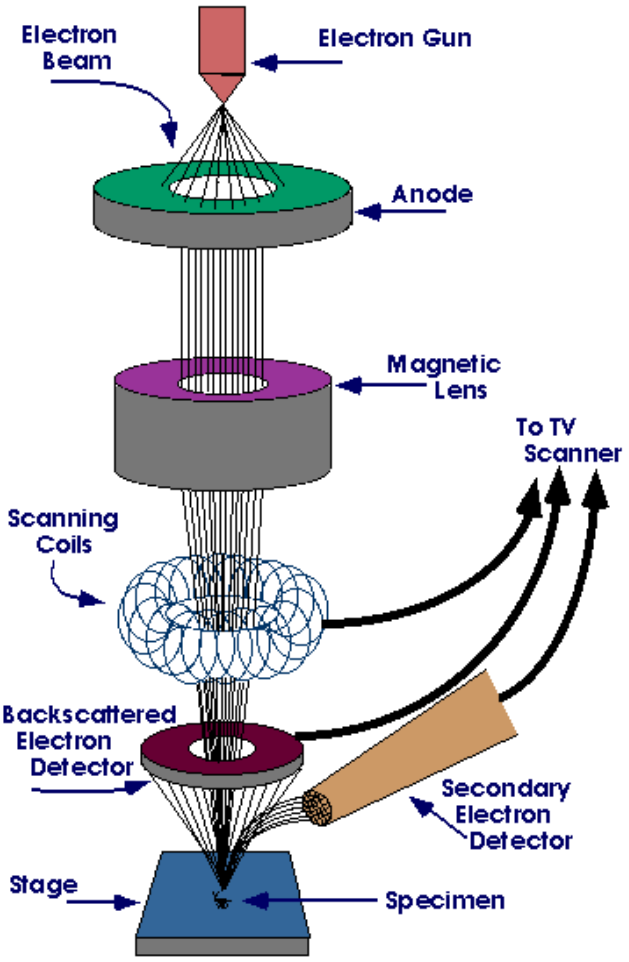

Fig. 3.2 Diagram of the SEM system

3.1.3 Transmission electron microscopy (TEM)

Transmission electron microscopy (TEM) is a microscopy technique where a beam of electrons is transmitted through an ultra thin specimen, interacting with the specimen as it passes through. TEM operates on a similar principle as the light microscope but instead of using light, TEM uses electrons as the source. The reason that TEM can have much better resolution than the regular light

microscope is based on the Rayleigh criterion.

$$\delta = \frac{0.61\lambda}{\mu \sin \beta}$$

where λ is the wavelength of the radiation, μ is the refractive index and β is the semi-angle of collection of the magnifying lens. Because of μ is variable and β is small, the resolution of light microscope is mainly determined by the wavelength of the light source.

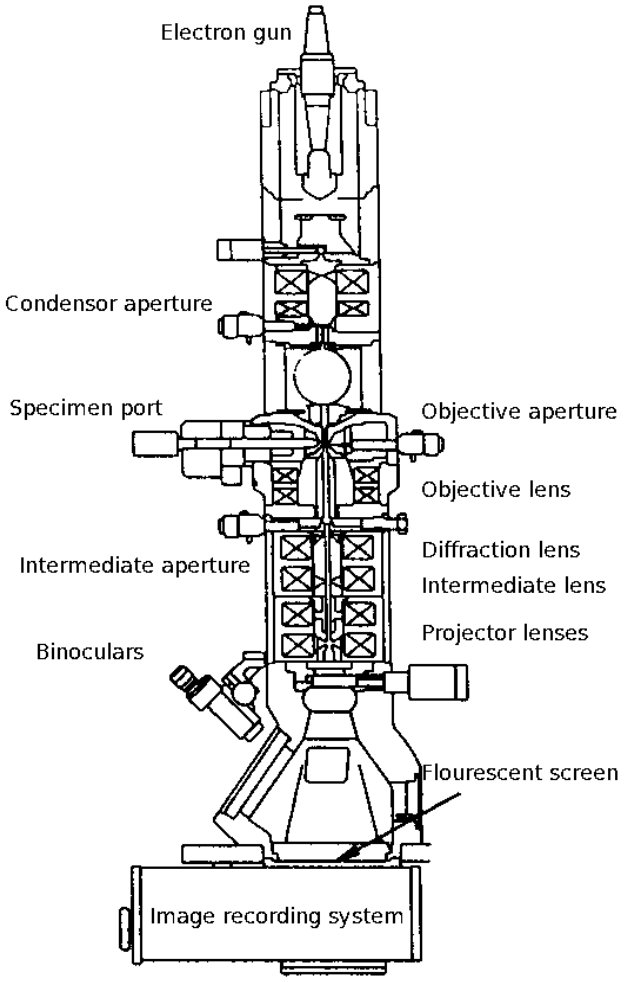

Fig. 3.3 Layout of optical components in a basic TEM

Based on theory of wave-particle duality, we know that electron has some wave-like properties:

$$\lambda = \frac{h}{p}$$

where h is the Planck's constant and p is the momentum of the electron. For regular TEM, the electron is accelerated through a potential of 100 keV, the electron wavelength can be described as:

$$\lambda = \frac{h}{\sqrt{2meU(1 + \frac{eU}{2mc^2})}}$$

The wavelength of the electron under this potential is 0.0037nm. The light microscope has the light source wavelength of 390 to 700 nm. In this regard, the resolution of electron microscope has been improved significantly [4].

The electron gun at the top of the microscope emits the electrons that travel through vacuum in the column of the microscope. The TEM uses electromagnetic lenses to focus the electrons into the focused beam which then travels through the specimen under examination. At the bottom of the microscope the unscattered electrons hit a fluorescent screen, which gives rise to a "shadow image" of the specimen with its different parts displayed in varied darkness according to their density. The image can be studied directly for information like crystal sizes, orientation and lattice parameter.

Two basic modes of TEM operation are used widely. One is the bright-field and the other is the dark-field imaging mode. The bright field mode can directly use the size of the objective aperture to determine the information of the final image. The dark field mode only utilize the light scattered by the sample and

enters the objective lens which makes specimens appear bright and the background is dark [5]. High resolution imaging is usually performed under bright field mode.

3.1.4 Matrix assisted laser desorption ionization/time of flight Mass Spectrometry (MALDI-TOF-MS)

Matrix-assisted laser desorption/ionization (MALDI) is a soft ionization technique used in mass spectrometry, allowing the analysis of biomolecules and large organic molecules, which tend to be fragile and fragment when ionized by more conventional ionization methods [6]. MALDI has the advantages of producing mostly singly charged parent ions so that the spectra are more suitable for mixture analysis [7]. However, the mass resolution of a linear time-of-flight MALDI mass spectrometer is usually low for molecules with a high mass to charge ratio (M/Z) due to the broad energy spread of these large molecules [8].

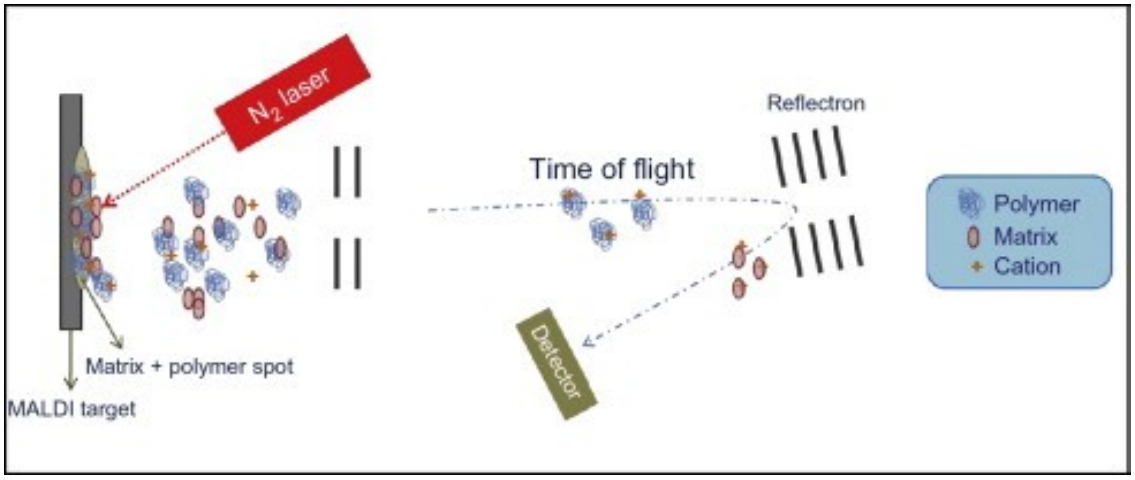

Fig. 3.4 MALDI: Matrix Assisted Laser Desorption Ionization

Sample is mixed with excess matrix (M) and dried on a MALDI plate. Laser flash ionizes matrix molecules. Sample molecules are ionized by particles transfer from matrix:

$$MH^+ + A \rightarrow M + AH^+.$$

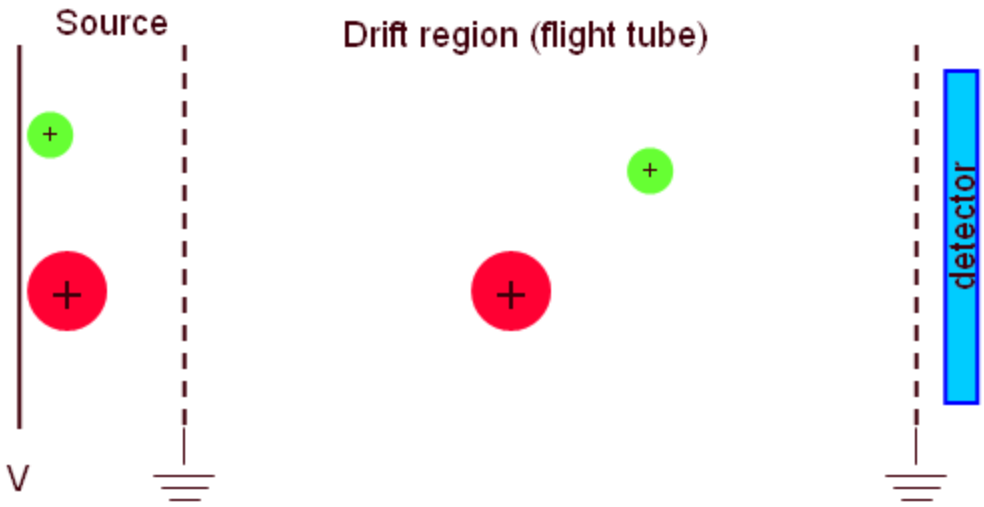

Fig. 3.5 Time-of-flight mass analyzer

In the TOF mass spectrometry, Ions are formed in pulses. Because of that small ions reach the detector before large ones, by measuring the time for ions to reach the detector, we can identify each ion from the sample molecule [9].

3.1.5 Atomic Resolution Scanning Tunneling Microscopy (STM)

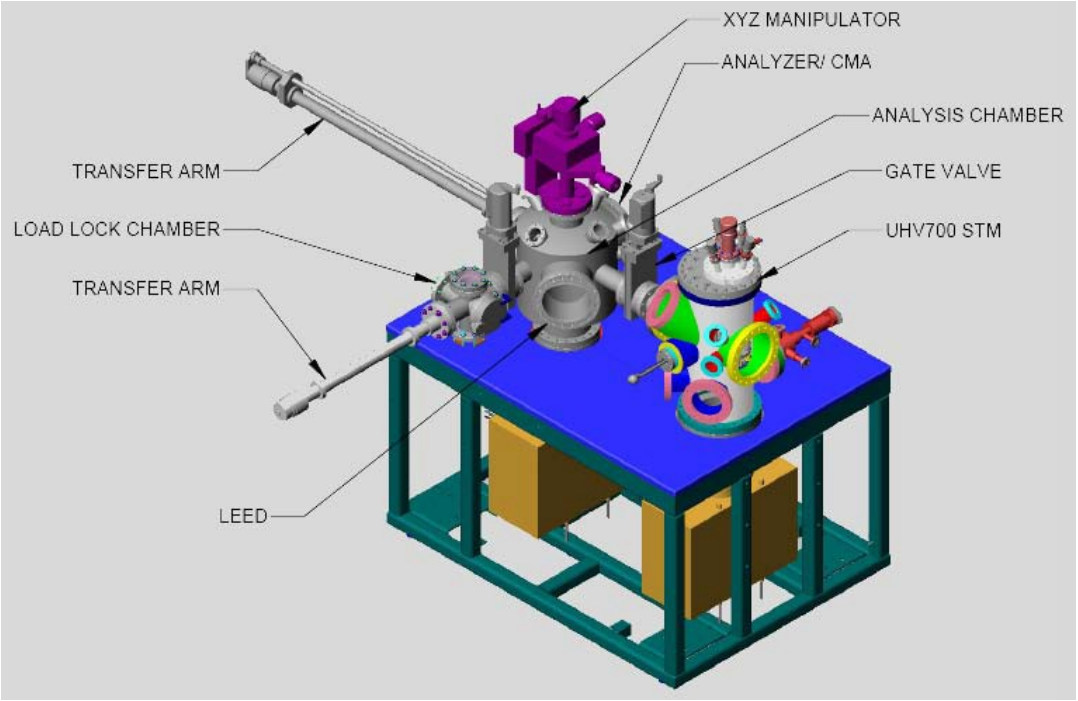

Fig. 3.6 RKH 7500 Variable-Temperature Ultra-High Vacuum Scanning Tunneling Microscope

The study of surfaces is an important part of physics, with particular applications in semiconductor physics and microelectronics. In chemistry, surface reactions also play an important part, for example in catalysis.

A scanning tunneling microscope (STM) is a microscopy instrument that gives 3-D images of the sample surface at atomic resolution. The resolution of the STM can reach 1 Å. The working principle is a conducting probe (tungsten or Pt/Ir tip) is placed very near the sample surface, before a bias (voltage difference) applied between the tip and the sample surface. In this case, electrons can tunnel through the vacuum from one to another. The resulting tunneling current is a determined by tip position, applied voltage, and the local density of state of the sample. Information can be gained by monitoring the current during the process of the tip scanning across the surface, and is usually displayed in 3-D image form. STM sample preparation is very challenging, as it requires extremely clean, conductive and stable crystal surfaces. Also the STM instrument need to be well

maintained for sharp tips, excellent vibration control, and sophisticated electronics [10-12]. The STM works best with conducting materials, but it is also possible to fix organic molecules on a surface and study their structures.

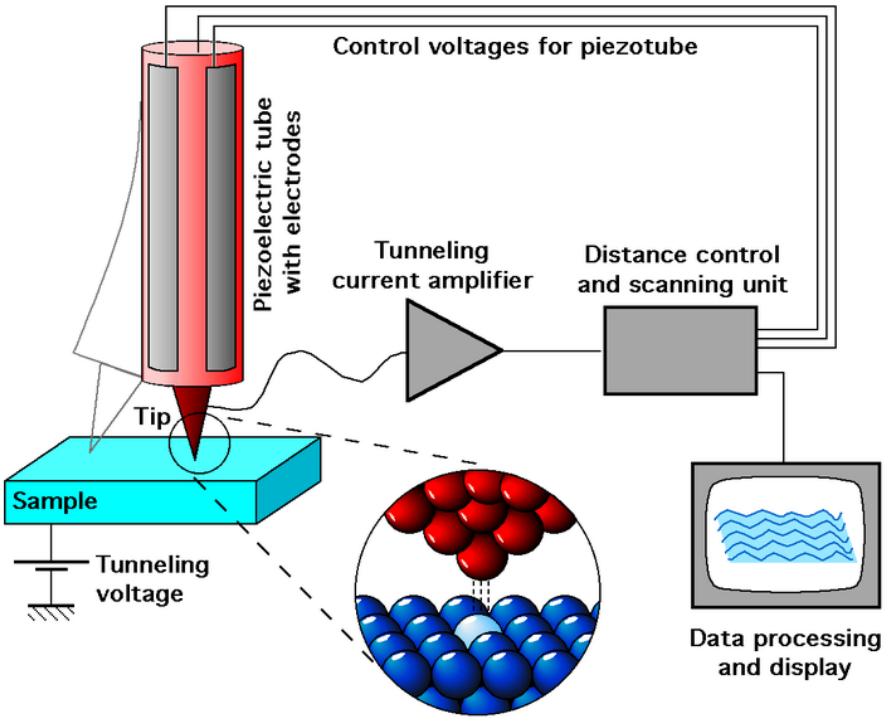

Fig. 3.7 Schematic view of an STM

3.2 Catalysts characterization

3.2.1 Liquid phase reactor

The experiments were done in a custom made 250 ml Pyrex reactor and 8 cm aperture with a quartz lid on top. Water jacket surrounding the reactor was

connected to a refrigerating circulator for which the temperature was set at 10 °C. The Xenon lamp (Model 67005, Newport Inc.) was placed on the top side of the reactor. The spectral region of emission was selected by using optical filters. The light intensity was measured by an Optical power meter (Model 71580, Newport Inc.).

3.2.2 Liquid chromatography

Liquid chromatography was defined in the early 1900s by the work of the Russian botanist, Mikhail S. Tswett. His pioneering studies focused on separating compounds (leaf pigments), extracted from plants using different solvents in a column packed with particles. High performance liquid chromatography (or high pressure liquid chromatography, HPLC) is a form of column chromatography used frequently in biochemistry and analytical chemistry to separate, identify, and quantify compounds based on their idiosyncratic polarities and interactions with the column's stationary phase [13, 14]. HPLC is an advanced form of column chromatography. It utilizes high pressures (100 – 400 atmospheres) to force the solvent through instead of relying on gravity to drip through a column. You can also use a much smaller size for the column packing materials which can give a greater surface area for interactions between the stationary phase and the molecules flowing past it. This allows a much better separation of the components of the mixture.

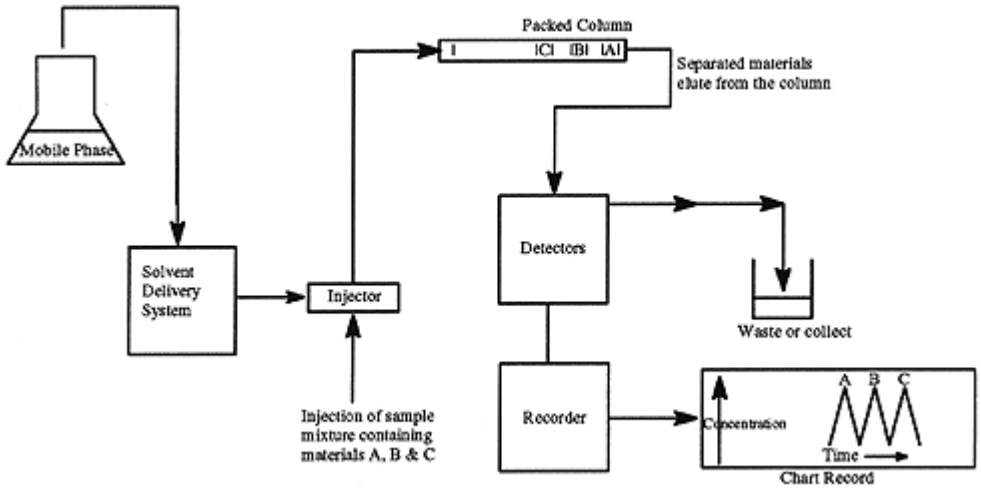

Fig. 3.8 Block diagram showing the components of an HPLC instrument

In 2004, further advances in instrumentation and column technology were made in liquid chromatography in order to achieve significant progress in various factors such as resolution, speed, and sensitivity [15]. Columns with smaller particles (1.7 micron) and instrumentation with specialized capabilities designed to deliver mobile phase at 15,000 psi were needed to achieve a new level of performance. A new system had to be holistically created to perform ultra-performance liquid chromatography, now known as UPLC technology [16]. This provides a glimpse of what we may expect in the future.

In this project, the HPLC system was mainly used for determining the concentration of the organic molecules (phenol) and identifying product molecules (catechol) by using a set of standards. For phenol degradation, the first step is the oxidation of the phenol to catechol. This step was crucial to determine the reaction mechanism of photocatalytic oxidation of phenol. Figure 3.9 shows the chromatogram of the phenol degradation. The phenol peak was integrated and used to determine the concentration of the reactant and the catechol peak is for determining the concentration of the product.

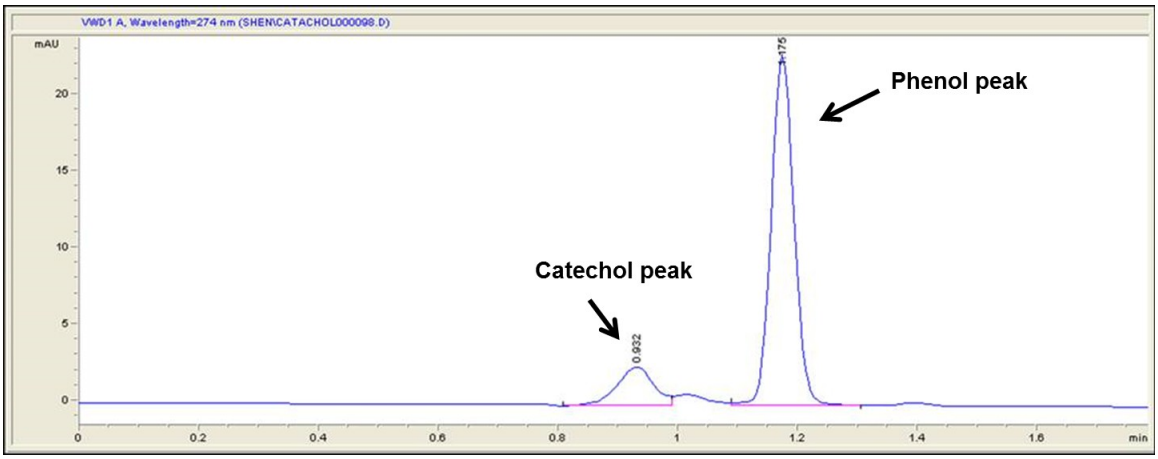

Fig. 3.9 chromatogram of the phenol degradation reaction

3.2.3 Diffuse reflectance infrared Fourier transform spectroscopy (DRIFTS)

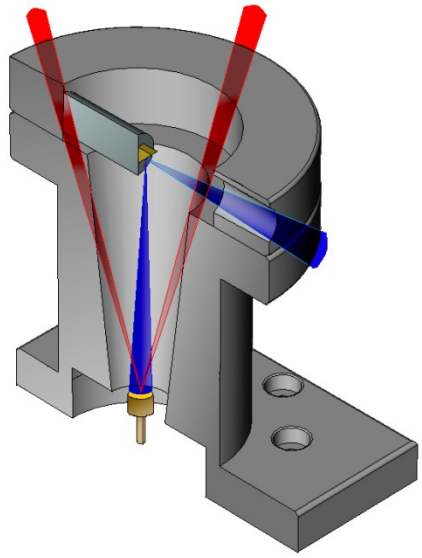

Fig 3.10 DRIFT Cell sketch

Diffuse reflectance infrared Fourier transform spectroscopy is a technique that collects and analyzes scattered IR energy. It is used for analysis of fine particles, powder sand films [17].

When the beam of IR enters the sample, it can be either reflected off the surface or transmitted through the sample. The beam that reflects off the surface is typically lost. The beam that passes through a particle can either be reflected by the next particle or be transmitted through the next particle again. This phenomenon of transmission-reflectance can occur many times in the sample. Finally, all scattered IR light is collected by a spherical mirror which is focused onto the IR detector. Because of the detected IR light is partially absorbed by the particles of the sample surface, it carries the information of the sample under IR region [18].

Our system is based on Nicolet 6700 FTIR equipped with Smart Collector. The Smart Collector also contains environmental chamber, which gives a capability to conduct the in-situ experiments under the controlled temperature and pressure. In our project, we have modified the DRIFTS unit to deliver the UV light to the surface of the samples (Figure 3.11). This arrangement gives us a unique capability to study the photocatalytic reaction using DRIFTS. The output of the chamber is connected to NO_X chemiluminescent analyzer, which can monitor the gas phase composition.

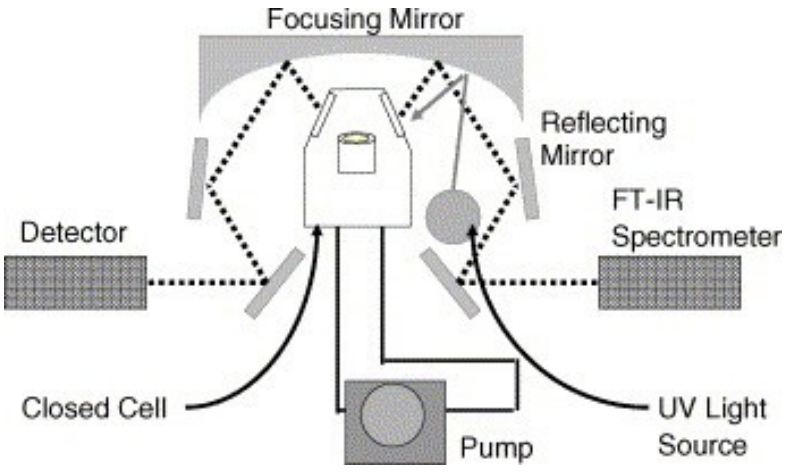

Fig. 3.11 Schematic diagram of DRIFTS cell [19]

3.3 Catalytic testing

3.3.1 Liquid Phase testing

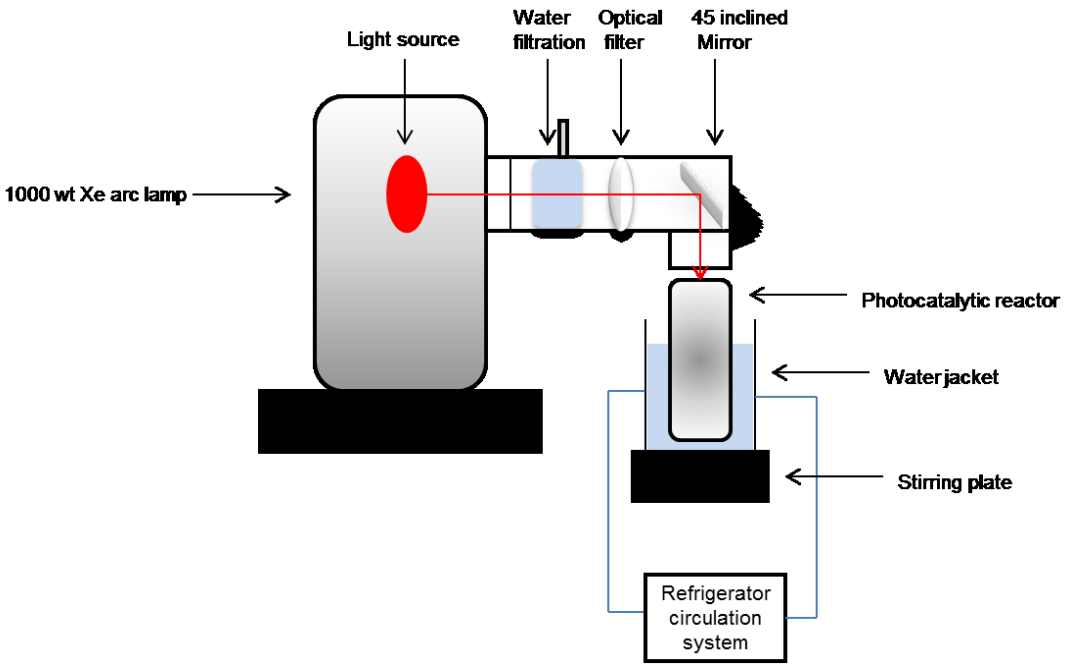

Fig. 3.12 Schematic diagram of liquid phase photocalytic reactor

The experiments were done in a custom made 250 ml Pyrex reactor with a quartz lid and water jack surrounded in a constant temperature of 10 °C. The solution was continuously stirred during the whole procedure. The catalyst was exposed to Xenon lamp (Newport Model 67005) providing radiation range from 200 nm up to 2500 nm. Optical filters were used to select the optical range from 255 nm above. 200 ml (20 mg/L) of phenol aqueous solution was added into the reactor. Then 200 mg of different catalysts samples were introduced into the

solution. Initially the solution was stirred under darkness for 30 min to eliminate the adsorption effect. Samples were periodically withdrawn from the solution, filtered through 0.45 um membrane and transfer to HPLC vials for further analysis. The analysis was done in HPLC, Agilent 1200 which determines the concentration of the phenol. The phenol conversion rates (C/Co) were calculated and plotted with duration time (hrs). The trend line of these dots would have an exponential fitting and gives an equation of

$$y = e^{-kx}$$

In this equation, k stands for the first order rate constant of the phenol degradation reactions which was often used as the indication of determining the efficiency of the catalysts. Fig 3.13 illustrates this reaction using benchmark photocatalysts TiO_2 P25 and the rate constant is 0.161. In this thesis, this rate constant would be often used as the baseline for comparison of other developed novel catalysts.

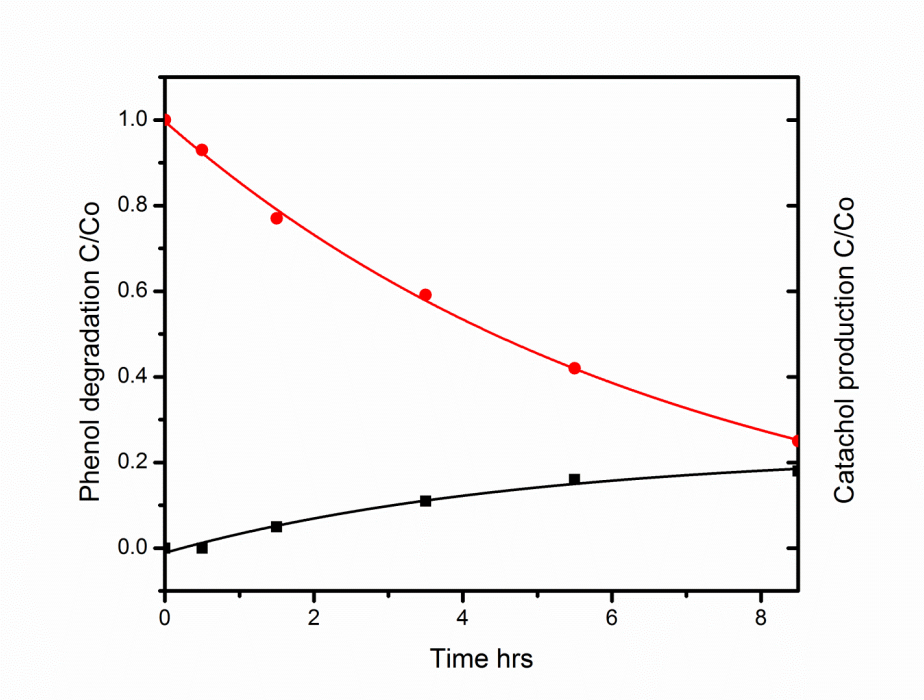

Fig. 3.13 Time dependence of phenol degradation and catachol production of TiO_2 P25

3.3.2 Gas Phase testing

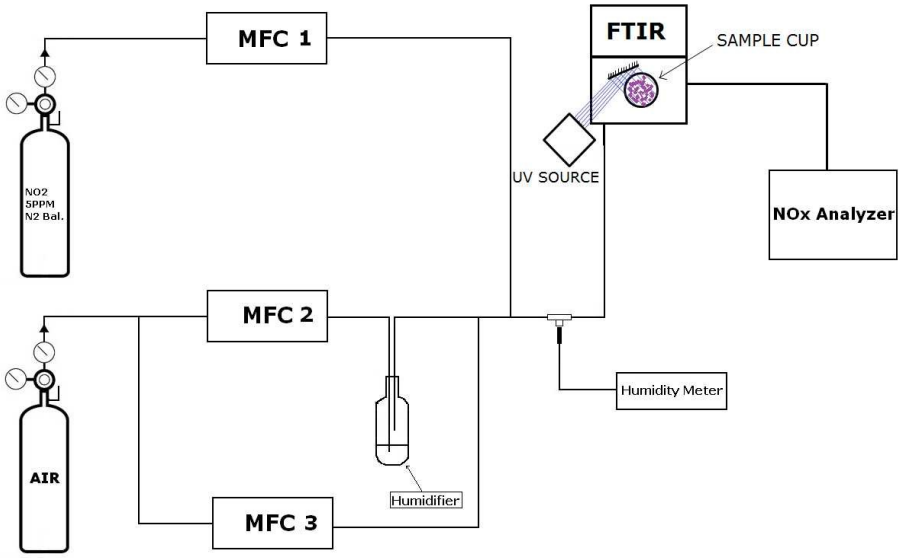

Fig. 3.14 DRIFTS setup for the gas phase catalytic testing

Modified TiO_2 catalysts were loaded on the cup in the environmental chamber with humid air (90-95% RH) at 10 sccm flowing for 12-16 hrs to saturate the catalysts surface with moisture. Before starting the NO_2 flow, the IR spectra were taken to use as background to minimize the IR signals related to water adsorption on the surface. NO_2 at 20 sccm was then allowed to flow. This caused the humidity to stabilize at about 30-35%. We believe that the photocatalytic oxidation reaction is partly governed by the generation hydroxyl radicals formed when the water adsorbed on the surface reacts with positively charged holes. These radicals subsequently react with the pollutants there by oxidizing. While the absence of moisture results in very low photocatalytic activity an excess of it can actually lead to decrease in activity due to establishing a diffusion barrier to NO_2 molecules. However, it is also possible that NO_2 can be dissolved in liquid water layer and form NO_3^- which can subsequently react with charges of hydroxyl

radicals generated by photocatalysts. The initial concentration of the NO_2 in the cylinder was 4.82 ppm. After adjusting the concentration through various dilution steps as shown in Figure 3.14, the final NO_2 concentration in environmental chamber was 3.21 ppm. The IR spectrum was taken continuously during the course of the experiment to monitor the reaction products adsorbed on TiO_2 surface. Once the NO_2 levels stabilized as determined by DRIFTS data, the UV lights were turned on and both the DRIFTS data and NO_X data were monitored simultaneously. The total experiment time was around 36 – 48 hrs.

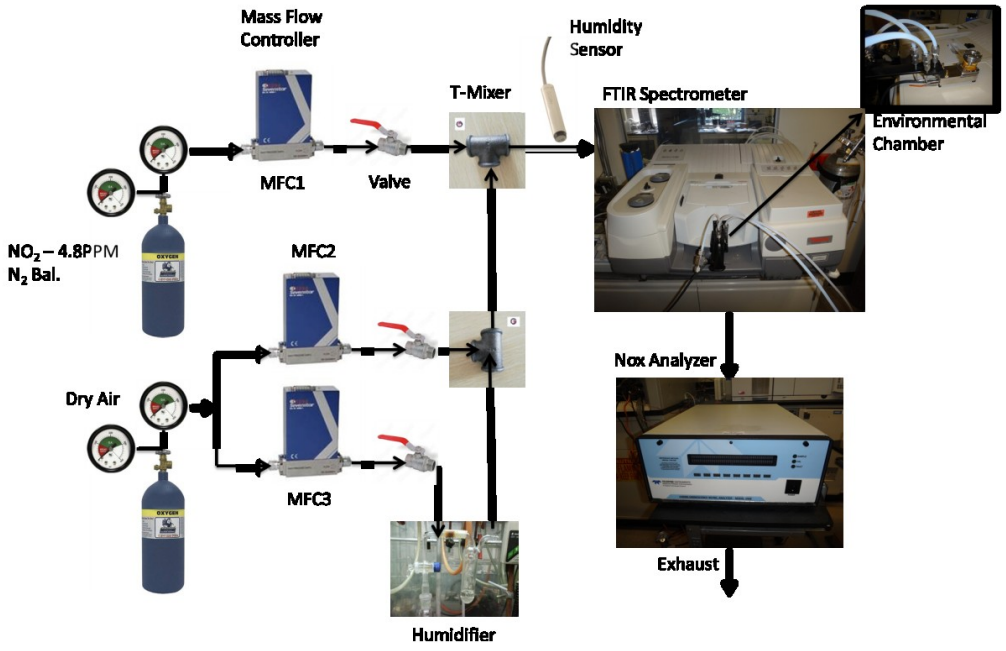

Fig. 3.15 Schematic of custom designed Diffuse Reflectance Fourier Transform Spectroscopy

Figure 3.16 shows NOx analyzer data for TiO_2 P25 sample. We used the the NO_2 conversion ((Co-C)/Co) as our indication for gas phase catalytic activity. The NO_2 conversion of P25 sample which is about 5 % was used as the gas phase benchmark conversion for evaluating developed photocatalysts.

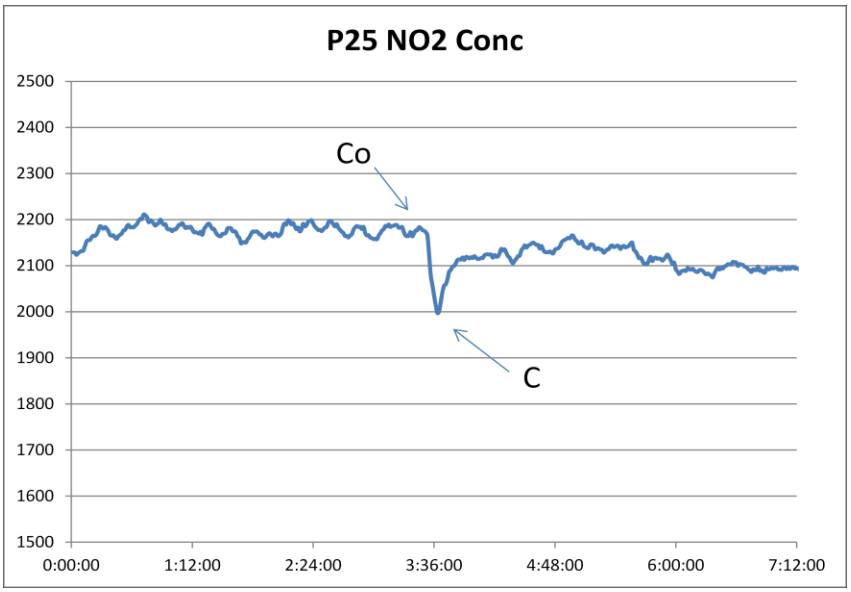

Fig. 3.16 Time dependent NO_2 concentration for TiO_2 P25

Reference:

[1] W.O. Milligan, A Review of the Application of X-Ray and Electron Diffraction Methods to Contact Catalysis, Phys Rev, 67 (1945) 197-197.

[2] G.J. Millar, M.L. Nelson, P.J.R. Uwins, In situ imaging of catalytic etching on silver during methanol oxidation conditions by environmental scanning electron microscopy, J Catal, 169 (1997) 143-156.

[3] M. Vrinat, L. Demourgues, Study of Unsupported Sulfided Co-Mo Catalysts - Scanning Electron-Microscopy and Catalytic Activity in Hydrodesulfurization, Cr Acad Sci Ii, 293 (1981) 1045-1048.

[4] M.A. Haque, M.T.A. Saif, In-situ tensile testing of nano-scale specimens in SEM and TEM, Exp Mech, 42 (2002) 123-128.

[5] H. Watanabe, M. Ichikawa, Development of a multifunctional surface analysis system based on a nanometer scale scanning electron beam: Combination of ultrahigh vacuum-scanning electron microscopy, scanning reflection electron microscopy, Auger electron spectroscopy, and x-ray photoelectron spectroscopy, Rev Sci Instrum, 67 (1996) 4185-4190.

[6] W.C. Chang, L.C.L. Huang, Y.S. Wang, W.P. Peng, H.C. Chang, N.Y. Hsu, W.B. Yang, C.H. Chen, Matrix-assisted laser desorption/ionization (MALDI) mechanism revisited, Anal Chim Acta, 582 (2007) 1-9.

[7] M. Karas, F. Hillenkamp, Laser Desorption Ionization of Proteins with Molecular Masses Exceeding 10000 Daltons, Anal Chem, 60 (1988) 2299-2301.

[8] K. Tang, S.L. Allman, R.B. Jones, C.H. Chen, Quantitative-Analysis of Biopolymers by Matrix-Assisted Laser-Desorption, Anal Chem, 65 (1993) 2164-2166.

[9] V.V. Laiko, S.C. Moyer, R.J. Cotter, Atmospheric pressure MALDI/ion trap mass spectrometry, Anal Chem, 72 (2000) 5239-5243.

[10] Q.H. Wu, J.Y. Kang, Applications of fast scanning tunneling microscopy: A review, Mater Manuf Process, 22 (2007) 22-27.

[11] A.A. Bukharaev, Diagnosis of a Surface by Scanning-Tunneling-Microscopy

(Review), Ind Lab+, 60 (1994) 589-598.
[12] T.E. Feuchtwang, P.H. Cutler, Tunneling and Scanning Tunnel Microscopy - a Critical-Review, Phys Scripta, 35 (1987) 132-140.
[13] R.E. Majors, High-Performance Liquid-Chromatography Columns and Column Technology - State-of-Art Review, J Chromatogr Sci, 15 (1977) 333-333.
[14] S.J. Schwartz, J.H. Vonelbe, High-Performance Liquid-Chromatography of Plant Pigments - a Review, J Liq Chromatogr, 5 (1982) 43-73.
[15] D. Guillarme, J. Ruta, S. Rudaz, J.L. Veuthey, New trends in fast and high-resolution liquid chromatography: a critical comparison of existing approaches, Anal Bioanal Chem, 397 (2010) 1069-1082.
[16] M.E. Swartz, UPLC (TM): An introduction and review, J Liq Chromatogr R T, 28 (2005) 1253-1263.
[17] M.C. Raphulu, J. McPherson, E. van der Lingen, J.A. Anderson, M.S. Scurrell, Investigation of the active site and the mode of Au/TiO2 catalyst deactivation using Diffuse Reflectance Infrared Fourier Transform Spectroscopy (DRIFTS) (vol 43, pg 21, 2010), Gold Bull, 43 (2010) 334-344.
[18] D.M. Byler, H. Susi, Examination of the Secondary Structure of Proteins by Deconvolved Ftir Spectra, Biopolymers, 25 (1986) 469-487.
[19] S. Kataoka, E. Lee, M.I. Tejedor-Tejedor, M.A. Anderson, Photocatalytic degradation of hydrogen sulfide and in situ FT-IR analysis of reaction products on surface of TiO2, Appl Catal B-Environ, 61 (2005) 159-163.

Chapter 4. Sub-nanomater gold particles synthesis and characterization

4.1 Introduction

Photocatalysis is a very important area of catalytic research, which has a potential to address both environmental and energy issues. One viable strategy to increase the photocatalytic efficiency of existing photocatalysts is to modify them with metal nanoparticles [1-4]. Several recent advances in gold nanoparticles (AuNPs) synthesis and applications have lead to the discovery of highly unusual magnetic, optical and catalytic properties [5-11].

It has been known that the gold nanoparticles less than 10 nm in diameter display electronic properties, which are quite different from those of bulk gold, reflecting a discrete electronic band structure of these nanoparticles. The supported gold has shown a significant activity for both gas phase and liquid phase reactions based on the previous work [12-19]. However, when gold particles are above 10 nm in size, they show chemical inertness and are often regarded as a poor catalysts [20].

The first study of gold nanoparticles on environmental photocatalytic applications showed that these nanoparticles are very active photocatalysts for decomposition of chlorophenol [21]. One possible reason for such improvement is the reduction of work function of the TiO_2 surface at the Au-TiO_2 interface, resulting in the facilitation of photoexcited electron transfer from TiO_2 to O_2, which is often viewed as a rate-limiting step in photocatalytic reactions [22-24].

It is important to mention that the impact of modifying the TiO_2 surface with sub-nm gold particles on the rate of photocatalytic reactions in both gas and liquid phase oxidation reactions is currently unknown. There is, however, an existing literature on the synthesis of such sub-nm particles. For example, gold nanoparticles Au_n ($n<13$) have been recently synthesized [25] using a procedure requiring complicated purification cycles [26, 27]. This approach can be further improved by introducing the bidentate phosphine ligands, which can optimize the size and uniformity of the nanoparticles [28-30]. Our project explores a relative

simple procedure for synthesis of highly stable Au clusters through the introduction of diphosphine ligands. It also studies applications of these catalysts for both liquid and gas-phase photocatalytic reactions. A novel component in photocatalytic testing of the AuNPs modified materials is based on a new generation of Diffuse Reflectance Fourier Transform Spectroscopy (DRIFTS) instrument modified with the UV light source. This approach allowed us to monitor the surface of the catalysts in-situ, which was extremely valuable to complement the gas phase data.

4.2 Experimental

4.2.1 Catalyst preparation

The synthetic method of Au nanoparticles synthesis was based on simple and straightforward procedure, which was developed based on modification of a previously published approach [31]. Titania (P25, Degussa, 50 m^2/g, 70% Anatase, 30% Rutile) was used as a support. For each preparation, 200mg of support and Triphenylphosphine gold(I) chloride [$(C_6H_5)_3PAuCl$, Strem Chemicals] with different ratios were used in order to achieve expected gold loadings (0.5, 1.0, 1.5, 2.5 and 5 wt. %).

$Au(PPh_3)Cl$ was dissolved in $CHCl_3$ to reach a final concentration of 10^{-3} mol/L. About 10^{-3} mol/L $P(Ph)_2(CH_2)_4P(Ph)_2$ was subsequently added to the mixture to achieve the target cluster size. Finally, $5 \bullet 10^{-3}$ mol/L of the reducing agent (aborane-tert-butylamine complex) was added under continuous stirring for 24 hours at room temperature. The unsupported gold clusters were then characterized by UV-Vis spectroscopy and Matrix Assisted Laser Desorption Ionization–Time of Flight Mass Spectrometry (MALDI-TOF MS). The gold deposition procedure on TiO_2 powders was achieved by varying the ratios of TiO_2 and AuNPs precursors developed in the previous step. About 200 mg of TiO_2 was

added to 20 ml of dichloromethane, followed by addition of AuNPs precursors. The mixture was stirred overnight, followed by thermal activation (150 °C, 2 h) in vacuo. The final powder was then washed with acetone. All gold modified samples were stored in darkness under nitrogen and tested within 2 weeks of preparation. The resulting products were characterized by Transmission Electron Microscopy (TEM, JEOL JEM-2100F).

4.2.2 Techniques of characterization

Scanning Transmission Electron Microscopy (Hitachi HD2700C), Ultraviolet-visible spectroscopy (Thermo Evolution 3000) and Matrix-assisted Laser Desorption/Ionization Time of Flight Mass Spectrometer (MALDI-TOF MS, ABI Voyager DE-STR with 337 nm UV laser) were used as the characterization methods to identify the gold clusters size and composition. DRIFTS (Thermo Nicolet 6700) and High Performance Liquid Chromatography (HPLC, Agilent Technologies 1200) were used for catalytic testing.

4.2.3 Catalytic reactions

The Au-TiO_2 catalysts were tested for oxidation of phenol and NO_2 in liquid and gas phase respectively.

The liquid phase photocatalytic experiment was carried out in a custom made temperature controlled Pyrex reactor loaded with the photocatalysts. The UV light source was Xenon lamp (Newport Model 67005) modified with optical filters, which cut off UV radiation below 320 nm to minimize the photolysis reactions. The temperature inside the reactor was maintained at 20 ^{o}C by using refrigerating recirculation. The photocatalytic experiments utilized 200 ml (20 mg/L) of phenol aqueous solution which was added into the reactor. Then 200 mg of catalysts with variable gold loadings were introduced into the solution. The

solution was stirred for 30 min before turning on the light to eliminate to account for pollutant adsorption on the surface of the catalyst. Samples were periodically withdrawn from the reactor, filtered through 0.45 μm membranes and transferred to HPLC vials for further analysis. The analysis was done using HPLC instrument described earlier.

The DRIFTS experiments were conducted in a novel photocatalytic system, which allowed simultaneous observations of both surface and gas phase reaction products under the UV illumination. This setup was based on a modified environmental chamber housed in the Smart Collector DRIFTS accessory (Thermo Fisher Scientific Inc.). This accessory was integrated into Nicolet 6700 FT-IR (Thermo Fisher Scientific Inc.) spectrometer equipped with liquid nitrogen cooled MCT (HgCdTe) detector. The catalyst surface was irradiated with UV light based on a UV LED source (λ=365nm, 50 mW, Prizmatix) and fiber optic cable (SH 8001, Mitsubishi Rayon Co. Ltd.). The temperature inside the cell was measured by thermocouple (Thermo Scientific temperature controller) and was maintained at 27 ^{0}C.

The spectral data recorded during the DRIFTS experiments was within the 4000-600 cm^{-1} spectral range with a resolution of 4 cm^{-1}. The experimental protocol included equilibration step, where the humidified air (RH 92 ±2.5%) was flowing through the chamber at 10 ccm for over 12 hours. Following the equilibration step, 3 ppm NO_2 gas feed was introduced into the chamber. Once the NO_2 concentration in the cell had stabilized, the UV light was turned on for approximately 6 hours. The analysis of the gas phase products was conducted by chemiluminescent NO_x analyzer (Model 200E, Teledyne Technologies Inc.).

4.3 Results and discussion

4.3.1 Characterization of Au-TiO_2

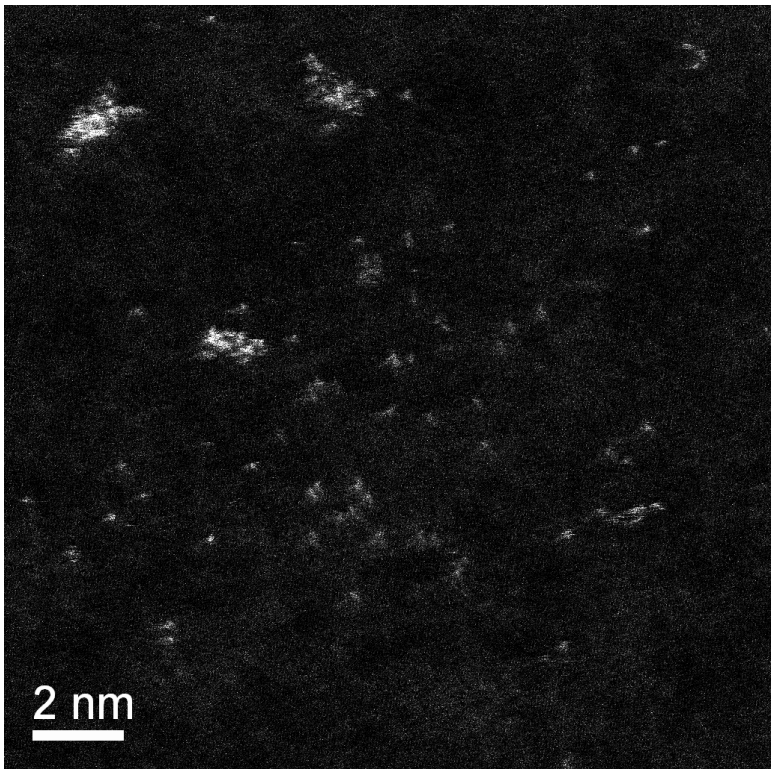

Fig. 4.1 STEM image of ultra small unsupported gold nanoparticles

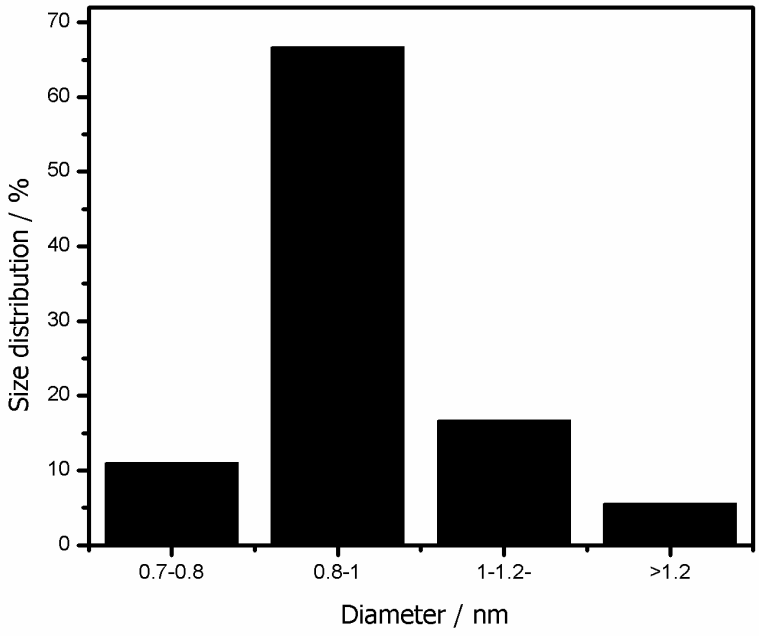

Fig. 4.2 Histogram of unsupported gold nanoparticles

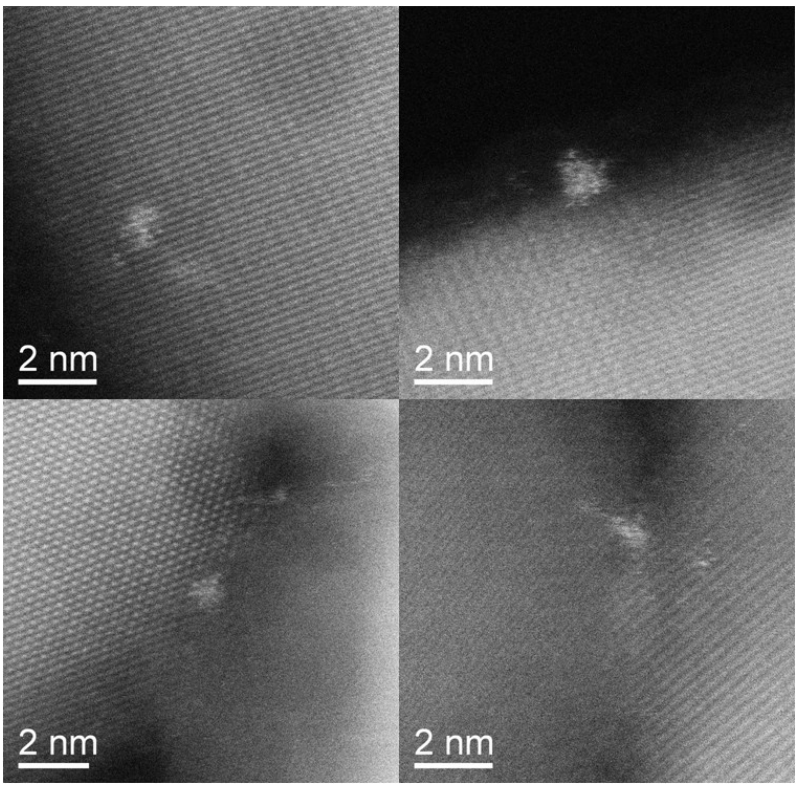

Fig. 4.3 STEM images of ultra small gold nanoparticles supported on TiO_2

Figure 4.1 shows the STEM image of the unsupported gold nanoparticles deposited on TEM carbon grid from chloroform solution. This image indicates that the average gold cluster size was approximately 0.8 ± 0.1 nm according to the histogram (Figure 4.2) with a significant number of isolated gold atoms uniformly distributed throughout the sample. This result shows that both sub-nanometer clusters and single gold atoms are present in chloroform solution before the deposition and thermal activation. Figure 4.3 shows the STEM images of gold nanoparticles deposited on TiO_2 P25. The bright spots observed in the STEM image were gold nanoparticles, which are similar to the work by Flytzani-Stephanopoulos *et al.* [32] on Au supported on iron oxide. The average size of the supported gold particles was 0.88 nm. This result is consistent with the unsupported Au cluster TEM data, except for the fact that no significant presence of individual Au atoms was observed. One possible explanation of this result is a

substantial agglomeration of Au atoms due to thermal activation step, although the limitations of the STEM instrument in imaging at such a high resolution should be also taken into consideration.

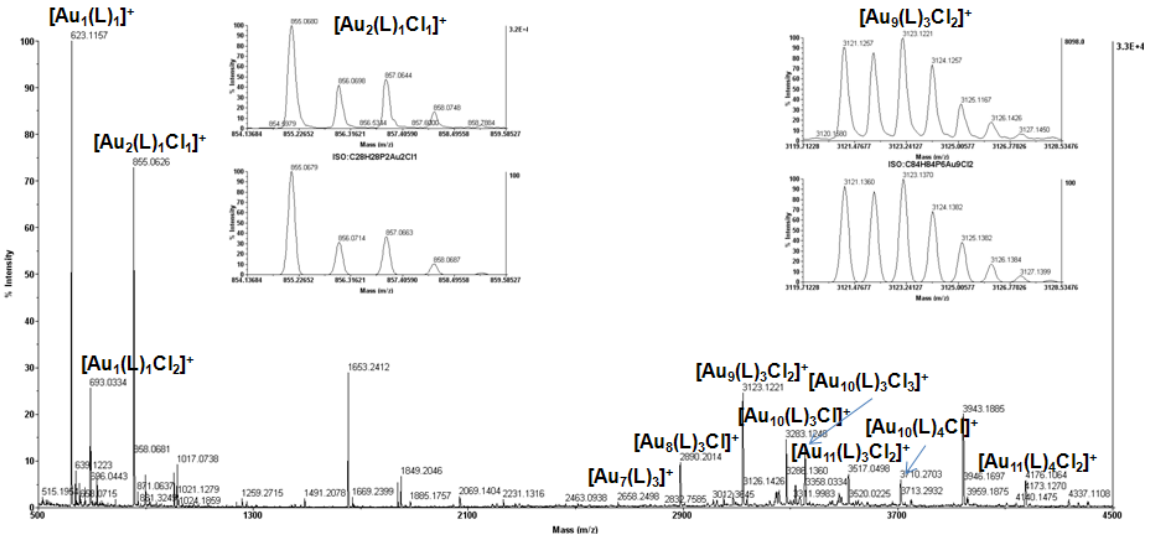

Fig. 4.4 MALDI mass spectrum for gold clusters (500-4500 m/z) (Insert shows the experimental isotopic distribution of Au clusters containing 2 and 9 Au atoms along with theoretical isotopic distribution of the same clusters)

Figure 4.4 shows the MALDI-TOF mass spectrum of unsupported gold nanoparticles before their deposition on TiO_2 surface. More specifically, it displays mass region of 500 to 4500 m/z. These results indicate that each Au cluster contains 8-11 Au atoms, which is consistent with TEM analysis. The insert in Figure 4.4 displays the experimental isotopic distribution of Au clusters containing 2 and 9 Au atoms along with theoretical isotopic distribution of the same compound. A significant similarity between these spectra confirms the structure of the $[Au_9(L)_3Cl_2]^+$ cluster. Similarly to the previously described STEM results, it also indicates a significant presence of Au_1 and Au_2 precursors. The ratio of intensities for signals attributed to Au_9 and $Au_{1/2}$ species is approximately 1:3.However, one has to be careful to relate the ratio of intensities to the actual

abundance ratio, given the uncertainties related to the instrument's response to each species and significant difficulties in obtaining a reliable calibration curve.

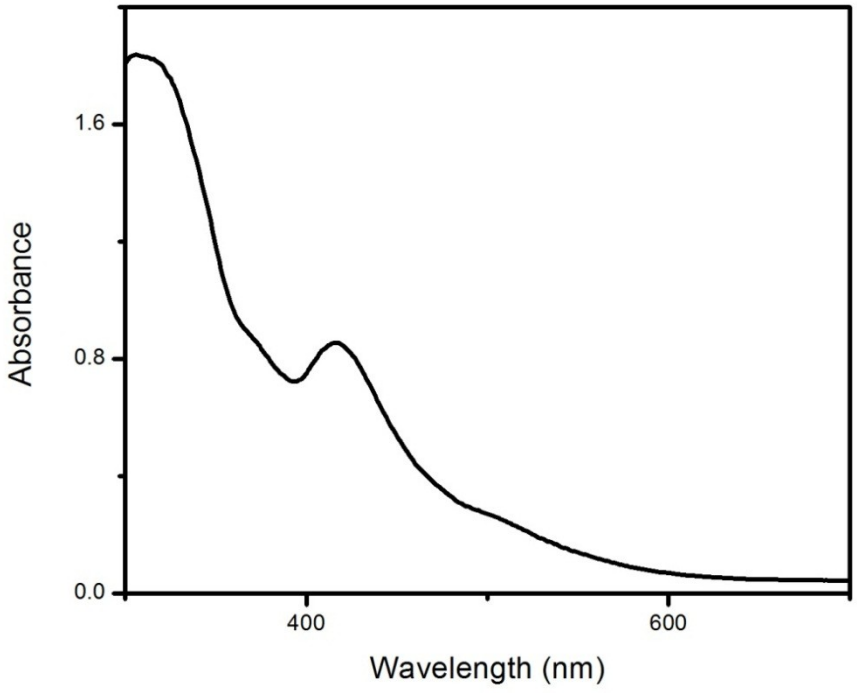

Fig. 4.5 UV-Vis optical absorption spectrum of Au nanoparticles in chloroform

The UV-vis optical absorption spectrum of unsupported Au clusters obtained by UV-Vis spectrometer is shown in Figure 4.5. It exhibits two peaks at around 310 and 415 nm. In case of particles below 1.5 nm in size, the assumption of continuous surface plasmon band is no longer valid, and particles can be regarded as atomic gold clusters with discrete electronic states [33, 34]. Therefore, the 310 nm peak can be interpreted as the ligand-to-metal charge transfer (LMCT) originated from Au-Cl charge transfer [35-37]. The peak at 415 nm indicates 5d$\rightarrow$6s interband transitions in the Au_{11}^{3+} core [38]. These peak positions are in agreement with the previously reported UV-Vis spectra of phosphine-stabilized undecagold (Au_{11}) clusters [25, 26].

4.3.2 Catalytic results

4.3.2.1 Liquid phase catalytic activity

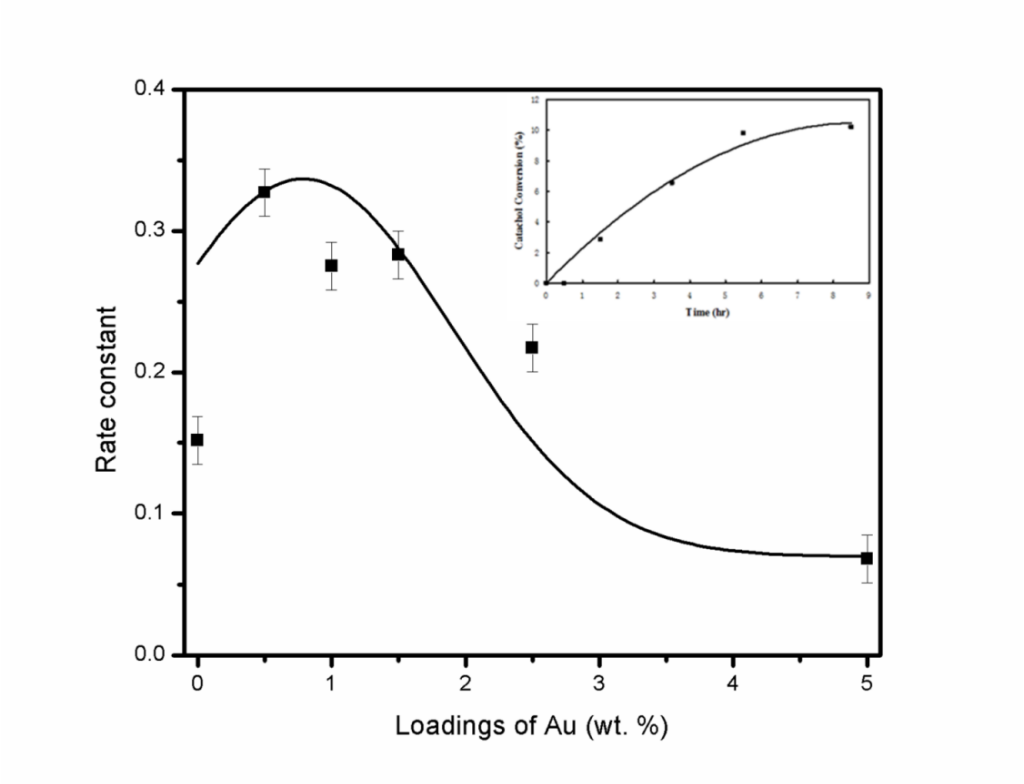

Fig. 4.6 Photocatalytic activities of Au modified TiO_2 for phenol oxidation at different Au loadings. Insert shows the time dependent production of catechol of 0.5 wt. % of Au loading

Figure 4.6 shows the photocatalytic activity of the Au-TiO_2 for liquid phase oxidation of phenol. It indicates a significant increase in activity of Au-TiO_2 catalyst as compared to that of the unmodified one. The highest catalytic activity was observed at 0.5 wt. % of gold loading. This catalyst had about 2 times better performance than that of an unmodified one. A further increase in Au loadings resulted in a decrease of activity, with 5 wt. % Au sample exhibiting the lowest activity. This sample performed noticeably worse than the unmodified TiO_2. The insert in Figure 4.6 shows the time dependent production of catechol, which was

one of the major intermediates in the phenol oxidation reaction. It confirms that the disappearance of phenol from solution is due to photocatalytic reaction rather than due to just adsorption on the catalyst surface.

4.3.2.1 Liquid phase catalytic activity

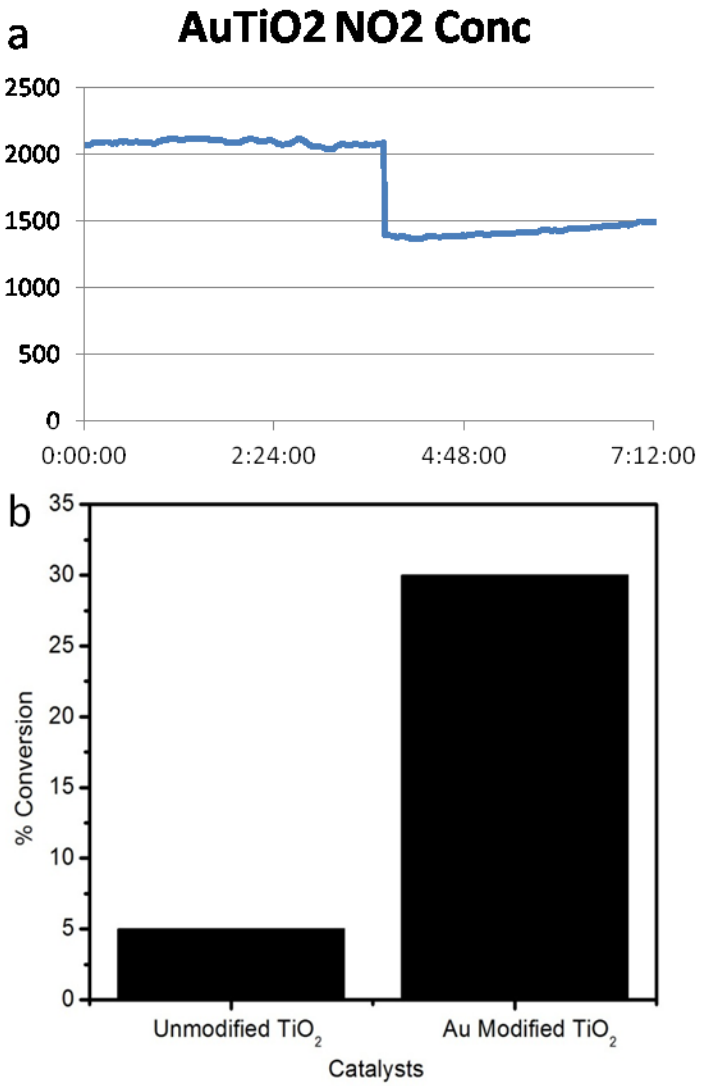

Fig. 4.7 a) Time dependent NO_2 conversion for Au modified TiO_2, b) Photocatalytic conversion of NO_2 by: (a) unmodified TiO_2; (b) 0.5 wt. % of Au modified TiO_2

The gas phase data for NO_2 conversion on Au modified (0.5 wt. %) and unmodified TiO_2 catalysts exposed to the UV light are shown in Figure 4.7. It displays a dramatic increase in activity of the Au modified sample as compared to that of the unmodified one. The improvement in NO_2 conversion by a factor of 6 is quite remarkable, given a rather modest gold loading. Relating this result to the ratio of Au_9 to Au_{12} species can help to clarify the role of Au clusters and will be a subject of a future work. It is important to mention that the presence of Au_1 and Au_2 species have been shown to significantly increase the catalyst activity for various heterogeneous reactions, however, the role of Au_1 and Au_2 in photocatalytic reactions is still unknown [39, 40]

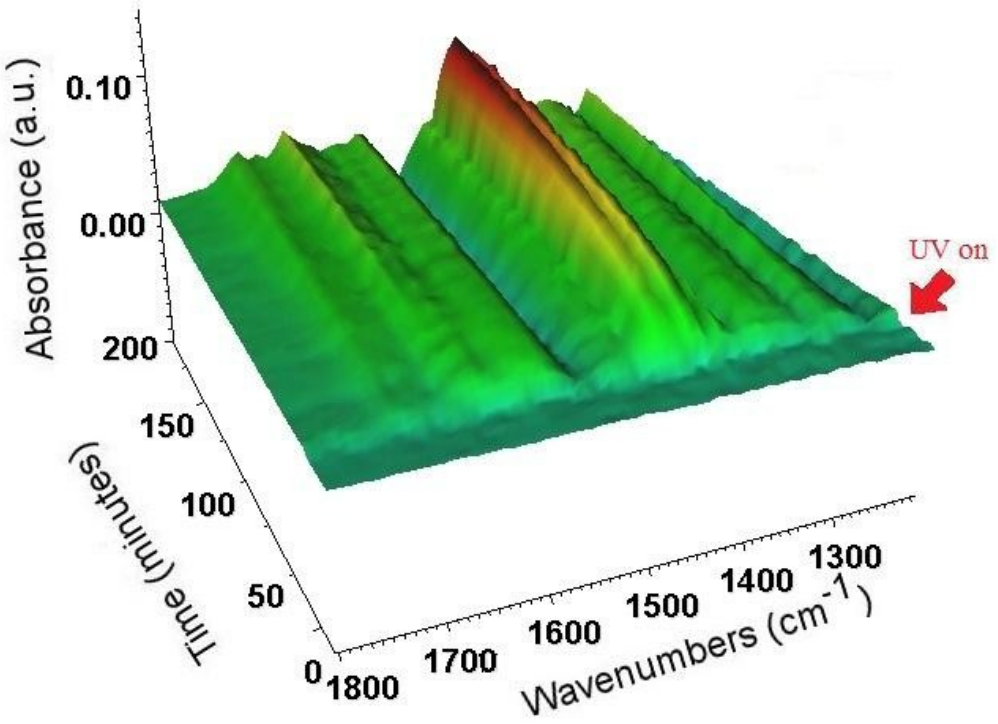

Fig. 4.8 Time dependent DRIFT spectra for the in-situ photocatalytic oxidation of NO_2 on Au modified TiO_2 catalyst

An important advantage of our system as compared to other setups is its capability to monitor the surface adsorbed products. Figure 8 shows time resolved DRIFTS spectra of Au modified sample exposed to NO_2 under illumination. The inflection point on the 3D time-resolved DRIFTS spectra coincides with turning on the UV light, illustrating a striking increase in the surface adsorbed reaction products. Several peaks appearing in Figure 4.8 can be assigned to nitrite, nitrate and nitrosyl species as described below.

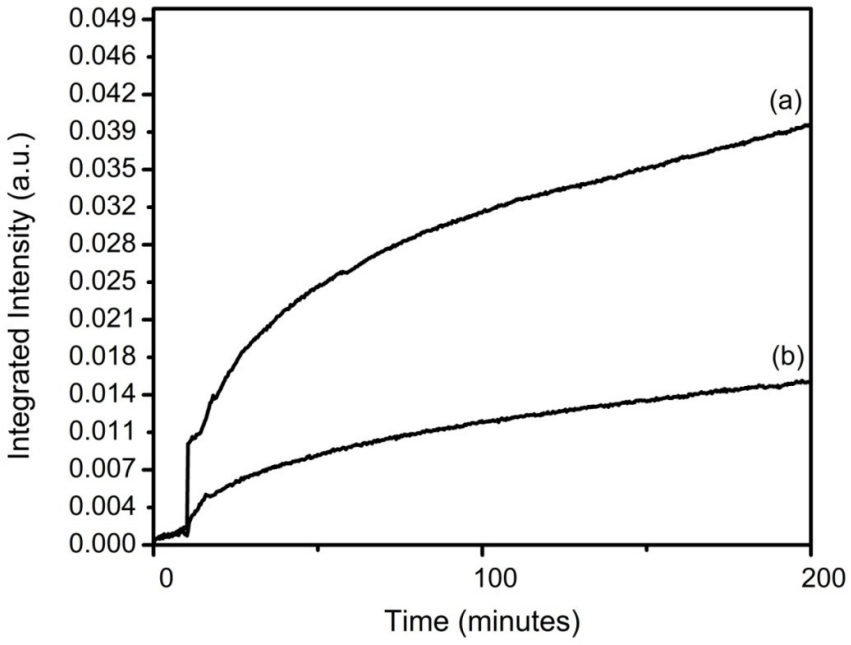

Fig. 4.9 Integrated intensity of surface adsorbed nitrite and nitrate by: (a) 0.5 wt. % of Au modified TiO_2 (b) unmodified TiO_2

The rate of reaction products accumulation can be illustrated by plotting the integrated IR intensity of the spectral region between 1200 and 1800 cm^{-1} as a function of time. Figure 4.9 shows the integrated IR intensity for Au modified and unmodified samples, indicating that Au modified sample is much more active for NO_2 conversion as compared to that of unmodified sample.

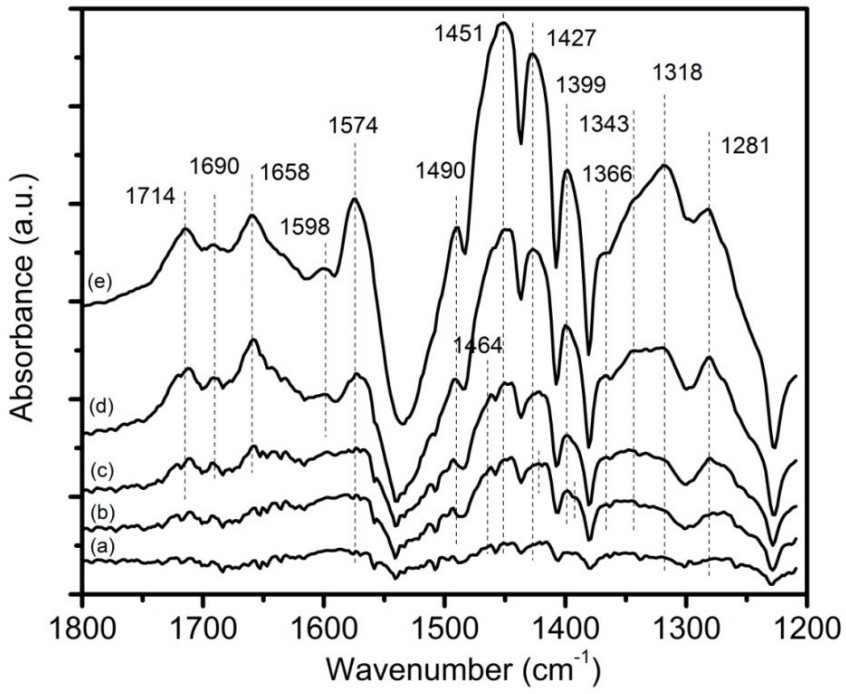

Fig. 4.10 Time dependent DRIFT spectra of NO_2 reaction products on Au modified TiO_2. (a): 0 min, (b): 60 min, (c): 120 min, (d): 180 min, (e): 200 min

In order to illustrate the surface adsorbed reaction products, the DRIFTS spectra recorded at various stages of photocatalytic reaction are shown in Figure 4.10. After approximately 30 minutes of the UV exposure several distinct peaks at 1447, 1421 and 1399 cm^{-1} were observed. These peaks grew parallel to each other sharpening and increasing in intensity as the experiment progressed, with the peaks at 1447 and 1421 cm^{-1} red shifting to corresponding peaks at 1451 and 1427 cm^{-1}. The peaks at 1451 and 1427 cm^{-1} were the most prominent peaks in the recorded spectra. Several transient peaks, which appeared in the intermediate stages of the experiments, included the peak at 1464 cm^{-1} and a very weak shoulder at 1399 cm^{-1}. In the final spectrum the 1464 cm^{-1} peak was most likely obscured by the dominant nature of the peak at 1451 cm^{-1} while the 1399 cm^{-1} has completely disappeared from the spectrum.

In addition to the peaks mentioned above, two distinct features were observed in the 1400-1200 cm^{-1} region, namely the broad band in the 1375-1315 cm^{-1} region and the smaller feature in 1290-1235 cm^{-1} part of the spectrum. The feature at 1375-1315 cm^{-1} can be deconvoluted into 3 broad bands at 1366, 1350 and 1325 cm^{-1}. All these bands substantially increased in intensity over the course of the experiments, with 1325 cm^{-1} feature sharpening and shifting to 1318 cm^{-1} in the final spectra.

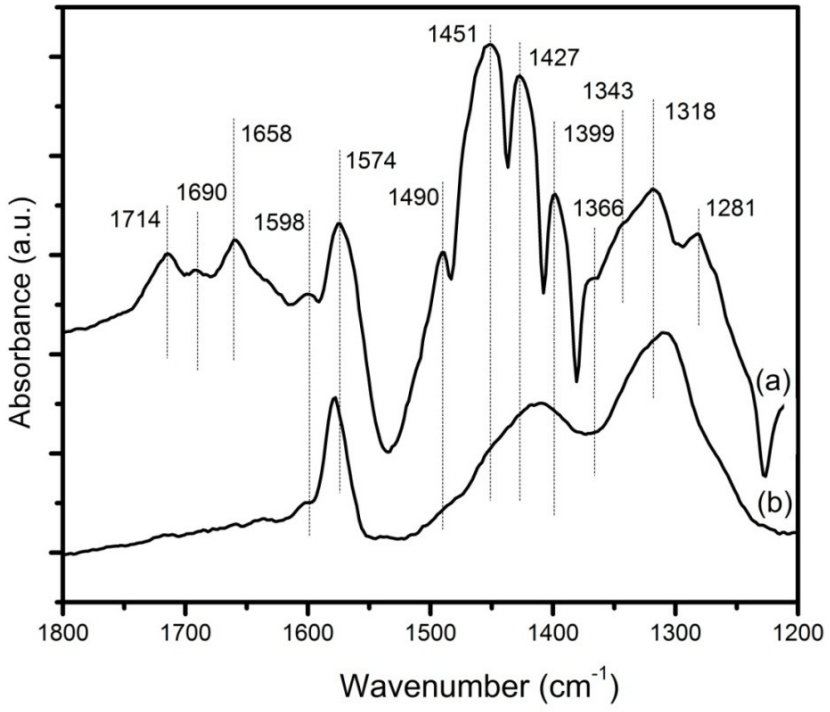

Fig. 4.11 Final DRIFT spectra obtained for NO_2 reaction products adsorbed on: (a) 0.5 wt. % of Au modified TiO_2 (b) unmodified TiO_2

The broad feature detected in 1600-1560 cm^{-1} region sharpened and grew steadily along with the peak observed at 1658 cm^{-1} over the course of the experiment while forming a shoulder at 1598 cm^{-1} on the high wavenumber side

of 1574 cm^{-1} peak midway through the experiment. These features were also visible in the unmodified catalyst (Figure 4.11).

A comparison of the baseline subtracted spectra of modified and unmodified catalysts is show in the Figure 11. The peaks at 1399 and 1427 cm^{-1} can be attributed to contribution from both M-NO_2 and solvated nitrate species [41, 42]. The feature at 1490 cm^{-1}, which appears alongside the most intense peak in the spectra, corresponds to the unidentate nitrito or intrate species. The peak at 1658 cm^{-1} can be assigned to bridging nitrate species while the peak at 1281 cm^{-1} can be attributed to either bidentate nitrate or monodentate nitrate or have contributions from both species [41, 42]. The bands at 1714 and 1690 cm^{-1} are generally assigned to mononitrosyl species [43, 44]. Although the primary species detected in the gas phase were attributed to NO_2, we have observed the elevated level of NO for Au-TiO_2 catalysts. The presence of gas phase NO for modified catalysts and the absence of this reaction product for unmodified catalysts are consistent with the observation of surface adsorbed mononitrosyl species. The common peaks appearing in both Au modified and unmodified catalysts were 1598, 1574 and 1318 cm^{-1} features associated with M-NO_2 and bidentate nitrate species [41]. The band at 1413 cm^{-1} in the unmodified catalyst spectra can be also assigned to M-NO_2 species; however, considering the broad nature of the peak, it can be a combination of 2 or more unresolved peaks resulting from both M-NO_2 and solvated nitrate species.

4.4 Conclusion

Our results unambiguously show that sub-nanometer Au modified TiO_2 samples exhibit significant activity for liquid and gas-phase oxidation reactions. The presence of sub-1 nm clusters was confirmed by TEM, MALDI-TOF MS and UV-vis spectroscopy. The catalytic data show a remarkable improvement in activity due to Au deposition. The new generation of UV source modified DRIFTS

was used to monitor NO_2 reactions with illuminated photocatalysts. The results revealed a significant presence of nitrate, nitrite and nitrosyl species on the surface after turning on the UV light, which was consistent with the gas phase data.

Reference:

[1] V. Subramanian, E.E. Wolf, P.V. Kamat, Influence of metal/metal ion concentration on the photocatalytic activity of TiO2-Au composite nanoparticles, Langmuir, 19 (2003) 469-474.

[2] M. Haruta, N. Yamada, T. Kobayashi, S. Iijima, Gold Catalysts Prepared by Coprecipitation for Low-Temperature Oxidation of Hydrogen and of Carbon-Monoxide, J Catal, 115 (1989) 301-309.

[3] H. Tsunoyama, H. Sakurai, T. Tsukuda, Size effect on the catalysis of gold clusters dispersed in water for aerobic oxidation of alcohol, Chem Phys Lett, 429 (2006) 528-532.

[4] G. Bond, Source of the catalytic activity of gold nanoparticles, Gold Bull, 43 (2010) 88-93.

[5] C.L. Nehl, H.W. Liao, J.H. Hafner, Optical properties of star-shaped gold nanoparticles, Nano Letters, 6 (2006) 683-688.

[6] M.C. Daniel, D. Astruc, Gold nanoparticles: Assembly, supramolecular chemistry, quantum-size-related properties, and applications toward biology, catalysis, and nanotechnology, Chemical Reviews, 104 (2004) 293-346.

[7] K.L. Kelly, E. Coronado, L.L. Zhao, G.C. Schatz, The optical properties of metal nanoparticles: The influence of size, shape, and dielectric environment, Journal of Physical Chemistry B, 107 (2003) 668-677.

[8] Y.G. Sun, Y.N. Xia, Shape-controlled synthesis of gold and silver nanoparticles, Science, 298 (2002) 2176-2179.

[9] A. Dawson, P.V. Kamat, Semiconductor-metal nanocomposites. Photoinduced fusion and photocatalysis of gold-capped TiO2 (TiO2/Gold) nanoparticles, Journal of Physical Chemistry B, 105 (2001) 960-966.

[10] C.B. Almquist, P. Biswas, The photo-oxidation of cyclohexane on titanium dioxide: an investigation of competitive adsorption and its effects on product formation and selectivity, Applied Catalysis a-General, 214 (2001) 259-271.

[11] P. Boarini, V. Carassiti, A. Maldotti, R. Amadelli, Photocatalytic oxygenation

of cyclohexane on titanium dioxide suspensions: Effect of the solvent and of oxygen, Langmuir, 14 (1998) 2080-2085.

[12] L. Ilieva-Gencheva, G. Pantaleo, N. Mintcheva, I. Ivanov, A.M. Venezia, D. Andreeva, Nano-structured gold catalysts supported on CeO2 and CeO2-Al2O3 for NOx reduction by CO: Effect of catalyst pretreatment and feed composition, J Nanosci Nanotechno, 8 (2008) 867-873.

[13] J.C. Fierro-Gonzalez, J. Guzman, B.C. Gates, Role of cationic gold in supported CO oxidation catalysts, Top Catal, 44 (2007) 103-114.

[14] Q. Fu, H. Saltsburg, M. Flytzani-Stephanopoulos, Active nonmetallic Au and Pt species on ceria-based water-gas shift catalysts, Science, 301 (2003) 935-938.

[15] J.H. Teles, S. Brode, M. Chabanas, Cationic gold(I) complexes: Highly efficient catalysts for the addition of alcohols to alkynes, Angewandte Chemie-International Edition, 37 (1998) 1415-1418.

[16] L. Prati, M. Rossi, Gold on carbon as a new catalyst for selective liquid phase oxidation of diols, Journal of Catalysis, 176 (1998) 552-560.

[17] A. Wood, M. Giersig, P. Mulvaney, Fermi level equilibration in quantum dot-metal nanojunctions, J Phys Chem B, 105 (2001) 8810-8815.

[18] M. Valden, X. Lai, D.W. Goodman, Onset of catalytic activity of gold clusters on titania with the appearance of nonmetallic properties, Science, 281 (1998) 1647-1650.

[19] M. Haruta, Size- and support-dependency in the catalysis of gold, Catal Today, 36 (1997) 153-166.

[20] M. Haruta, Catalysis of gold nanoparticles deposited on metal oxides, Cattech, 6 (2002) 102-115.

[21] A. Orlov, D.A. Jefferson, N. Macleod, R.M. Lambert, Photocatalytic properties of TiO2 modified with gold nanoparticles in the degradation of 4-chlorophenol in aqueous solution, Catal Lett, 92 (2004) 41-47.

[22] V. Subramanian, E.E. Wolf, P.V. Kamat, Catalysis with TiO2/gold nanocomposites. Effect of metal particle size on the Fermi level equilibration, Journal of the American Chemical Society, 126 (2004) 4943-4950.

[23] M.A. Henderson, W.S. Epling, C.H.F. Peden, C.L. Perkins, Insights into

photoexcited electron scavenging processes on TiO2 obtained from studies of the reaction of O-2 with OH groups adsorbed at electronic defects on TiO2(110), Journal of Physical Chemistry B, 107 (2003) 534-545.

[24] A.L. Linsebigler, G.Q. Lu, J.T. Yates, Photocatalysis on Tio2 Surfaces - Principles, Mechanisms, and Selected Results, Chemical Reviews, 95 (1995) 735-758.

[25] K.P. Hall, D.M.P. Mingos, HOMONUCLEAR AND HETERONUCLEAR CLUSTER COMPOUNDS OF GOLD, Progress in Inorganic Chemistry, 32 (1984) 237-325.

[26] W. Jahn, Review: Chemical aspects of the use of gold clusters in structural biology, Journal of Structural Biology, 127 (1999) 106-112.

[27] D. Safer, L. Bolinger, J.S. Leigh, Undecagold Clusters for Site-Specific Labeling of Biological Macromolecules - Simplified Preparation and Model Applications, Journal of Inorganic Biochemistry, 26 (1986) 77-91.

[28] Y. Yanagimoto, Y. Negishi, H. Fujihara, T. Tsukuda, Chiroptical activity of BINAP-stabilized undecagold clusters, Journal of Physical Chemistry B, 110 (2006) 11611-11614.

[29] C.E. Briant, K.P. Hall, D.M.P. Mingos, Structural Studies on Mixed Iron Gold Clusters with Bidentate Tertiary Phosphine-Ligands, Journal of the Chemical Society-Chemical Communications, (1983) 843-845.

[30] J.W.A. Vandervelden, F.A. Vollenbroek, J.J. Bour, P.T. Beurskens, J.M.M. Smits, W.P. Bosman, Gold Clusters Containing Bidentate Phosphine-Ligands - Preparation and X-Ray Structure Investigation of [Au5(Dppmh)3(Dppm)](No3)2 and [Au13(Dppmh)6](No3)N, Recueil Des Travaux Chimiques Des Pays-Bas-Journal of the Royal Netherlands Chemical Society, 100 (1981) 148-152.

[31] M.F. Bertino, Z.M. Sun, R. Zhang, L.S. Wang, Facile syntheses of monodisperse ultrasmall Au clusters, J Phys Chem B, 110 (2006) 21416-21418.

[32] L.F. Allard, A. Borisevich, W.L. Deng, R. Si, M. Flytzani-Stephanopoulos, S.H. Overbury, Evolution of gold structure during thermal treatment of Au/FeOx catalysts revealed by aberration-corrected electron microscopy, J Electron Microsc, 58 (2009) 199-212.

[33] S. Link, M.A. Ei-Sayed, Optical properties and ultrafast dynamics of metallic nanocrystals, Annual Review of Physical Chemistry, 54 (2003) 331-366.

[34] L. Balogh, D.A. Tomalia, Poly(amidoamine) dendrimer-templated nanocomposites. 1. Synthesis of zerovalent copper nanoclusters, Journal of the American Chemical Society, 120 (1998) 7355-7356.

[35] S. Ivanova, C. Petit, V. Pitchon, A new preparation method for the formation of gold nanoparticles on an oxide support, Applied Catalysis a-General, 267 (2004) 191-201.

[36] M. Ito, T. Tsukatani, H. Fujihara, Preparation and characterization of gold nanoparticles with a ruthenium-terpyridyl complex, and electropolymerization of their pyrrole-modified metal nanocomposites, J Mater Chem, 15 (2005) 960-964.

[37] T.H. Peter Kracke, Howard Saltsburg, and Maria Flytzani-Stephanopoulos, CO Oxidation on Unsupported Dendrimer-Encapsulated Gold Nanoparticles, J. Phys. Chem. C, 39 (2010) 16401–16407.

[38] Y.Y. Yang, S.W. Chen, Surface manipulation of the electronic energy of subnanometer-sized gold clusters: An electrochemical and spectroscopic investigation, Nano Letters, 3 (2003) 75-79.

[39] G.J. Hutchings, Nanocrystalline gold catalysts: A reflection on catalyst discovery and the nature of active sites, Gold Bull, 42 (2009) 260-266.

[40] A.A. Herzing, C.J. Kiely, A.F. Carley, P. Landon, G.J. Hutchings, Identification of active gold nanoclusters on iron oxide supports for CO oxidation, Science, 321 (2008) 1331-1335.

[41] M.A. Debeila, N.J. Coville, M.S. Scurrell, G.R. Hearne, The effect of calcination temperature on the adsorption, of nitric oxide on Au-TiO2: Drifts studies, Applied Catalysis a-General, 291 (2005) 98-115.

[42] G.M. Underwood, T.M. Miller, V.H. Grassian, Transmission FT-IR and Knudsen cell study of the heterogeneous reactivity of gaseous nitrogen dioxide on mineral oxide particles, Journal of Physical Chemistry A, 103 (1999) 6184-6190.

[43] M.A. Debeila, N.J. Coville, M.S. Scurrell, G.R. Hearne, Direct observation of thermally activated NO adsorbate species on Au-TiO2: DRIFTS studies, Journal

of Molecular Catalysis a-Chemical, 219 (2004) 131-141.

[44] R.V. Mikhaylov, A.A. Lisachenko, B.N. Shelimov, V.B. Kazansky, G. Martra, G. Alberto, S. Coluccia, FTIR and TPD Analysis of Surface Species on a TiO2 Photocatalyst Exposed to NO, CO, and NO-CO Mixtures: Effect of UV-Vis Light Irradiation, Journal of Physical Chemistry C, 113 (2009) 20381-20387.

Chapter 5. Size and Shape Dependency Studies on Gold Nanoparticles for Catalysis

5.1 Introduction

Numerous studies have been focused on understanding the properties that affect the catalytic performance of metal nanoparticles. Such studies investigated interactions between the deposited metals and the supports, deposition methods and etc [1-16]. At a current stage, size and shape dependencies of the nanoparticles have gained significant amount of attention due to a recognition of them being one the most crucial parameters, which affect the catalytic behaviors of metal/semiconductor catalysts [17-29]. For the previous years, there are a lot of publications focused on the metal nanoparticle size, where the most promising catalytic activities were achieved when particle size were less than 10 nm [30, 31]. In order to develop more precise structure-activity relations, researchers are now trying to exercise more precise control of the number of atoms in metal clusters e.g. Au_n ($n<20$), and study their catalytic behaviors [32].

Previous reports have explained the distinct reactivity of NPs with different shapes based on prevalence of several crystalline facet substrates [33, 34]. For example, Zaera et al. demonstrated that the independent control of Pt particle size and shape during catalyst manufacture can be utilized to design of highly selective catalysts [33]. Cuenya et al. stated that Pt nanoparticles on TiO_2 (110) showed very different catalytic performances between flat and round (3D) in their geometric shape [35]. These results not only suggest that some of the catalytic reactions are structure sensitive, but also highlight the roles that particle size and particle shape may play together in defining selectivity in those catalytic processes. It is important to point out that the nanoparticle size and the interaction between metal and support both have significant impact on the most stable NP shapes. Therefore, the shape dependence cannot be simply investigated separately from the effects of substrate and particle size.

A comprehensive picture summarizing some of the models described in literature was given by Cho, Fig. 1 [36]. This figure illustrates the models, which assign the enhanced and size-dependent reactivity of gold clusters to different contributions, namely to: (i) small metal clusters displaying non-metallic behavior (quantum size effects), (ii) the presence of higher densities of low coordinated atoms, (iii) excess electronic charge in the step edges of the metal particles, and (iv) NP–support interactions (active perimeter sites). In this section, we will focus on the size-dependent aspects (i–iii) and will dedicate future sections to the importance of the cluster support (iv).

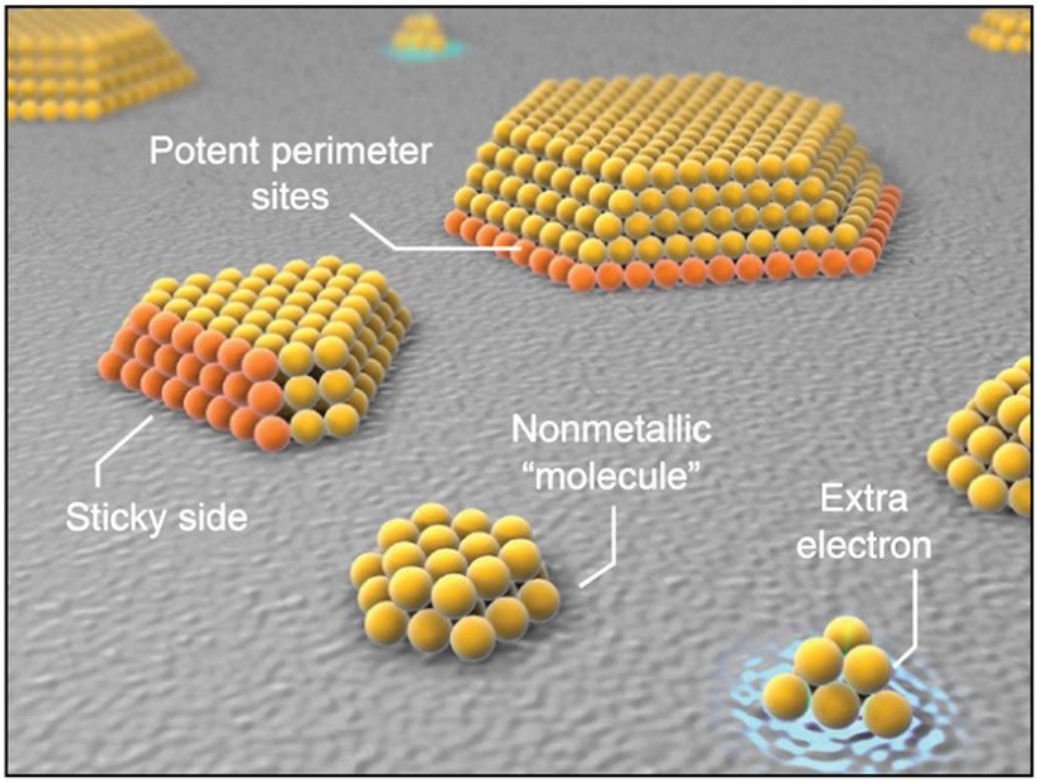

Fig. 5.1 Possible mechanisms responsible for the enhanced reactivity of nanoscale gold nanoclusters

One of the biggest challenges for this type of research is to determine the eventual size and shape of the metal clusters. Once they were deposited on the substrate, the shape will be influenced by metal-support interactions and will be different from that of unsupported clusters. Also it is important to mention that shape of the particles will be modified by potential particle agglomeration, especially due to deprotection of nanoparticles from either ligands or surfactants, which are used to keep the separated in the solution. In this work, we report the deposition and imaging of size-selected Au and Pt nanoparticles deposited on both TiO_2 powders and (110) single crystals. In order to get high resolution of the images, we used atomic resolution scanning tunneling microscopy (STM) to observe the surface morphology after cluster deposition coupled with density functional theory (DFT) calculations to explore the possible cluster geometries. The geometry and size were then discussed in terms of NPs catalytic performances in both liquid and gas phase reactions.

5.2 Experimental Conditions

Au clusters with organic ligands were synthesized via established methods mentioned in the previous chapters. Samples with different gold loadings and particle sizes were synthesized. Both regular and sub-nm Au nanoparticles were deposited on TiO_2 P25 powder. Two different preparation methods were employed in this work including ligands exchange and photodeposition methods However, only sub-nm Au samples were deposit on the single crystalline TiO_2 (110) for size and shape dependency study..

STM experiments were performed in an ultrahigh vacuum (UHV) chamber equipped with an RHK-100 variable temperature STM with a cluster deposition device system, and X-ray photoelectron spectrometer (XPS). The base pressure is less than 2×10^{-10} torr, and a cluster deposition chamber with maximum deposition pressure $<10^{-9}$ torr. The cleaning of TiO_2 (110) surface was achieved by multiple cycles (20 to 30) of Ar^+ ion sputtering (1 keV, 20 min), followed by

annealing at 800 K for 20 min until a well-defined (1 × 1) low energy diffraction (LEED) pattern was observed. STM image of the TiO_2 single crystal was described in Figure 5.2 and few impurities (1 × 2) were observed from the images. The treatment described above has also created bulk oxygen vacancies making the single crystal conductive, which is important for the STM imaging.

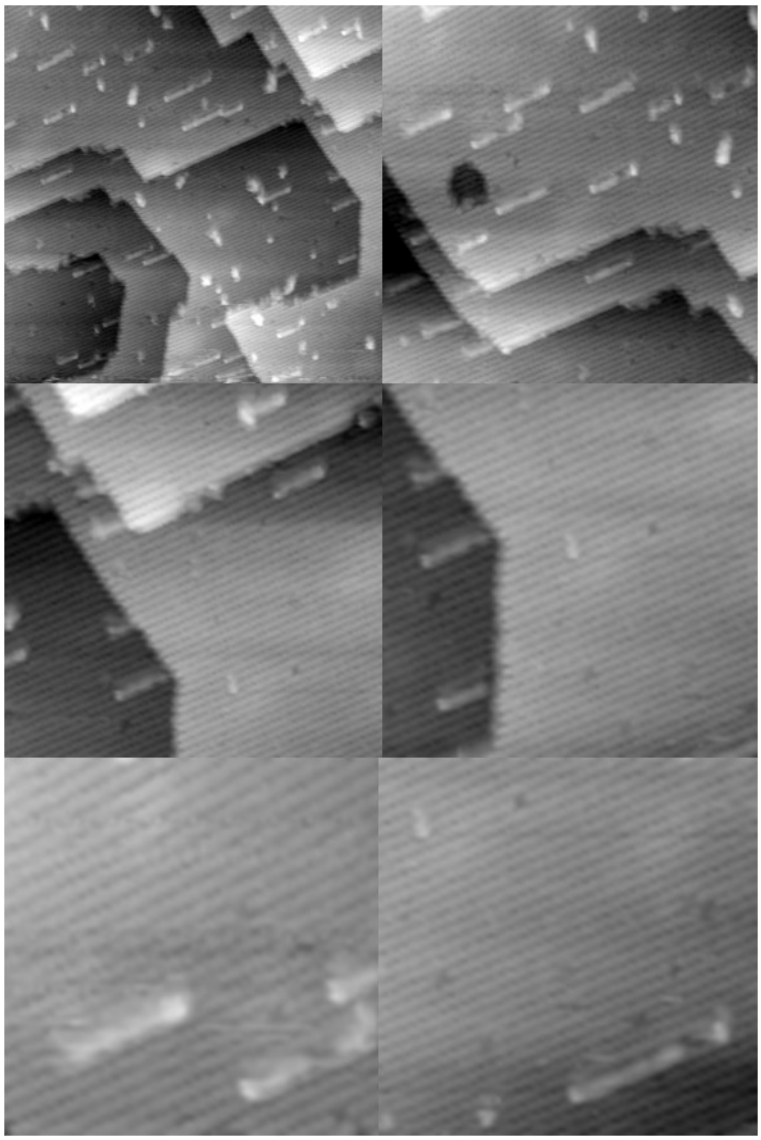

Fig. 5.2 STM images for TiO2 (110) single crystal

The solution containing metal nanoparticles was degassed for several

cycles and attached into the UHV chamber. Clusters were deposited onto the single crystal surface via the custom made dosser system. The sample was then annealed at 100 ^{0}C for 30 min in order to de-protect the ligands.

STM observations were performed using a low-temperature scanning tunneling microscope (LT-STM) attached to a surface analysis chamber. Then, the samples were imaged using a LT-STM with a tungsten tip. STM images of the surface were acquired at 80 K in a constant current mode. The typical operating parameters were a sample bias in the range of +1 to +3 V and a tunneling current of 0.06–0.08 nA.

Photocatalytic reactions in liquid and gas phase were mentioned in details elsewhere in this dissertation. Although the imaging was done on single crystals and catalytic results were obtained in powder system, there is still a possibility to extract some useful information on the effect of particle size on catalytic activity. More specifically, , we have chosen 1 wt. % Au loaded on TiO_2 powder samples as a basis of this discussion, given that those samples have shown the most promising catalytic activities.

5.3 Results and Discussion

5.3.1 Shape effects of the Au nanoparticles

Figure 5.3 shows atomic-resolution images of the ligands protected Au nanoclusters. The images were obtained using a scanning tunneling microscope with a tungsten tip. the results indicate that the gold nanoparticles are well dispersed onto the TiO_2 crystal surface.

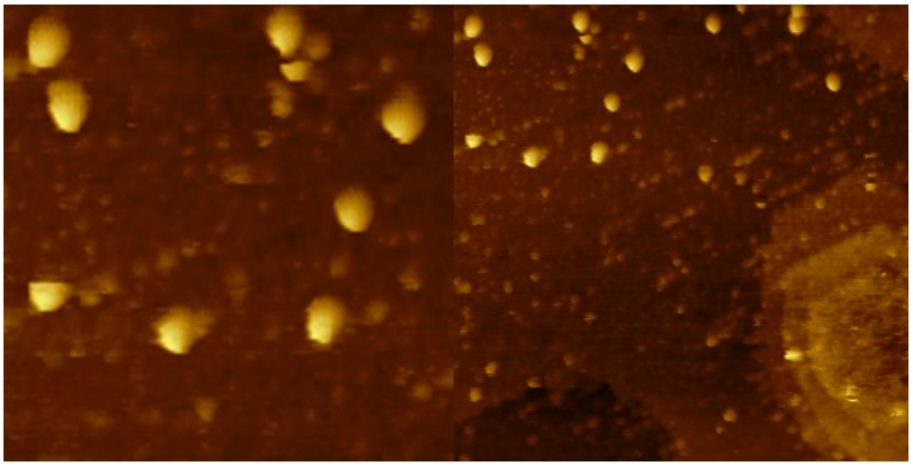

Fig. 5.3 STM images for Au nanoparticles modified TiO_2 (110) single crystal

Figure 5.4 shows the 3D images for the Au nanoparticles on TiO_2 (110) surface. It can be observed from the images that the ligand protected Au nanoparticles are approximately 1.5 nm in height. One cannot use STM image to measure the precise diameter of the nanoparticles due to the inaccuracy of the distance between the tip and the sample steps edges. It is important to point out that the size of the nanoparticle showed on the STM images does not reflect the actual gold cluster size but the one derived from ligand protected gold.

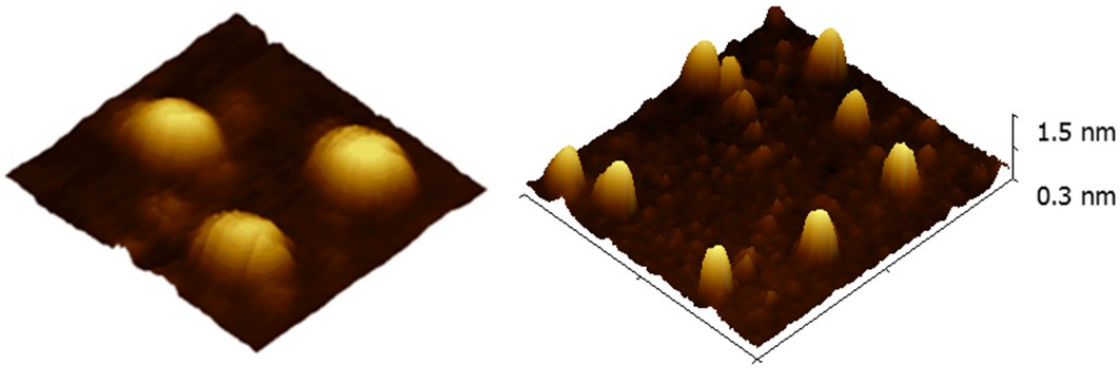

Fig. 5.4 3D STM images for Au modified TiO_2 (110) single crystal

Density functional theory (DFT) study of the sub-nm Au nanoparticles was conducted by Yan Li et al. in Brookhaven National Laboratory. Figure 5.5 shows the DFT-optimized geometries of Au nanoparticles. In theory, we gave out 4 different possible Au_n (n=11) structures. In these 4 possible structures, we can get the energy state of each structure and determine which one has the highest potential to become the most likely geometry for the A_{11} nanoparticles. Since the flatter geometry structured Au has smaller energy values, (Eg (a) =1.0< Eg(c) =1.2 < Eg (b) =1.7 < Eg (d) =2.1), we can concluded that there is a substantial difference in both shape and electronic properties between charged and neutral bare Au clusters as well as between bare and ligand-protected ones which might affect the shape of supported co-catalysts. It is important to point out that the surface termination also has significant influence on the shape/dimension of the Au cluster.

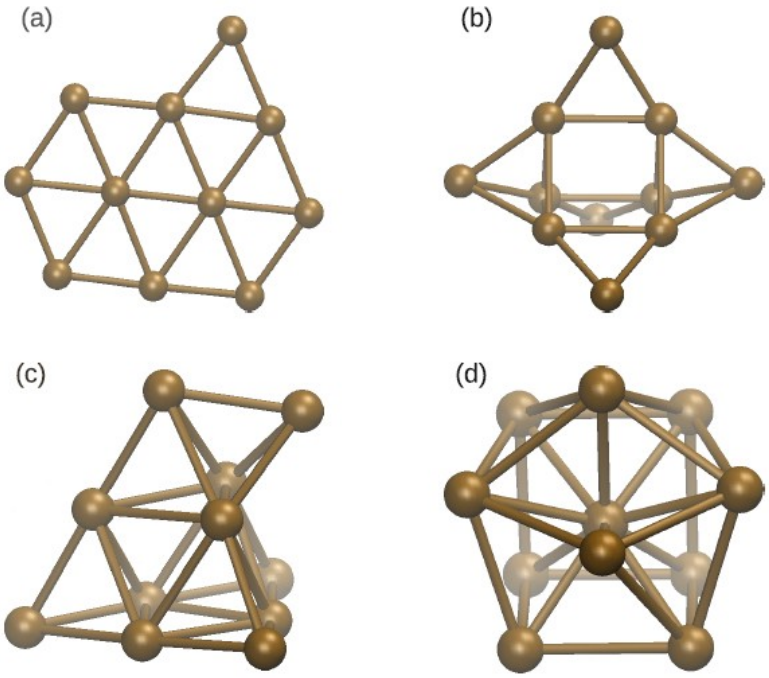

Fig. 5.5 DFT-optimized geometries of Au clusters: (a) bare Au_{11}^- and Au_{11}^0, (b) bare Au_{11}^+, (c) bare Au_{11}^{3+} and (d) $[Au_{11}(PH_3)_8Cl_2]^+$ and $[Au_{11}(PH_3)_{10}]^{3+}$ (only Au atoms are shown).

Figure 5.6 shows the comparison between the experimental UV-Vis spectra and the theoretical computed optical spectra for ligand-protected $Au11^{+}$ and $Au9^{+}$ clusters. It demonstrates the fact that they are in reasonable agreement with each other. Also, the fact that theory can be used to confirm and explain the physical origins of the peaks in the observed UV-vis is extremely promising development.

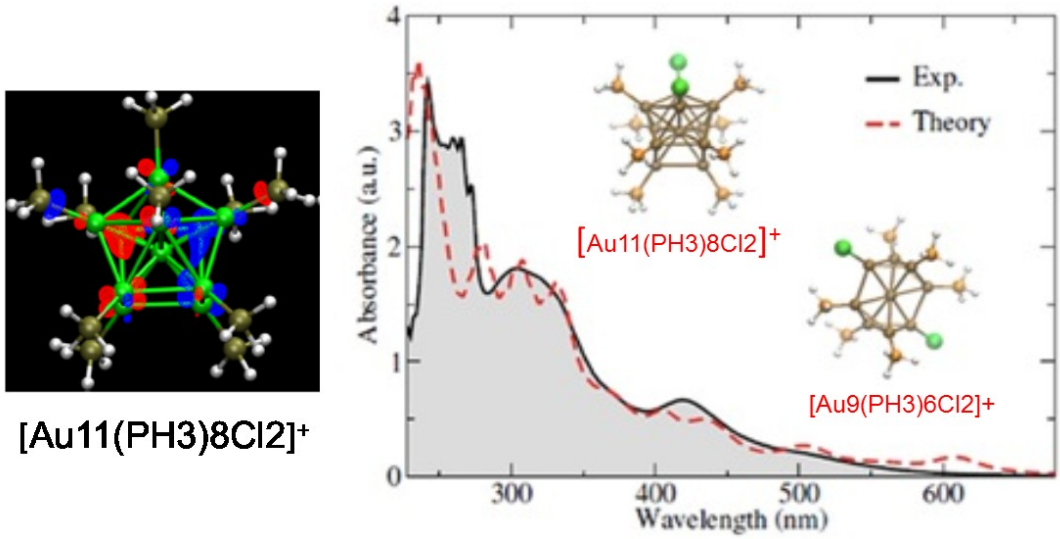

Fig. 5.6 computed optical absorption spectra (red line) in comparison with experimental UV-Vis spectrum (dark line)

Based on preliminary DFT calculations, Au11 nanoparticles possess non-metallic properties, as highlighted by significant HOMO-LUMO separation. Although no detailed mechanistic explanation for charge transfer between Au and TiO2 is available, one might invoke an analogy of semiconductor-semiconductor photocatalytic system. The coupling of two semiconductors having different energy levels for their corresponding conduction and valence bands can lead to formation of the interfacial charge transfer and band bending. Such process can increase the charge lifetime due to enhanced charge transfer and better charge separation in the system. There are two different cases in such a system: only one semiconductor is illuminated and activated, and both two semiconductor are illuminated and activated. In the first case, given the right alignment of conduction and valence bands, the electrons generated in the illuminated

semiconductor with the conduction band is more negative transfer to the inactive semiconductor leaving the holes in the activated semiconductor. When both semiconductors are illuminated and activated, photoelectrons will accumulate at the semiconductor with higher conduction band, while positive holes will accumulate at the one with lower valence band. Such charge transfer in both cases can yield an irreversible vectorial transfer under certain conditions. In both cases, charge separation is enhanced. It is quite possible that in case of Au-TiO_2 system both gold and TiO_2 are activated to achieve this outstanding catalytic effect, however, this needs to be further studied using both theoretical and experimental tools.

5.3.2 Size dependency study for catalytic performance

High-resolution TEM analysis was carried out in JEOL 3000F instrument (300 keV), which is located at the Center for Functional Nanomaterials (CFN), Brookhaven National Laboratory.

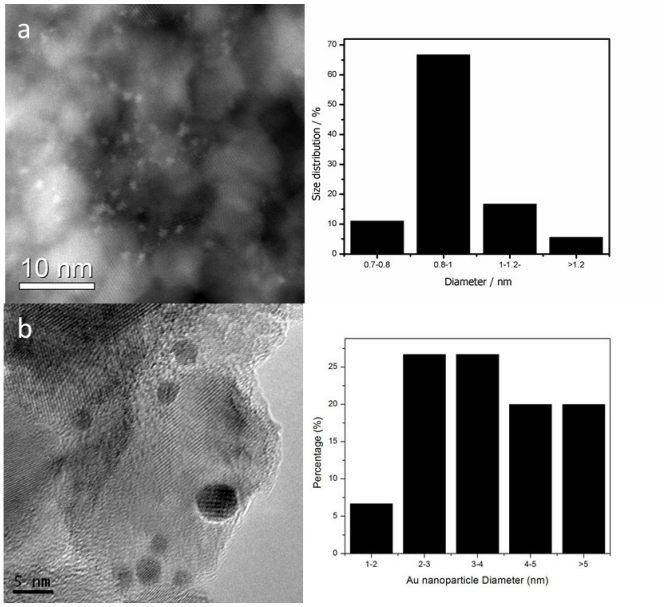

Fig. 5.7 TEM images of: (a) Sub-nanometer Au-TiO_2; (b) regular size Au-TiO_2 with size distributions

The TEM images of the gold nanoparticles supported on TiO_2 and their size distribution histograms are shown in Figure 5.7. Two types of samples were prepared: one with regular (above 1 nm) size of gold and another one with sub-nm size. Two different procedures were employed to make the nanoparticles. One was to utilize ligand exchange reaction described previously to achieve sub-nm dimensions, while surfactant based method of synthesis was used to make above-1 nm samples. The results in Figure 5.7 demonstrate a successful modification of TiO_2 surfaces with Au nanoparticles ranging from 1 to 6 nm for larger gold and from 0.7 to 1.2 nm for sub-nm gold samples. The average size of the sub-nm Au was 0.96 nm and the regular size Au is around 3.6 nm. Both the particle size distributions indicate that both sub-nm and regular size Au nanoparticles were uniformly dispersed on the support and no significant agglomeration has occurred after the polymer removal.

5.3.2.1 Gas phase catalytic activity

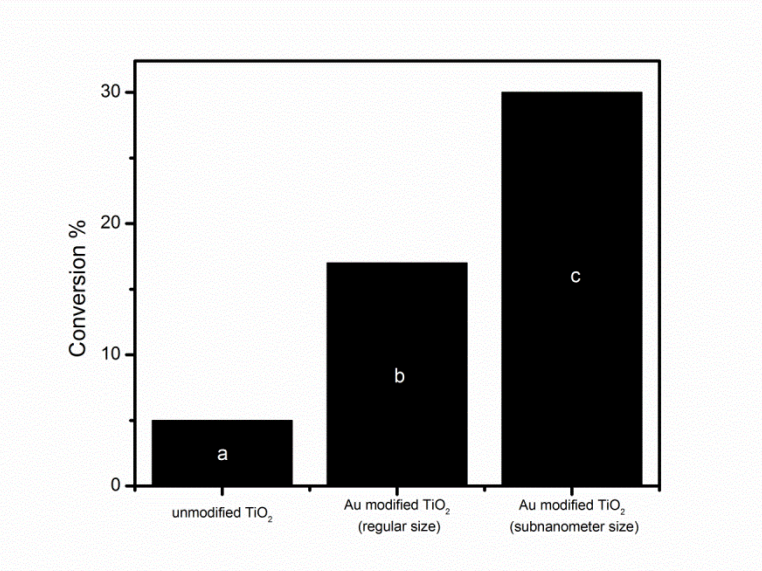

Fig. 5.8 Photocatalytic conversion of NO_2 by: (a) unmodified TiO_2; (b) 1 wt. % of regular size Au-TiO_2; (c) 1 wt. % of sub-nm Au-TiO_2

In order to develop a comprehensive picture of catalytic behavior of Au nanoparticles as a function size, we conducted both gas and liquid phase reaction experiments. The gas phase data for NO_2 conversion on Au modified (1 wt. %) and unmodified TiO_2 catalysts exposed to the UV light are shown in Figure 5.8. It is obvious to see both sub-nm and regular size Au modified catalysts exhibited an increase in activity, albeit to a different degree. The sub-nm Au modified TiO_2 showed approximately 6 times increase in activity as compared to that of unmodified sample. The sample modified with larger Au particles exhibited an increase in NO_2 conversion by a factor of 3. There are several reasons lead to this outstanding increase compared with two different Au nanoparticles. First, superior catalytic properties can arise due to the difference of the metal particle size which gives nanoparticles increased surface to volume ratios. The size of the Au is thus crucial to its catalytic properties. Another factor causing this drastic catalytic increase for sub-nm range of Au nanoparticles is its shape effect. The sub-nm Au can potentially show a 2 D “flat shaped” geometry according to the DFT calculation while regular size Au remains a 3 D geometry. Several studies demonstrated that different shapes contain different number of binding sites for the gold, which gives different reaction pathways [40]. As observed in the DRIFTS results, for regular size Au only oxidation reaction was discovered during the NO_2 removal. However, NO was detected for the sub-nm Au modified TiO_2 which suggest that both oxidation and reduction pathways for NO_2 removal were present.

5.3.2.2 Liquid phase catalytic activity

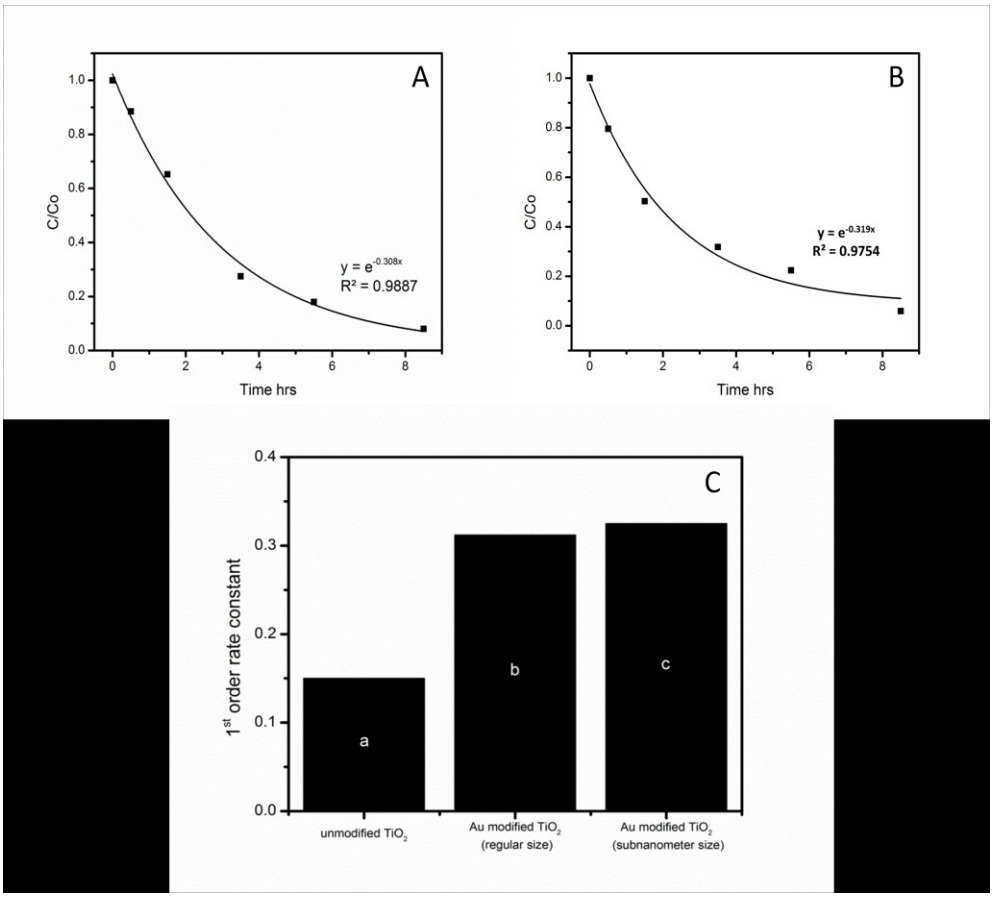

Fig. 5.9 A,B) Time dependence phenol oxidation of regular size Au-TiO_2 and sub-nm Au-TiO_2. C) Photocatalytic rate constant by: (a) unmodified TiO_2; (b) 1 wt. % of regular size Au-TiO_2; (c) 1 wt. % of sub-nm Au-TiO_2

Similarly, there was also a significant increase in activity for phenol degradation due to modification with Au as compared to the unmodified TiO_2. The 1 wt. % Au modified the catalyst results in more than doubling of the first order rate constant as compared of the plain TiO_2. This behavior was consistent with the studies, where a comparable increase in activity for phenol and chlorophenol photocatalytic degradation was observed [37-39]. However, the difference in behavior of Au particle in sub-nm range vs. regular size range was not significant (within the error bar value) in case of phenol oxidation reaction, which is totally different to the behavior of Au nanoparticles in NO_2 oxidation reaction. When the Au nanoparticle size is reduced to sub-nm range is that it no longer remains metallic. Instead, it shows HOMO-LUMO gap which can be interpreted as loss of

metallic properties. Therefore, sub-nm Au modified TiO_2 can be interpreted as a semiconductor-semiconductor system and can initiate a total different reaction mechanism as compared to the metallic Au modified TiO_2. The difference in catalytic behavior for phenol and NO_2 removal is also significant. The increased activity for NO_2 removal for sub-nm Au can be attributed to an extra reduction reaction pathway related to NO_2 transformation to NO. However, there is no reduction reaction pathways appear to be present in case of phenol removal perhaps due to a different position of redox potential for this reaction. This might account for a comparable activity in catalytic phenol removal reaction for both regular and sub-nm Au nanoparticles.

5.4 Conclusion

Sub-nm Au clusters were deposited on TiO_2 single crystal (110) and imaged using STM. TiO_2 powder samples show significant improvement when deposited with Au nanoparticles in liquid phase oxidation reaction with phenol. Moreover, we also found that sub-nm Au shows a very different reaction mechanism as compared to that for larger particles in gas phase.

Reference:

[1] H. Feng, J.A. Libera, P.C. Stair, J.T. Miller, J.W. Elam, Subnanometer Palladium Particles Synthesized by Atomic Layer Deposition, Acs Catal, 1 (2011) 665-673.

[2] M. Chatterjee, Y. Ikushima, Y. Hakuta, H. Kawanami, In situ synthesis of gold nanoparticles inside the pores of MCM-48 in supercritical carbon dioxide and its catalytic application, Adv Synth Catal, 348 (2006) 1580-1590.

[3] J.R. Croy, S. Mostafa, L. Hickman, H. Heinrich, B.R. Cuenya, Bimetallic Pt-Metal catalysts for the decomposition of methanol: Effect of secondary metal on the oxidation state, activity, and selectivity of Pt, Appl Catal a-Gen, 350 (2008) 207-216.

[4] H. Vijwani, S.M. Mukhopadhyay, Palladium nanoparticles on hierarchical carbon surfaces: A new architecture for robust nano-catalysts, Appl Surf Sci, 263 (2012) 712-721.

[5] E. Castillejos, E. Gallegos-Suarez, B. Bachiller-Baeza, R. Bacsa, P. Serp, A. Guerrero-Ruiz, I. Rodriguez-Ramos, Deposition of gold nanoparticles on ZnO and their catalytic activity for hydrogenation applications, Catal Commun, 22 (2012) 79-82.

[6] K. Kwon, S.A. Jin, C. Pak, H. Chang, S.H. Joo, H.I. Lee, J.H. Kim, J.M. Kim, Enhancement of electrochemical stability and catalytic activity of Pt nanoparticles via strong metal-support interaction with sulfur-containing ordered mesoporous carbon, Catal Today, 164 (2011) 186-189.

[7] H.R. Choi, H. Woo, S. Jang, J.Y. Cheon, C. Kim, J. Park, K.H. Park, S.H. Joo, Ordered Mesoporous Carbon Supported Colloidal Pd Nanoparticle Based Model Catalysts for Suzuki Coupling Reactions: Impact of Organic Capping Agents, Chemcatchem, 4 (2012) 1587-1594.

[8] M.J. Weber, A.J.M. Mackus, M.A. Verheijen, C. van der Marel, W.M.M. Kessels, Supported Core/Shell Bimetallic Nanoparticles Synthesis by Atomic Layer Deposition, Chem Mater, 24 (2012) 2973-2977.

[9] F.P. Hu, P.K. Shen, Y.L. Li, J.Y. Liang, J. Wu, Q.L. Bao, C.M. Li, Z.D. Wei, Highly Stable Pd-Based Catalytic Nanoarchitectures for Low Temperature Fuel Cells, Fuel Cells, 8 (2008) 429-435.

[10] D.D. Das, A. Sayari, Applications of pore-expanded mesoporous silica 6. Novel synthesis of monodispersed supported palladium nanoparticles and their catalytic activity for Suzuki reaction, J Catal, 246 (2007) 60-65.

[11] R. Narayanan, M.A. El-Sayed, Carbon-supported spherical palladium nanoparticles as potential recyclable catalysts for the Suzuki reaction, J Catal, 234 (2005) 348-355.

[12] C.M.Y. Yeung, S.C. Tsang, Noble Metal Core-Ceria Shell Catalysts For Water-Gas Shift Reaction, J Phys Chem C, 113 (2009) 6074-6087.

[13] T. Xu, C.K. Lin, C. Wang, D.L. Brewe, Y. Ito, J. Lu, Synthesis of Supported Platinum Nanoparticles from Li-Pt Solid Solution, J Am Chem Soc, 132 (2010) 2151-+.

[14] F. Behafarid, B.R. Cuenya, Nanoepitaxy Using Micellar Nanoparticles, Nano Lett, 11 (2011) 5290-5296.

[15] J.A. Enterkin, K.R. Poeppelmeier, L.D. Marks, Oriented Catalytic Platinum Nanoparticles on High Surface Area Strontium Titanate Nanocuboids, Nano Lett, 11 (2011) 993-997.

[16] O. Lopez-Acevedo, K.A. Kacprzak, J. Akola, H. Hakkinen, Quantum size effects in ambient CO oxidation catalysed by ligand-protected gold clusters, Nat Chem, 2 (2010) 329-334.

[17] J.Y. Park, C. Aliaga, J.R. Renzas, H. Lee, G.A. Somorjai, The Role of Organic Capping Layers of Platinum Nanoparticles in Catalytic Activity of CO Oxidation, Catal Lett, 129 (2009) 1-6.

[18] N. Semagina, L. Kiwi-Minsker, Palladium Nanohexagons and Nanospheres in Selective Alkyne Hydrogenation, Catal Lett, 127 (2009) 334-338.

[19] K. An, G.A. Somorjai, Size and Shape Control of Metal Nanoparticles for Reaction Selectivity in Catalysis, Chemcatchem, 4 (2012) 1512-1524.

[20] P. Alexandridis, Gold Nanoparticle Synthesis, Morphology Control, and Stabilization Facilitated by Functional Polymers, Chem Eng Technol, 34 (2011)

15-28.
[21] D.Y. Murzin, Kinetic analysis of cluster size dependent activity and selectivity, J Catal, 276 (2010) 85-91.
[22] A.Z. Li, J.X. Zhao, D.T. Pierce, Silica nanoparticles for template synthesis of supported Pt and Pt-Ru electrocatalysts, J Colloid Interf Sci, 351 (2010) 365-373.
[23] Y.X. Zhang, H.L. Ding, Y.Y. Liu, S.S. Pan, Y.Y. Luo, G.H. Li, Facile one-step synthesis of plasmonic/magnetic core/shell nanostructures and their multifunctionality, J Mater Chem, 22 (2012) 10779-10786.
[24] R. Narayanan, M.A. El-Sayed, Catalysis with transition metal nanoparticles in colloidal solution: Nanoparticle shape dependence and stability, J Phys Chem B, 109 (2005) 12663-12676.
[25] R. Ma, N. Semagina, Nanoparticle Shape Effect Study as an Efficient Tool to Reveal the Structure Sensitivity of Olefinic Alcohol Hydrogenation, J Phys Chem C, 114 (2010) 15417-15423.
[26] H.B. Pan, C.M. Wai, One-Step Synthesis of Size-Tunable Rhodium Nanoparticles on Carbon Nanotubes: A Study of Particle Size Effect on Hydrogenation of Xylene, J Phys Chem C, 114 (2010) 11364-11369.
[27] F. Lu, Y. Zhang, L.H. Zhang, Y.G. Zhang, J.X. Wang, R.R. Adzic, E.A. Stach, O. Gang, Truncated Ditetragonal Gold Prisms as Nanofacet Activators of Catalytic Platinum, J Am Chem Soc, 133 (2011) 18074-18077.
[28] O.D. Lyons, N.E. Musselwhite, L.M. Carl, K.A. Manbeck, A.L. Marsh, Synthesis, Characterization, and Reaction Studies of a PVP-Capped Platinum Nanocatalyst Immobilized on Silica, Langmuir, 26 (2010) 16481-16485.
[29] A.B.R. Mayer, Formation of noble metal nanoparticles within a polymeric matrix: nanoparticle features and overall morphologies, Mat Sci Eng C-Bio S, 6 (1998) 155-166.
[30] N. Clement, G. Patriarche, K. Smaali, F. Vaurette, K. Nishiguchi, D. Troadec, A. Fujiwara, D. Vuillaume, Large Array of Sub-10-nm Single-Grain Au Nanodots for use in Nanotechnology, Small, 7 (2011) 2607-2613.
[31] M.P. Mallin, C.J. Murphy, Solution-phase synthesis of sub-10 nm Au-Ag alloy nanoparticles, Nano Lett, 2 (2002) 1235-1237.

[32] E.M. Fernandez, J.M. Soler, L.C. Balbas, Planar and cagelike structures of gold clusters: Density-functional pseudopotential calculations, Phys Rev B, 73 (2006).

[33] I. Lee, R. Morales, M.A. Albiter, F. Zaera, Synthesis of heterogeneous catalysts with well shaped platinum particles to control reaction selectivity, P Natl Acad Sci USA, 105 (2008) 15241-15246.

[34] S. Mostafa, F. Behafarid, J.R. Croy, L.K. Ono, L. Li, J.C. Yang, A.I. Frenkel, B.R. Cuenya, Shape-Dependent Catalytic Properties of Pt Nanoparticles, J Am Chem Soc, 132 (2010) 15714-15719.

[35] B.R. Cuenya, J.R. Croy, S. Mostafa, F. Behafarid, L. Li, Z.F. Zhang, J.C. Yang, Q. Wang, A.I. Frenkel, Solving the Structure of Size-Selected Pt Nanocatalysts Synthesized by Inverse Micelle Encapsulation, J Am Chem Soc, 132 (2010) 8747-8756.

[36] A. Cho, Connecting the dots to custom catalysts, Science, 299 (2003) 1684-1685.

[37] M.A. Centeno, M.C. Hidalgo, M.I. Dominguez, J.A. Navio, J.A. Odriozola, Titania-supported gold catalysts: Comparison between the photochemical phenol oxidation and gaseous CO oxidation performances, Catal Lett, 123 (2008) 198-206.

[38] A. Orlov, M.S. Chan, D.A. Jefferson, D. Zhou, R.J. Lynch, R.M. Lambert, Photocatalytic degradation of water-soluble organic pollutants on TiO2 modified with gold nanoparticles, Environ Technol, 27 (2006) 747-752.

[39] M.A. Debeila, N.J. Coville, M.S. Scurrell, G.R. Hearne, The effect of calcination temperature on the adsorption, of nitric oxide on Au-TiO2: Drifts studies, Appl Catal a-Gen, 291 (2005) 98-115.

[40] MB, Boucher; S. Goergen;N. Yi, M. Flytzani-Stephanopoulos, 'Shape effects' in metal oxide supported nanoscale gold catalysts, Phys. Chem. Chem. Phys., 13 (2011) 2517-2527.

Chapter 6. Experimental demonstration of beneficial effects of sub-nanometer platinum particles for photocatalysis

6.1 Introduction

Catalytic applications of metal nanoparticles have been an exciting area of chemistry research, leading to many promising applications [1-4]. It is also known that light induced catalytic reactions (i.e. photocatalysis) can be enhanced by modifying the semiconductor surfaces with metal nanoparticles [5-14]. These studies showed that catalytic behaviour of metal nanoparticles exhibits a strong size dependency, which can be used to tune these reactive interfaces to achieve high activity and selectivity for various types of reactions [15-18]. These adjustments to nanoparticles size can be accomplished by several synthetic procedures described in the recent literature [19-22].

In addition to controlling size of nanoparticles, another potentially transformative idea is to independently control particle sizes and shapes. This approach may offer additional means for producing a new generation of very active catalysts [19]. For example, the particle shape in micelle-templated nanoparticle synthesis can be tuned by altering micelle shapes. This can be achieved by introducing various salts to initiate a preferential crystal growth via selective capping mechanism coupled with reverse micelles based synthesis in a supersaturated regime [23, 24]. One interesting example of controlling nanoparticles size and shape is given in the recent publication by Cuenya *et al.,* where sub-nm Pt particles of different shapes were synthesized by controlling the metal-salt/polymer-head ratio in the reverse micelles solutions [25, 26]. The catalytic activities of these particles were tested for selective oxidation of propanol, where the highest activity was observed for 2D bilayer nanoparticles. However, the above mentioned approach of controlling the nanoparticle shape has never been applied for photocatalytic reactions.

It is well known that modification of powder semiconductor photocatalysts with metal nanoparticles can often lead to substantial increase in catalytic activity for various reactions [27-29]. However, surface modification with such noble

metals as Pt appears to produce mixed results. For example, some publications concluded that Pt had a negative impact on TiO_2 photocatalytic activity for phenol oxidation reaction [30, 31], whereas Kowalska *et al.* Found that Pt can actually increase photocatalytic activity of TiO_2 for the same reaction [32]. Similarly to Kowalska's work, enhancements due to Pt deposition have been also observed in other photocatalytic oxidation reactions [33-35].

Given the issues discussed above, this work has focused on several unexplored areas of Pt modified TiO_2 catalysis. Firstly, it explores sub-nm range of Pt nanoparticles, which is a new approach to tuning the photocatalytic activity. Secondly, this work focuses on both gas phase and liquid phase oxidation reaction to assess the enhancement effect of Pt for two distinctly different photocatalytic systems. Phenol photocatalytic degradation is a very well known approach of removing a pollutant of a significant environmental concern [36]. Similarly, the gas phase reaction is focused on NO_2, which is well known priority pollutant of a substantial concern for air quality. Thirdly it concentrates on Pt nanoparticles of flat geometry following the recent developments by Cuenya et al [25, 26], which is a completely unexplored approach in photocatalytic area. Fourthly, it assesses the advantages of sub-nm particles versus the larger ones for two different reactions. And lastly, this project uses a very innovative methodology for *in-situ* gas phase composition analysis coupled with simultaneous observations of surface adsorbed species using the UV light modified Diffuse Reflectance Fourier Transform Spectroscopy (DRIFTS) unit [37]. This analytical approach allowed us to observe photocatalytic reactions in real time to understand both surface and gas phase processes.

6.2 Experimental

6.2.1 Preparation of sub-nm Pt nanoparticles

TiO_2 used in our experiments was P25, which consisted of both rutile and anatase phases of titania in approximately 80/20 ratio. The P25 point of zero charge (pzc) is 6.8 ± 0.2 as described in several literature sources [38, 39]. Sub-nm Pt NPs were synthesized by a modified inverse micelle encapsulation method, which can achieve a high degree of uniformity of particle size [25, 26]. The synthetic steps to make Pt-TiO_2 are described in supplementary information. More specifically, diblock copolymers Poly(styrene)-block-poly-(2vinylpyridine) were dissolved in a nonpolar solvent (toluene), thereby inducing formation of spherical nanocages known as reverse micelles. The size-selectivity of Pt NPs was achieved by modifying metal-salt/polymer-head (P2VP) ratio [40]. In order to attain a sub-nm size of the Pt NPs, the molar ratio of $H_2PtCl_6 \cdot 6H_2O$ to P2VP selected for our study was 0.1. This preparation procedure was followed by the NPs deposition on powder TiO_2 (P25, Sigma Aldrich) , where we prepared 0.5, 1 and 2 wt. % Pt modified samples. All the samples were then stir-dried overnight followed by encapsulating polymer removal (400 °C, 24 hrs.) in *vacuo.* The samples were then reduced in H_2 at 400 °C for 2 hrs and characterized by the Scanning Transmission Electron Microscope (STEM, Hitachi HD2700C).

6.2.2 Preparation of regular size Pt nanoparticles

The regular size Pt nanoparticles were synthesized and deposited by a modified photodeposition method [41]. Various ratios of H_2PtCl_6 and TiO_2 were added into a customized reactor, where 20 vol % of methanol was put in as a sacrificial reagent. The reactor was illuminated by a 300 W Xenon lamp (>320nm), while the solution was continuously stirred for 1h. The platinum particles deposited onto the TiO_2 surface occurred via photoreduction mechanism. The resulting products were collected, filtered on 0.45 μm filters, washed with DI water 3 times and dried in oven at 60 °C for 6 hrs. The size distribution of the Pt nanoparticles was investigated in the Transmission Electron

Microscope (TEM, JEOL JEM-2100F). The XRD patterns of P25 TiO_2 and Pt-TiO_2 have been described elsewhere [42]. Given low loading and small size of platinum particles, there were no characteristic peaks attributed to Pt for both regular and sub-nm size Pt-TiO_2 samples. Similarly, no distinct differences in BET surface area for P25 and the platinum modified TiO_2 were observed.

6.2.3 Photocatalytic testing in phenol oxidation reaction

The Pt-TiO_2 catalysts were tested in both liquid and gas phases for oxidation reaction of phenol and NO_2 respectively. The liquid phase phenol oxidation experiment was carried out in a custom made temperature controlled Pyrex reactor. The UV light source was Xenon lamp (Newport Model 67005) modified with optical filters (λ>320 nm, Edmund Optics). A water filter was also introduced to eliminate the IR part of irradiation. The original concentration of the phenol is 20 mg/L. The initial pH for the phenol solution was 5.5. Then the liquid phenol samples were periodically withdrawn from the solution and transferred to HPLC vials. A further analysis was conducted by using Agilent 1200 HPLC for concentration determination.

6.2.4 Photocatalytic testing in NO_x oxidation reaction

The gas phase photocatalytic reaction was conducted in our custom modified environmental chamber, which was incorporated into the Diffuse Reflectance Fourier Transform (DRIFT) spectrometer. We used 4000-600 cm^{-1} spectral range averaged over 32 scans with a resolution of 4 cm^{-1}. The UV light was delivered to the sample surface through a fiber optics system. This system, based on a Smart Collector optical assembly, represents a significant improvement in its analytical capabilities as compared to a regular DRIFT

system. This setup can perform not only the gas phase analysis but also a simultaneous observation of surface adsorbed reaction products. The sample that exhibited the highest activity for phenol oxidation (1 wt. % Pt modified TiO_2) was loaded into the environmental chamber. It was then exposed to NO_2 concentration of 3.21 ppm, while humidity was maintained at 30-35% RH. The rationale for choosing these levels of humidity was based on our previous experiments for NO_2 conversion on P25-TiO_2, where we did not observe significant differences in NO_2 conversion rates in 20-70% RH range. The IR spectra showing the surface mediated conversion of NO_2 to nitrates and nitrites were taken *in-situ* during the course of the experiment. The gas phase concentration of NO_2 under UV illumination was monitored by the NO_x analyser (Teledyne Instruments Model 200E).

6.3 Results and Discussion

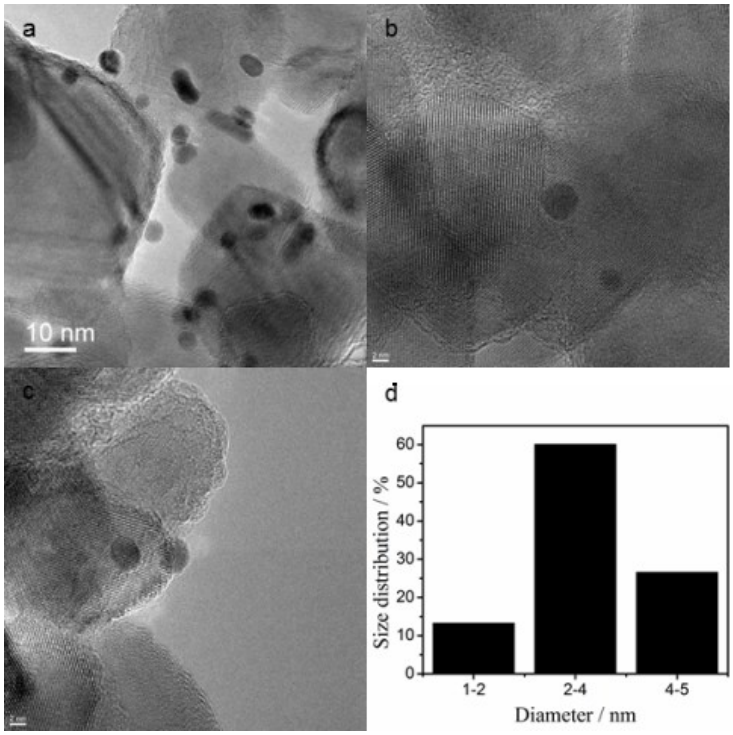

Fig. 6.1 (a,b,c): TEM images of 1 wt. % of regular size Pt-TiO_2; (d): Pt nanoparticles size distribution (Particle size distribution was based on several TEM images)

Several samples with different loadings and particle sizes were synthesized. They included both regular and sub- nm Pt nanoparticles deposited on TiO_2. Two different methods of preparation employed in this work included inverse micelle encapsulation and photodeposition methods. Figure 6.1 shows the TEM image of Pt nanoparticles supported on TiO_2, which were synthesized by photodeposition method. The corresponding histogram shown in Figure 1d indicates that the average size of the Pt particles is 3.3 nm. This particle size is consistent with the previously published data, where the authors used a similar synthetic method [41]. Figure 6.2 shows the STEM images of sub-nm platinum nanoparticles supported on TiO_2, which were prepared by the inverse micelle encapsulation method. The preparation conditions chosen for synthesis were aimed at achieving a flat geometry of Pt nanoparticles, as described by Cuenya *et al* [43]. The particle size distribution (Figure 1d) indicates that Pt nanoparticles were uniformly dispersed on the support and no significant agglomeration has occurred after the polymer removal. The average size of the Pt nanoparticles was 0.85 nm. In order to understand the reactivity of Pt particles we tested the prepared photocatalysts for liquid and gas phase oxidation reactions, such as liquid phase oxidation of phenol and gas phase oxidation of NO_2. Our results indicate a markedly different behaviour of Pt nanoparticles in these two reactions. Moreover, they also indicate that size of Pt nanoparticles has a pronounced effect on the photocatalytic activity.

6.3.1 Liquid phase catalytic activity

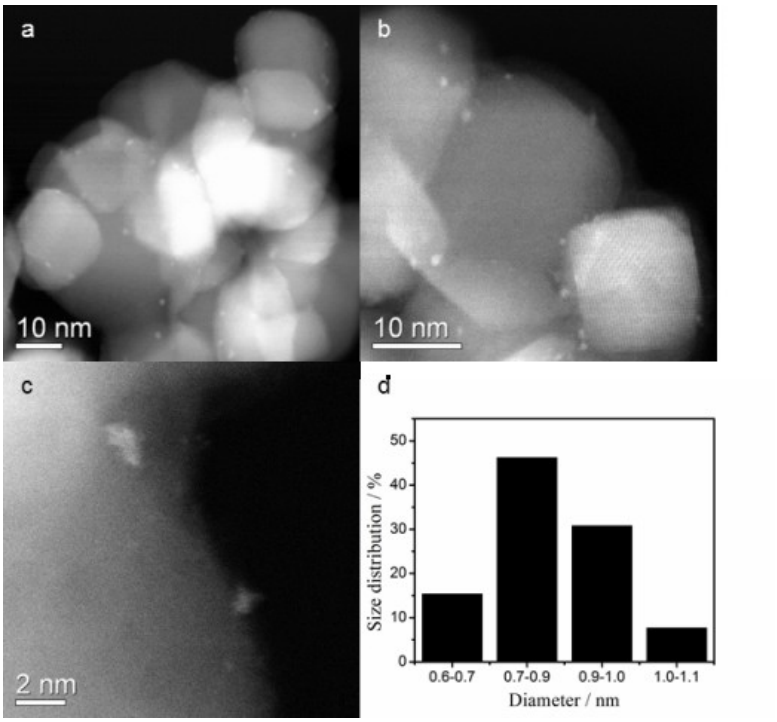

Fig. 6.2 (a,b,c): STEM images of 1 wt. % of sub-nm Pt-TiO_2; (d): Pt nanoparticles size distribution.

Figure 6.3 shows the photocatalytic activities of our catalysts for different loadings of sub-nm Pt. The highest catalytic activity was observed at 1 wt. % of the Pt loading. Increasing the Pt loading beyond 1 wt. % resulted in a decrease of activity. The improvement in phenol oxidation rate constant by a factor of 4 is quite substantial, especially given the fact that relatively modest Pt loadings were used.

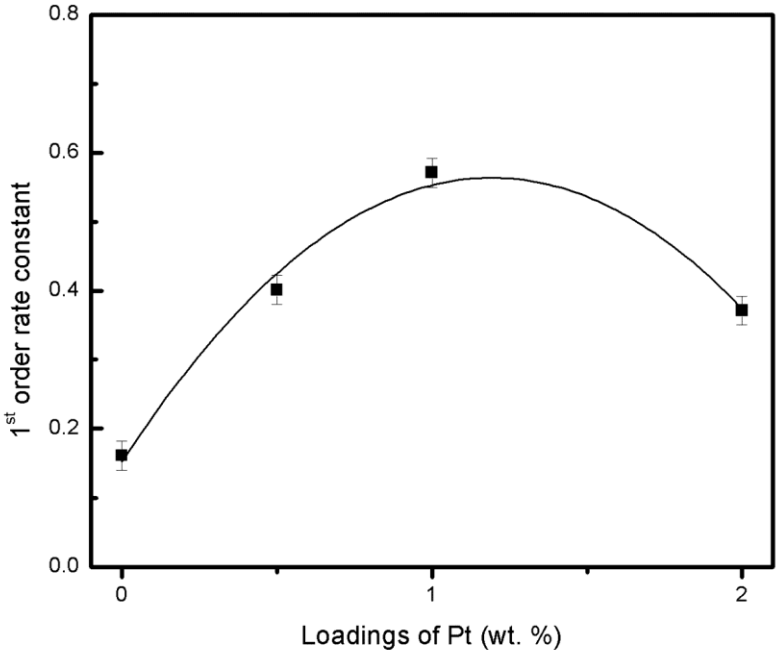

Fig. 6.3 Photocatalytic activity of sub-nm Pt -TiO_2 for phenol oxidation at different Pt loadings (0.5, 1 and 1 wt. %)

Part A of the Figure 6.4 shows the time dependent phenol conversion and catechol production for sub-nm and regular size Pt modified TiO_2 (1wt. %). The R^2 values for exponential dependence were 0.9953 for sub-nm Pt-TiO_2 and 0.989 for regular size Pt-TiO_2 indicating that the data can be well described by a pseudo first order kinetics. Catechol is an intermediate product of phenol oxidation, which implies that phenol disappearance is not merely due to the phenol adsorption. This data also indicate a very good correspondence between phenol disappearance and catechol production, where a more active catalyst as measured by phenol conversion had also a much higher activity for catechol production. Part B of the Figure 6.4 shows a comparison of photocatalytic activities of TiO_2 P25, 1 wt. % of sub-nm Pt modified TiO_2 and a regular size Pt -TiO_2. As compared to unmodified TiO_2, the photocatalytic activity of larger Pt

nanoparticles has decreased by 30%, to the catalytic behaviour of the sub-nm Pt particles described above. These observations provide a novel insight into size-dependent activity of Pt nanoparticles in the photocatalytic reactions, which are not dissimilar to observations of Pt behaviour in oxidation reactions conducted in the absence of light [25, 26]. Moreover, our results also provide an important interpretation of some of the discrepancies found in Pt-TiO_2 literature, where authors came up with contradictory conclusions about the benefits of using Pt to increase the photocatalytic activity. Given that imaging of the sub-nm Pt is not always trivial for regular TEM as compared to STEM, and such particles might be present in the catalysts described in above-mentioned literature; it is quite conceivable that the role of these nanoparticles for activity enhancement is overlooked in the published data. It appears that the presence of sub-nm Pt in the sample can be the main factor contributing to substantial catalytic activity enhancement. This is also consistent with other published catalytic work where the beneficial properties of sub-nm Pt particles were observed for 2-propanol oxidation reaction in the absence of light [26]. Given all of the above, we believe that our results present the first ever experimental observation of beneficial effects of sub-nm Pt particles in photocatalytic reactions.

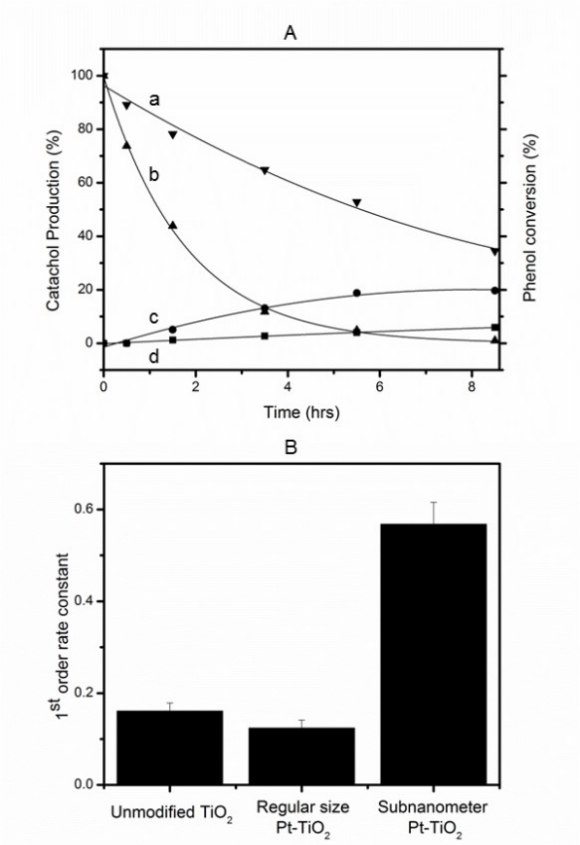

Fig. 6.4 (A) Time dependent phenol conversion of (a) regular size Pt-TiO_2; (b) sub-nm Pt-TiO_2 and catechol production of (c) sub-nm Pt - TiO_2; (d) regular size Pt-TiO_2; (B) Photocatalytic activity comparison of the TiO_2 P25, 1 wt. % of sub-nm and regular size Pt -TiO_2 for phenol oxidation reaction

6.3.2 Gasphase catalytic activity

In order to develop a more comprehensive picture of sub-nm Pt behaviour in photocatalytic reactions, we also conducted gas phase photocatalytic oxidation experiments. The gas phase data for NO_2 conversion on Pt modified (1 wt. %) and unmodified TiO_2 catalysts exposed to the UV light are shown in Figure 6.5 In contrast to liquid phase data, both sub-nm and regular size Pt modified catalysts exhibited an increase in activity, albeit to a different degree. The sub-nm Pt modified TiO_2 showed approximately 5 times increase in activity as compared to that of unmodified sample. The sample modified with larger Pt particles exhibited

an increase in NO_2 conversion by a factor of 2, which is completely different from 30% decrease in phenol oxidation rate for the same sample. It appears that the behaviour of Pt might be dissimilar for different types of photocatalytic reactions and might also depend on the reaction medium (gas phase vs. liquid phase). It is important to mention that the NO_2 photocatalytic oxidation experiments were conducted in a unique Diffuse Reflectance Fourier Transform Spectroscopy (DRIFTS) system, which was custom-modified with fiber coupled to UV diode (λ=365 nm, 50 mW). A notable advantage of this system as compared to any other photocatalytic setups is in its capability of the real time monitoring of the surface adsorbed products, which is highly complementary to the gas phase chemical composition data.

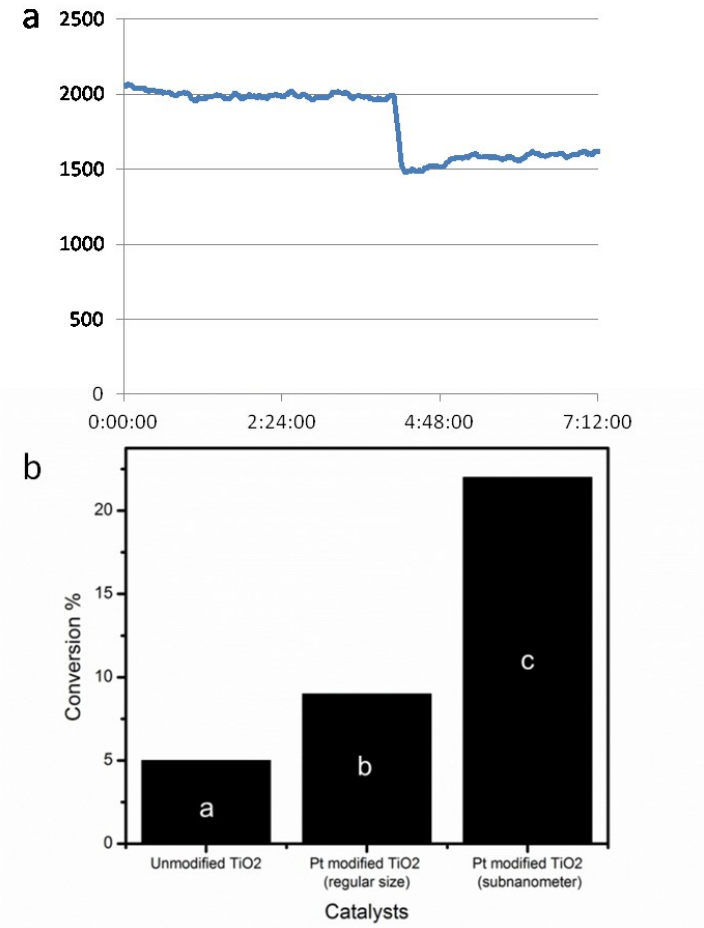

Fig. 6.5 a) Time dependent NO_2 for 1 wt. % sub-nm Pt-TiO_2, b) Photocatalytic conversion of NO_2 by: (a) unmodified TiO_2; (b) 1 wt. % of regular size Pt-TiO_2; (c) 1 wt. % of sub-nm Pt-TiO_2.

Figure 6.6 shows time resolved DRIFTS spectra of sub-nm and regular size Pt modified catalysts exposed to NO_2 under UV illumination. The 3-D spectra clearly indicate a substantial photocatalytic activity of both catalysts, with the inflection point noticeably coinciding with the start of illumination. The data also shows a substantially higher concentration of the reaction products adsorbed on the surface of sub-nm Pt-TiO_2 catalyst as evident by a much higher IR absorbance for this catalyst. This is consistent with the substantially enhanced gas phase NO_2 conversion for the same sample as compared to other catalysts (Figure 6.5). Each peak in Figure 6.6 signifies surface adsorbed reaction products, such as nitrite, nitrate and nitrosyl species. Our own observations, as well as literature data, point out several potentially important pathways for NO_2 reactions on UV-light activated TiO_2. For example, both oxidation and reduction pathway for NO_2 and NO_3 adsorbed on TiO_2 have been described in published work.[44, 45] These reactions can result in formation of NO and NO_3 in a gas phase and can also explain the composition of surface adsorbed products observed in our experiments [44].

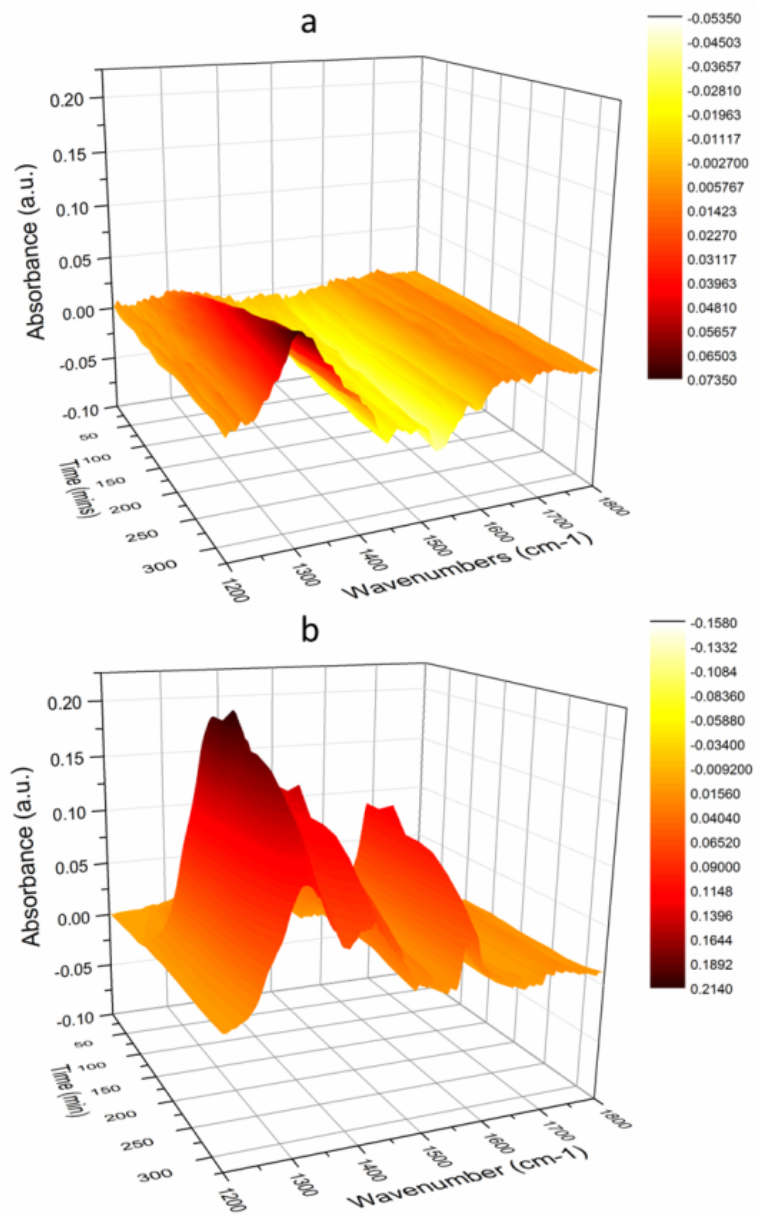

Fig. 6.6 Time dependent DRIFT spectra for the in-situ photocatalytic oxidation of NO_2 on (a) 1 wt. % of regular size Pt-TiO_2; (b) 1 wt. % of sub-nm Pt-TiO_2

A comparison of the DRIFT spectra of surface adsorbed reaction products for modified and unmodified catalysts is shown in Figure 6.7. The peaks present in both Pt modified and unmodified catalysts were located at 1575, 1417 and 1318 cm^{-1} wavelengths, which can be assigned to M-NO_2 and bidentate nitrate

species. These peaks, which are very pronounced in all the samples, indicate a certain degree of similarity in the reaction mechanisms for all three catalysts. The spectral features at 1506 cm^{-1} can be assigned to a monodentate nitrate. A more detailed analysis of a very pronounced peak at 1575 cm^{-1} indicate that the signal can be assigned to either bidentate or monodentate nitrate species, or possibly to contributions from both [45, 46]. The peaks at 1417 cm^{-1} can be attributed to contributions from both M-NO_2 and solvated nitrate species [47]. Finally, the most intense peak at 1318 cm^{-1} can be assigned to adsorbed symmetric nitro compounds $\square_s$ (M-NO_2) [48]. In addition to similarities in the IR spectra observed for modified and unmodified catalysts, there are also some notable differences. For example, the modified catalysts had a number of unresolved features in the areas of 1550-1450 cm^{-1} and 1800-1650 cm^{-1}, which are absent in the TiO_2 samples. In order to understand these differences it is important to note that NO_2 coordinated in the form of NO_2^- (nitrite) has ambidentate properties and is an extremely versatile ligand. In general, nitrite can be potentially coordinated to a metal in nine different ways, giving a rise in complexity of the IR spectra.[49] A detailed HREEL study of NO_2 chemisorption on Pt(111) by Koel *et al.* identified three isomers: μ-N,O-nitrito, nitrito, and three-coordinate nitrite [49]. According to that study, the inequality of the N-O bonds would contribute to additional spectral features in the 1200-1537 cm^{-1} IR region. The features at 1472 and 1457 cm^{-1}, which appear alongside the most intense peak in the spectra, correspond to monodentate nitrite [48, 50]. The bands at 1650 cm^{-1} are generally assigned to Pt-NO mononitrosyl. Although the primary reactive component of the gas phase was NO_2, NO concentration detected during the Pt-TiO_2 gas-phase reaction was higher than that during the P25 TiO_2 gas-phase reaction. These observations are consistent with observations Pt-NO mononitrosyl species mentioned above. [51] The broad peaks from 1650 to 1700 cm^{-1} also indicate weakly held species of adsorbed NO on Pt [52, 53]. Finally, despite nitrate species being present in all three samples, as indicated by appearance of 1575 cm^{-1} and 1417 cm^{-1} peaks discussed earlier in this paper, the intensities of these peaks were much lower for regular size Pt-TiO_2 samples. This might be indicative of altered reaction

pathways for NO_2 oxidation on regular size Pt as compared to that for sub-nm Pt-TiO_2 catalysts.

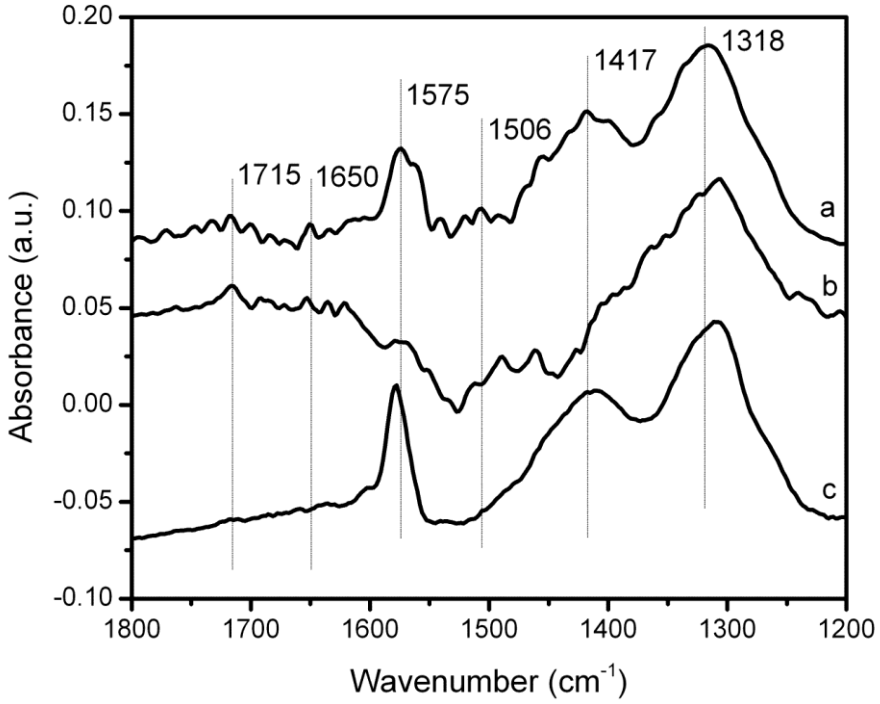

Fig. 6.7 Time dependent DRIFT spectra of NO_2 reaction products on: (a) sub-nm Pt-TiO_2; (b) regular size Pt-TiO_2; (c) unmodified TiO_2 P25

Given a novelty of the sub-nm Pt-TiO_2 catalysts, the rationale for beneficial effects of Pt enhancement still needs to be developed. Several explanations have been invoked to describe activity/inactivity of larger Pt nanoparticles. For example, an electron migration to Pt and resulting increase in rates of O_2 reduction have been suggested by several groups.[30, 35] Moreover, in case of P25, it was proposed that anatase-rutile mixture has already beneficial properties in terms of charge separation [54] and, as a result, the advantageous effects of Pt for electron-hole separation might be rather limited. Therefore, although platinum particles might still capture some electrons, it would not lead to further

decrease in recombination rate [31]. However, one might need to distinguish between gas phase and liquid phase photocatalytic reactions. For example, it was suggested that surface charge and formation of electric double layer in liquids might further decrease electron-hole recombination rate [1, 11] and therefore would reduce a positive impact of Pt nanoparticles in terms of charge separation. In contrast, in case of gas phase oxidation reactions, Pt deposition has been observed to result in significant enhancement in reaction rates, possibly due to the absence of the charged species present in solution [8, 55]. Although our gas-phase reactor contained both water vapour and oxygen, a much smaller concentration of water as compared to that in liquid phase reactor could have made a substantial impact on charge recombination rate. For example, some studies suggested that electron-capture is enhanced with the increasing water pressure, which might explain the difference in Pt behaviour in liquid vs. gas phase reactions [56]. Finally, the enhancements of photocatalytic activity due to localized surface plasmon resonance (LSPR) of Pt particles was also proposed, although it is important to note that these observations were done for metallic (i.e. large) Pt particles [57, 58].

In case of sub-nm particles, the above mentioned explanations might no longer be valid. Importantly, the electronic effects and non-metallic properties of these smaller particles need to be taken into account. For example, our collaborator's recent DFT calculations of electronic structures of sub-nm Au particles indicate a DFT gap between 1-1.7 eV depending on particle geometry [59]. Similar computational efforts are in progress for Pt sub-nm particles. However, the calculation of the Pt particles shows no DFT gap which indicates it remains metallic. This result suggests that the sub-nm Au and Pt promote very different mechanisms and can not be treated as having the same beneficial effects for catalytic reactions. Given that the initial intention of this work was to explore 2-D clusters, a further comparison of 2-D and 3-D geometry will be a subject of further investigations.

6.4 Conclusion

Our experiments indicate that Pt deposition on TiO_2 P25 exhibits very promising activity for several oxidation reactions. More specifically, we have demonstrated that sub-nm Pt modified TiO_2 samples have a particularly promising activity for environmentally relevant reactions, such as oxidation of phenol and NO_2. This activity was substantially higher than that observed on regular size supported Pt particles. We believe that this work is the first ever demonstration of applications of such small Pt clusters for both liquid and gas phase photocatalytic oxidation reactions. Moreover, we also found that sub-nm Pt promotes a very different reaction product distribution as compared to that for larger particles. These observations, enabled by a novel use of modified UV-source modified DRIFT spectroscopy, also indicate the Pt ability to affect both oxidation and reduction pathways of NO_2 removal from gas the phase.

References:

[1] M.R. Hoffmann, S.T. Martin, W.Y. Choi, D.W. Bahnemann, Environmental Applications of Semiconductor Photocatalysis, Chem Rev, 95 (1995) 69-96.

[2] M.A. Fox, M.T. Dulay, Heterogeneous Photocatalysis, Chem Rev, 93 (1993) 341-357.

[3] A.L. Linsebigler, G.Q. Lu, J.T. Yates, Photocatalysis on Tio2 Surfaces - Principles, Mechanisms, and Selected Results, Chem Rev, 95 (1995) 735-758.

[4] X. Chen, S.S. Mao, Titanium dioxide nanomaterials: Synthesis, properties, modifications, and applications, Chem Rev, 107 (2007) 2891-2959.

[5] H. Remita, E. Kowalska, C. Colbeau-Justin, J. Hupka, J. Belloni, Modification of titanium dioxide with platinum ions and clusters: Application in photocatalysis, J Phys Chem C, 112 (2008) 1124-1131.

[6] H. Tada, T. Kiyonaga, S. Naya, Rational design and applications of highly efficient reaction systems photocatalyzed by noble metal nanoparticle-loaded titanium(IV) dioxide, Chem Soc Rev, 38 (2009) 1849-1858.

[7] M.C. Daniel, D. Astruc, Gold nanoparticles: Assembly, supramolecular chemistry, quantum-size-related properties, and applications toward biology, catalysis, and nanotechnology, Chem Rev, 104 (2004) 293-346.

[8] S. Hwang, M.C. Lee, W. Choi, Highly enhanced photocatalytic oxidation of CO on titania deposited with Pt nanoparticles: kinetics and mechanism, Appl Catal B-Environ, 46 (2003) 49-63.

[9] Y.C. Xing, Synthesis and electrochemical characterization of uniformly-dispersed high loading Pt nanoparticles on sonochemically-treated carbon nanotubes, J Phys Chem B, 108 (2004) 19255-19259.

[10] R.A. Ganeev, R.I. Tugushev, T. Usmanov, Application of the nonlinear optical properties of platinum nanoparticles for the mode locking of Nd:glass laser, Appl Phys B-Lasers O, 94 (2009) 647-651.

[11] P.V. Kamat, Photophysical, photochemical and photocatalytic aspects of metal nanoparticles, J Phys Chem B, 106 (2002) 7729-7744.

[12] Y. Bai, W. Li, C. Liu, Z.H. Yang, X. Feng, X.H. Lu, K.Y. Chan, Stability of Pt nanoparticles and enhanced photocatalytic performance in mesoporous Pt-(anatase/TiO2(B)) nanoarchitecture, J Mater Chem, 19 (2009) 7055-7061.

[13] E. Kowalska, O.O.P. Mahaney, R. Abe, B. Ohtani, Visible-light-induced photocatalysis through surface plasmon excitation of gold on titania surfaces, Phys Chem Chem Phys, 12 (2010) 2344-2355.

[14] V. Iliev, D. Tomova, L. Bilyarska, A. Eliyas, L. Petrov, Photocatalytic properties of TiO2 modified with platinum and silver nanoparticles in the degradation of oxalic acid in aqueous solution, Appl Catal B-Environ, 63 (2006) 266-271.

[15] R.M. Lambert, A. Orlov, D.A. Jefferson, N. Macleod, Photocatalytic properties of TiO2 modified with gold nanoparticles in the degradation of 4-chlorophenol in aqueous solution, Catal Lett, 92 (2004) 41-47.

[16] P.V. Kamat, V. Subramanian, E.E. Wolf, Catalysis with TiO2/gold nanocomposites. Effect of metal particle size on the Fermi level equilibration, J Am Chem Soc, 126 (2004) 4943-4950.

[17] S. Kobayashi, K. Okamoto, R. Akiyama, H. Yoshida, T. Yoshida, Formation of nanoarchitectures including subnanometer palladium clusters and their use as highly active catalysts, J Am Chem Soc, 127 (2005) 2125-2135.

[18] S. Vajda, S. Lee, B. Lee, F. Mehmood, S. Seifert, J.A. Libera, J.W. Elam, J. Greeley, P. Zapol, L.A. Curtiss, M.J. Pellin, P.C. Stair, R.E. Winans, Oxidative Decomposition of Methanol on Subnanometer Palladium Clusters: The Effect of Catalyst Size and Support Composition, J Phys Chem C, 114 (2010) 10342-10348.

[19] I. Lee, R. Morales, M.A. Albiter, F. Zaera, Synthesis of heterogeneous catalysts with well shaped platinum particles to control reaction selectivity, P Natl Acad Sci USA, 105 (2008) 15241-15246.

[20] J.D. Aiken, R.G. Finke, A review of modern transition-metal nanoclusters: their synthesis, characterization, and applications in catalysis, J Mol Catal a-Chem, 145 (1999) 1-44.

[21] C. Burda, X.B. Chen, R. Narayanan, M.A. El-Sayed, Chemistry and

properties of nanocrystals of different shapes, Chem Rev, 105 (2005) 1025-1102.
[22] R.M. Rioux, H. Song, M. Grass, S. Habas, K. Niesz, J.D. Hoefelmeyer, P. Yang, G.A. Somorjai, Monodisperse platinum nanoparticles of well-defined shape: synthesise characterization, catalytic properties and future prospects, Top Catal, 39 (2006) 167-174.
[23] I. Lisiecki, Size, shape, and structural control of metallic nanocrystals, J Phys Chem B, 109 (2005) 12231-12244.
[24] A.R. Tao, S. Habas, P.D. Yang, Shape control of colloidal metal nanocrystals, Small, 4 (2008) 310-325.
[25] B.R. Cuenya, J.R. Croy, S. Mostafa, F. Behafarid, L. Li, Z.F. Zhang, J.C. Yang, Q. Wang, A.I. Frenkel, Solving the Structure of Size-Selected Pt Nanocatalysts Synthesized by Inverse Micelle Encapsulation, J Am Chem Soc, 132 (2010) 8747-8756.
[26] B.R. Cuenya, S. Mostafa, F. Behafarid, J.R. Croy, L.K. Ono, L. Li, J.C. Yang, A.I. Frenkel, Shape-Dependent Catalytic Properties of Pt Nanoparticles, J Am Chem Soc, 132 (2010) 15714-15719.
[27] M.I. Litter, Heterogeneous photocatalysis - Transition metal ions in photocatalytic systems, Appl Catal B-Environ, 23 (1999) 89-114.
[28] U. Diebold, The surface science of titanium dioxide, Surf Sci Rep, 48 (2003) 53-229.
[29] V. Subramanian, E.E. Wolf, P.V. Kamat, Catalysis with TiO2/gold nanocomposites. Effect of metal particle size on the Fermi level equilibration, J Am Chem Soc, 126 (2004) 4943-4950.
[30] C.A. Emilio, M.I. Litter, M. Kunst, M. Bouchard, C. Colbeau-Justin, Phenol photodegradation on platinized-TiO2 photocatalysts related to charge-carrier dynamics, Langmuir, 22 (2006) 3606-3613.
[31] B. Sun, A.V. Vorontsov, P.G. Smirniotis, Role of platinum deposited on TiO2 in phenol photocatalytic oxidation, Langmuir, 19 (2003) 3151-3156.
[32] E. Kowalska, H. Remita, C. Colbeau-Justin, J. Hupka, J. Belloni, Modification of titanium dioxide with platinum ions and clusters: Application in photocatalysis, J Phys Chem C, 112 (2008) 1124-1131.

[33] T.A. Egerton, J.A. Mattinson, The influence of platinum on UV and 'visible' photocatalysis by rutile and Degussa P25, J Photoch Photobio A, 194 (2008) 283-289.

[34] J.S. Lee, W.Y. Choi, Photocatalytic reactivity of surface platinized TiO2: Substrate specificity and the effect of Pt oxidation state, J Phys Chem B, 109 (2005) 7399-7406.

[35] D. Hufschmidt, D. Bahemann, J.J. Testa, C.A. Emilio, M.I. Litter, Enhancement of the photocatalytic activity of various TiO2 materials by platinisation, J Photoch Photobio A, 148 (2002) 223-231.

[36] A. Sclafani, L. Palmisano, M. Schiavello, Influence of the Preparation Methods of Tio2 on the Photocatalytic Degradation of Phenol in Aqueous Dispersion, J Phys Chem-Us, 94 (1990) 829-832.

[37] G. Ramakrishnan, S. Zhao, W.Q. Han, A. Orlov, Simultaneous observation of gas phase and surface species in photocatalytic reactions on nanosize Au modified TiO(2): The next generation of DRIFTS systems, Chem Eng J, 170 (2011) 445-450.

[38] P.K. Dutta, A.K. Ray, V.K. Sharma, F.J. Millero, Adsorption of arsenate and arsenite on titanium dioxide suspensions, J Colloid Interf Sci, 278 (2004) 270-275.

[39] P. Fernandez-Ibanez, F.J. de las Nieves, S. Malato, Titanium dioxide/electrolyte solution interface: Electron transfer phenomena, J Colloid Interf Sci, 227 (2000) 510-516.

[40] Y.H. Cho, J.E. Yang, J.S. Lee, Size control of polymeric nanoparticles from polystyrene-b-poly(2-vinylpyridine), Mat Sci Eng C-Bio S, 24 (2004) 293-295.

[41] J.S. Jang, S.H. Choi, H.G. Kim, J.S. Lee, Location and State of Pt in Platinized CdS/TiO2 Photocatalysts for Hydrogen Production from Water under Visible Light, J Phys Chem C, 112 (2008) 17200-17205.

[42] H.J. Fan, C.S. Lu, W.L.W. Lee, M.R. Chiou, C.C. Chen, Mechanistic pathways differences between P25-TiO2 and Pt-TiO2 mediated CV photodegradation, J Hazard Mater, 185 (2011) 227-235.

[43] S. Kielbassa, A. Habich, J. Schnaidt, J. Bansmann, F. Weigl, H.G. Boyen, P.

Ziemann, R.J. Behm, On the morphology and stability of Au nanoparticles on TiO2(110) prepared from micelle-stabilized precursors, Langmuir, 22 (2006) 7873-7880.

[44] G.M. Underwood, T.M. Miller, V.H. Grassian, Transmission FT-IR and Knudsen cell study of the heterogeneous reactivity of gaseous nitrogen dioxide on mineral oxide particles, J Phys Chem A, 103 (1999) 6184-6190.

[45] K. Hadjiivanov, V. Bushev, M. Kantcheva, D. Klissurski, Infrared-Spectroscopy Study of the Species Arising during No2 Adsorption on Tio2 (Anatase), Langmuir, 10 (1994) 464-471.

[46] J.C.S. Wu, Y.T. Cheng, In situ FTIR study of photocatalytic NO reaction on photocatalysts under UV irradiation, J Catal, 237 (2006) 393-404.

[47] M.A. Debeila, N.J. Coville, M.S. Scurrell, G.R. Hearne, The effect of calcination temperature on the adsorption, of nitric oxide on Au-TiO2: Drifts studies, Appl Catal a-Gen, 291 (2005) 98-115.

[48] K.I. Hadjiivanov, Identification of neutral and charged NxOy surface species by IR spectroscopy, Catal Rev, 42 (2000) 71-144.

[49] M.E. Bartram, R.G. Windham, B.E. Koel, The Molecular Adsorption of Nitrogen-Dioxide on Pt(111) Studied by Temperature Programmed Desorption and Vibrational Spectroscopy, Surf Sci, 184 (1987) 57-74.

[50] G. Ramis, G. Busca, F. Bregani, P. Forzatti, Fourier Transform-Infrared Study of the Adsorption and Coadsorption of Nitric-Oxide, Nitrogen-Dioxide and Ammonia on Vanadia Titania and Mechanism of Selective Catalytic Reduction, Appl Catal, 64 (1990) 259-278.

[51] C. Panja, B.E. Koel, Influence of alloyed Sn on adsorption and reaction of NO on Pt(100) surfaces, J Phys Chem A, 104 (2000) 2486-2497.

[52] B.A. Morrow, R.A. Mcfarlane, L.E. Moran, Infrared Study of the Reaction between No and O-2 and of the Adsorption of No2 on Platinum, J Phys Chem-Us, 89 (1985) 77-80.

[53] A. Rodes, R. Gomez, J.M. Orts, J.M. Feliu, J.M. Perez, A. Aldaz, In-Situ Ftir Spectroscopy Characterization of the No Adlayers Formed at Platinum Single-Crystal Electrodes in Contact with Acidic Solutions of Nitrite, Langmuir, 11 (1995)

3549-3553.

[54] T. Ohno, K. Sarukawa, K. Tokieda, M. Matsumura, Morphology of a TiO2 photocatalyst (Degussa, P-25) consisting of anatase and rutile crystalline phases, J Catal, 203 (2001) 82-86.

[55] E.A. Kozlova, A.V. Vorontsov, Influence of mesoporous and platinum-modified titanium dioxide preparation methods on photocatalytic activity in liquid and gas phase, Appl Catal B-Environ, 77 (2007) 35-45.

[56] A. Yamakata, T. Ishibashi, H. Onishi, Kinetics of the photocatalytic water-splitting reaction on TiO2 and Pt/TiO2 studied by time-resolved infrared absorption spectroscopy, J Mol Catal a-Chem, 199 (2003) 85-94.

[57] J. Zhang, L.P. Li, T.J. Yan, G.S. Li, Selective Pt Deposition onto the Face (110) of TiO2 Assembled Microspheres That Substantially Enhances the Photocatalytic Properties, J Phys Chem C, 115 (2011) 13820-13828.

[58] A.C. Chen, P. Holt-Hindle, Platinum-Based Nanostructured Materials: Synthesis, Properties, and Applications, Chem Rev, 110 (2010) 3767-3804.

[59] S. Zhao, G. Ramakrishnan, D. Su, R. Rieger, A. Koller, A. Orlov, Novel photocatalytic applications of sub-nanometer gold particles for environmental liquid and gas phase reactions, Appl Catal B-Environ, 104 (2011) 239-244.

Chapter 7. Photocatalytic properties of TiO_2 supported on SBA-15 mesoporous materials

7.1 Introduction

Application of TiO_2 for photocatalysis has become a very well established approach in environmental catalysis area [1, 2]. In addition to numerous advantages of using this material to degrade various toxic substances, there are also several limitations. For example, commercially available catalysts have relatively low surface area, which is an important factor hindering the photocatalytic activity. In order to address this limitation, several groups have developed supported TiO_2 photocatalysts [3, 4]. Such inorganic porous materials as Ordered Mesoporous Silicas (OMSs) are widely used as catalytic supports given their high thermal and chemical stability, as well as tunable surface composition and pore size [5, 6]. In the past 20 years there has been a rapid development of this field [7-9]. One example of the recently synthesized OMSs is SBA-15, which is considered to be one of most promising mesoporous silica based materials, given its commercial availability, high surface area, significant thermal stability and large pore sizes [8, 10-12]. Utilizing TiO_2 supported on SBA-15 materials for photocatalytic reactions is a promising area of research, given the limitations of the unsupported catalysts mentioned above [13, 14].

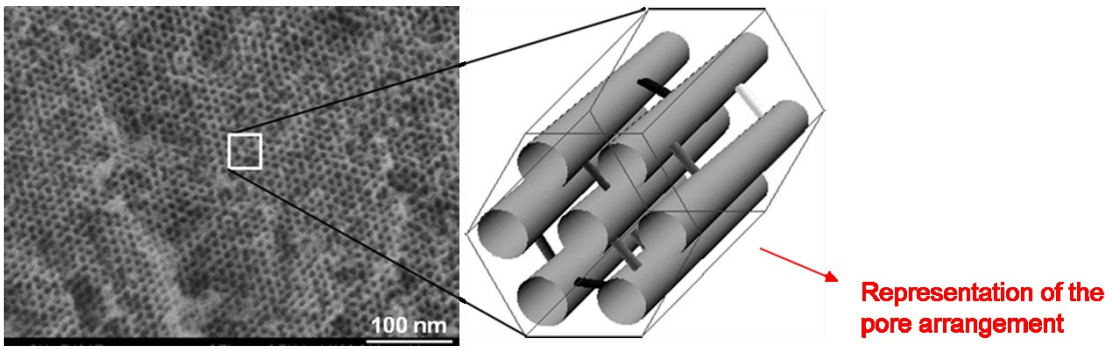

Diagram 7.1: structure demonstration of hexagonal SBA-15 mesoporous silica material

In addition to increasing the surface area of photocatalysts, another viable strategy to increase their activity is to modify them with metal nanoparticles [15, 16]. It has been observed that Au nanoparticles in the size range of 1-5 nm display electronic properties, which are quite different from those of bulk Au, reflecting a quantum confinement effect [17, 18]. This phenomenon was explored in various reactions, where Au nanoparticles exhibited very high catalytic activity [19, 20]. However, the impact of modification the TiO_2 surface with sub-nm Au particles on the rate of photocatalytic oxidation reactions is currently unknown.

In this study, a new generation of highly ordered mesoporous SBA-15 sieves, which have large pore diameter (22 nm) and short pore length (500 nm), were utilized as templates to facilitate photo-oxidation reactions [11, 21]. To the best of our knowledge, this is the first ever application of this type of SBA-15 molecular sieves in photocatalytic area. In order to increase the activity of the supported catalyst even further, sub-nm Au nanoparticles were deposited inside the pores of the TiO_2/SBA-15 sample. The samples mentioned above were characterized by SAXS, TEM, BET techniques and utilized for liquid phase oxidation of phenol [22].

7.2 Materials and methods

The synthesis and modification of the SBA-15 materials were based on the approach recently developed by Prof. Kruk's group at CUNY, Staten Island [11]. First, HCl was dissolved in water to reach a final concentration of 1.3 M. About 2.4 g of Pluronic P123 block copolymer (BASF; $EO_{20}PO_{70}EO_{20}$) was then added into the HCl solution and stirred for 3 hours. A mixture of 5.5 ml TEOS and 1.0 g of TIPB was added under continuously stirring and allowed to equilibrate for approximately 10 minutes. Afterwards, the mixture was kept at 17 °C for one day without stirring. It was subsequently heated in a closed autoclave at 130 °C for 2

days.

The SBA-15 mesoporous molecular sieves were calcined at high temperature (550°C, 4 hrs) to ensure the complete removal of the surfactants. Afterwards, they were added to 100 ml of butanol and kept in nitrogen atmosphere under constant stirring. Titanium butoxide was subsequently added into the solution to achieve 2 wt. % Ti loading on OMSs, which was followed by the addition of acetic acid to facilitate hydrolysis reaction. Afterwards, the prepared solution was stirred at room temperature for 12 hours and was subsequently evaporated at 60 °C. The sample was then calcined in oven at 550°C for 12 hours.

The gold synthesis of sub-nm particles was based on modified ligand exchange reaction described in our previous work [23]. About 200 mg of the TiO_2/SBA-15 sample was added to 20 ml of chloroform, followed by 0.5 wt. % addition of Au nanoparticles. The mixture was stirred overnight, followed by surfactant removal washed with dichloromethane with subsequent thermal activation (150°C, 2 h) in vacuo.

The resulting catalysts were tested for oxidation of phenol in liquid phase reaction. The liquid phase photocatalytic experiment was carried out in a custom made temperature controlled Pyrex reactor loaded with the photocatalysts. The UV light source was Xenon lamp (Newport Model 67005) modified with optical filters, which cut off UV radiation below 320 nm to minimize the photolysis reactions. Liquid samples were periodically withdrawn from the solution and transferred to HPLC vials for further analysis by Agilent 1200 HPLC.

Small-angle X-ray scattering (SAXS) measurements were performed at National Synchrotron Light Source at Brookhaven National Laboratory (BNL). Nitrogen adsorption isotherms for the SBA-15 samples were collected by Quantachrome Nova 1200 instrument. Prior to surface area measurements the samples were *in-situ* degassed under vacuum at 200 ^{o}C for 2 hrs.

7.3 Results and discussion

	Pore Diameter /nm (BJH adsorption)	Total Pore Volume (cm^3/g)	Surface area (m^2/g)
Silica template (MP00)	22.9102	1.659	462.181
1 wt. % loading of TiO_2 (MP01)	18.1400	1.463	392.789
5 wt. % loading of TiO_2 (MP05)	18.0003	1.382	393.87
10 wt. % loading of TiO_2 (MP10)	18.1066	1.365	395.645
25 wt. % loading of TiO_2 (MP25)	18.1282	1.217	361.406
50 wt. % loading of TiO_2 (MP50)	16.5357	1.010	308.453

Table 7.1 BET characterization results of SBA-15 mesoporous silica modified with different TiO_2 loadings

Table 7.1 shows BET data for SBA-15 samples with different TiO_2 loadings. Nitrogen adsorption isotherm of unmodified SBA-15 samples showed BET surface area of 276 m^2g^{-1}, which was much larger than that of TiO_2 P25 (50 m^2g^{-1}) considered to be one of the most active photocatalysts. The pore size was determined by BJH method. The results indicate a small decrease in OMSs surface area due to TiO_2 deposition. In addition, pore size and total pore volume decreased as the titania loading increased.

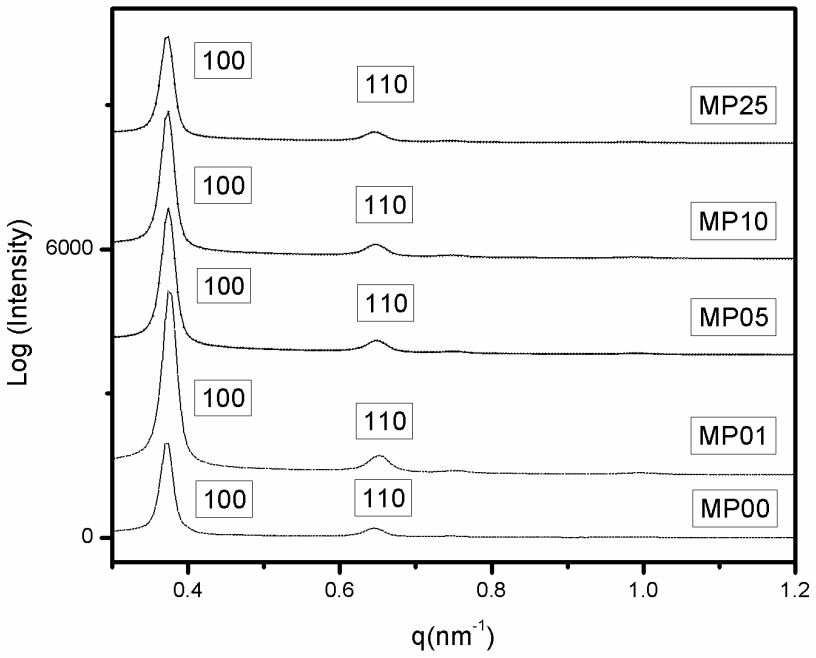

Fig. 7.1 XRD patterns at low angle of: (a) SBA-15 sample, (b) 1 wt. % of TiO_2/SBA-15, (c) 5 wt. % of TiO_2/SBA-15, (d) 10 wt. % of TiO_2/SBA-15, (e) 25 wt. % of TiO_2/SBA-15, (f) 1 wt. % of TiO_2/SBA-15.

Figure 7.1 shows an integrated SAXS patterns for different TiO_2/SBA-15 loadings. The position of the highest intensity peak on the SAXS pattern corresponds to (100) reflection with calculated interplanar spacings of 16.8 nm. The peaks of the pattern observed in Figure 7.1 can be indexed as reflections of the hexagonal structure [24]. It is important to note that the interplanar spacings remain the same regardless the TiO_2 loadings. This suggests that the silica framework was very stable and was not affected by titania deposition. The hexagonal structure of mesoporous samples was also confirmed by TEM images shown below.

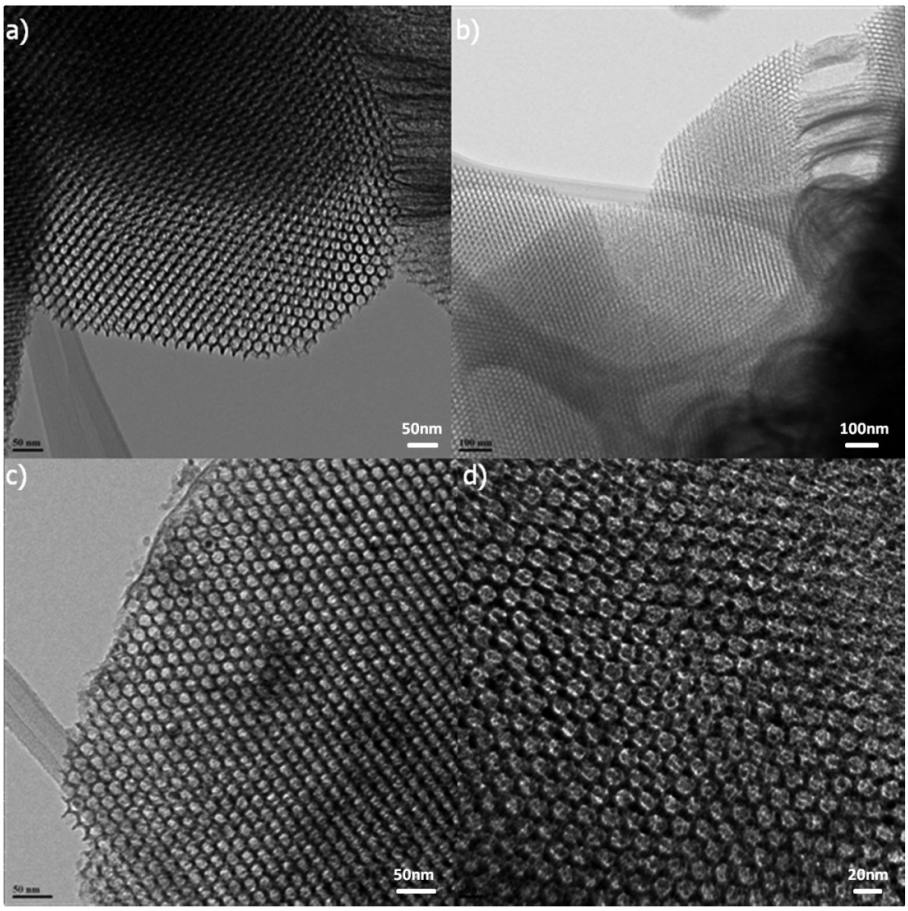

Fig. 7.2 TEM images of the mesoporous silica template and the TiO_2/SBA-15 samples: where (a) and (b) corresponds to unmodified SBA-15; and (c) and (d) shows 25 wt. % of TiO_2 modified SBA-15.

Figure 7.2 shows the TEM images of the mesoporous silica template and the TiO_2 modified SBA-15 catalysts with highly ordered 2D hexagonal (honeycomb) structure [11]. It shows homogeneous channels of which the diameter is about 20 nm, with a wall thickness of 5 nm. The introduction of titanium did not substantially alter the regular ordered structure of the mesopores, which was consistent with SAXS and BET results.

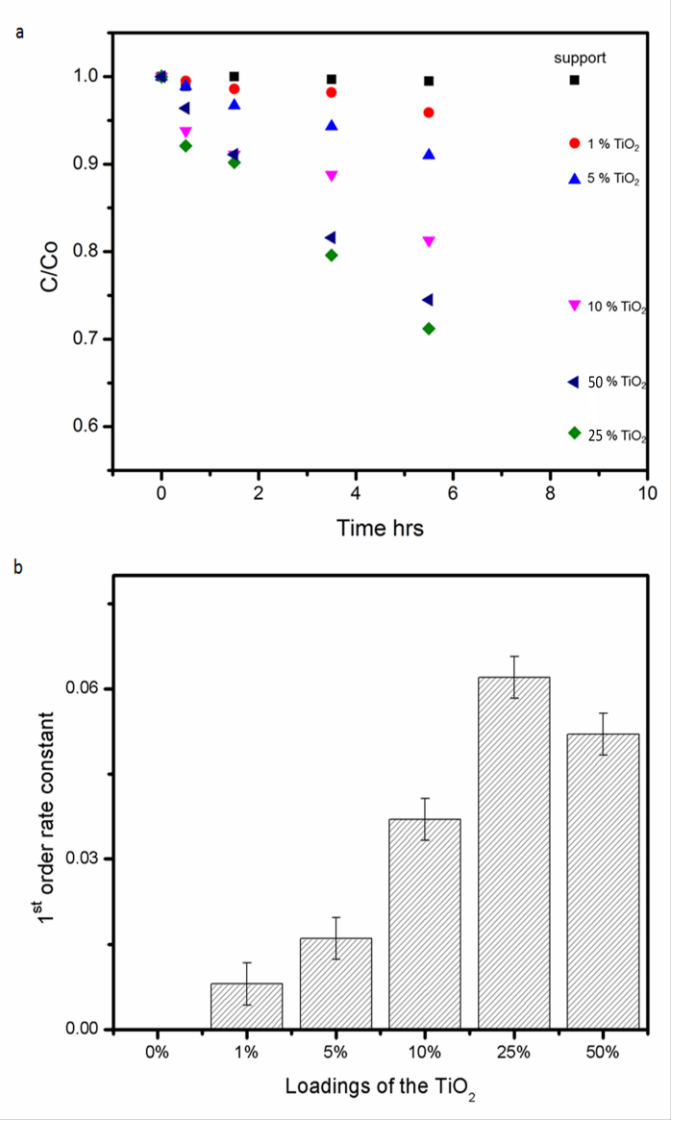

Fig. 7.3 a) Time dependent phenol degradation for titania modified SBA-15; b) Photocatalytic activity of the TiO_2/SBA-15 for phenol oxidation.

Figure 7.3 shows the photocatalytic activity of the TiO_2/SBA-15 for liquid phase oxidation of phenol. Unmodified mesoporous silica sample did not have any photocatalytic activity. However, TiO_2 modified samples exhibit a significant activity, which was a function of TiO_2 loading. The highest activity was observed at 25 wt. % of TiO_2 loading. A further increase in TiO_2 loading resulted in a decrease of activity, possibly due to a combination of factors including decrease in surface area, pore size and increase in TiO_2 particle size inside the channels

[25].

The figure7.4 (a) is the time dependent phenol oxidation for Au modified TiO_2/SBA-15. The insert of figure 7.4 (b) shows sub-nm unsupported gold clusters before their deposition on TiO_2 modified SBA-15. The STEM image indicates that the average size of the gold clusters was approximately 0.8 ± 0.1 nm with a significant number of isolated gold atoms distributed throughout the sample. Figure 7.4 (b) shows the photocatalytic activities for 25 wt. % TiO_2/SBA-15 samples. After deposited with 0.5 wt. % Au nanoparticles, the activity has increased by a factor of 2 as compared to unmodified sample, which indicates a significant beneficial effect of sub-nm Au particles for the overall catalytic performance.

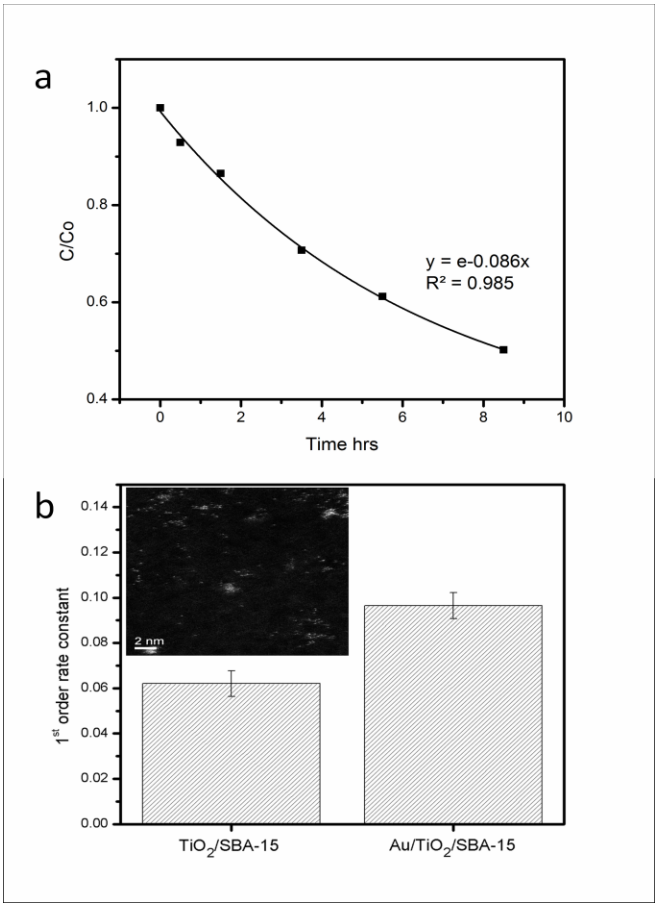

Fig. 7.4 a) Time dependent phenol oxidation of 1 wt. % of gold deposited on 25 wt. % of TiO_2/SBA-15; b) Photocatalytic activity of TiO_2/SBA-15 and 1 wt. % Au modified TiO_2/SBA-15.

7.4 Conclusions

As presented in the previous chapters, metal nanoparticles can have significant impact on catalytic performance. In this chapter, high surface area materials were introduced into the metal semiconductor system to further increase the photocatalytic activity. We have employed a novel mesoporous SBA-15 sieves with highly ordered porous structure and relatively short channels. These nanostructured materials were modified with TiO_2 and tested for liquid phase oxidation reactions. Our results show that TiO_2 modified mesoporous silica samples exhibit a significant photocatalytic activity for phenol degradation reactions. We have also introduced a new strategy of further increasing the TiO_2/SBA-15 activity by modifying it with novel sub- nm gold clusters.

References:

[1] M.R. Hoffmann, S.T. Martin, W.Y. Choi, D.W. Bahnemann, Environmental Applications of Semiconductor Photocatalysis, Chemical Reviews, 95 (1995) 69-96.

[2] O. Legrini, E. Oliveros, A.M. Braun, Photochemical Processes for Water-Treatment, Chemical Reviews, 93 (1993) 671-698.

[3] J.A. Byrne, B.R. Eggins, N.M.D. Brown, B. McKinney, M. Rouse, Immobilisation of TiO2 powder for the treatment of polluted water, Applied Catalysis B-Environmental, 17 (1998) 25-36.

[4] R.L. Pozzo, M.A. Baltanas, A.E. Cassano, Supported titanium oxide as photocatalyst in water decontamination: State of the art, Catalysis Today, 39 (1997) 219-231.

[5] L. Li, J.L. Shi, J.N. Yan, H.G. Chen, X.G. Zhao, SBA-15 supported quaternary ammonium salt: an efficient, heterogeneous phase-transfer catalyst, Journal of Molecular Catalysis a-Chemical, 209 (2004) 227-230.

[6] Y. Liu, T.J. Pinnavaia, Assembly of hydrothermally stable aluminosilicate foams and large-pore hexagonal mesostructures from zeolite seeds under strongly acidic conditions, Chemistry of Materials, 14 (2002) 3-+.

[7] Y. Wan, D.Y. Zhao, On the controllable soft-templating approach to mesoporous silicates, Chem Rev, 107 (2007) 2821-2860.

[8] D.Y. Zhao, J.L. Feng, Q.S. Huo, N. Melosh, G.H. Fredrickson, B.F. Chmelka, G.D. Stucky, Triblock copolymer syntheses of mesoporous silica with periodic 50 to 300 angstrom pores, Science, 279 (1998) 548-552.

[9] M. Kruk, M. Jaroniec, C.H. Ko, R. Ryoo, Characterization of the porous structure of SBA-15, Chem Mater, 12 (2000) 1961-1968.

[10] M.J. Lopez-Munoz, R. van Grieken, J. Aguado, J. Marugan, Role of the support on the activity of silica-supported TiO2 photocatalysts: Structure of the TiO2/SBA-15 photocatalysts, Catalysis Today, 101 (2005) 307-314.

[11] L.A. Cao, T. Man, M. Kruk, Synthesis of Ultra-Large-Pore SBA-15 Silica with Two-Dimensional Hexagonal Structure Using Triisopropylbenzene As Micelle Expander, Chemistry of Materials, 21 (2009) 1144-1153.

[12] R. Ryoo, S.H. Joo, M. Kruk, M. Jaroniec, Ordered mesoporous carbons, Adv Mater, 13 (2001) 677-681.

[13] K. Inumaru, T. Kasahara, M. Yasui, S. Yamanaka, Direct nanocomposite of crystalline TiO2 particles and mesoporous silica as a molecular selective and highly active photocatalyst, Chemical Communications, (2005) 2131-2133.

[14] R. Kato, N. Shimura, M. Ogawa, Controlled photocatalytic ability of titanium dioxide particle by coating with nanoporous silica, Chemistry Letters, 37 (2008) 76-77.

[15] V. Subramanian, E.E. Wolf, P.V. Kamat, Influence of metal/metal ion concentration on the photocatalytic activity of TiO2-Au composite nanoparticles, Langmuir, 19 (2003) 469-474.

[16] Q. Fu, H. Saltsburg, M. Flytzani-Stephanopoulos, Active nonmetallic Au and Pt species on ceria-based water-gas shift catalysts, Science, 301 (2003) 935-938.

[17] M. Valden, X. Lai, D.W. Goodman, Onset of catalytic activity of gold clusters on titania with the appearance of nonmetallic properties, Science, 281 (1998) 1647-1650.

[18] A. Wood, M. Giersig, P. Mulvaney, Fermi level equilibration in quantum dot-metal nanojunctions, Journal of Physical Chemistry B, 105 (2001) 8810-8815.

[19] A. Orlov, D.A. Jefferson, N. Macleod, R.M. Lambert, Photocatalytic properties of TiO2 modified with gold nanoparticles in the degradation of 4-chlorophenol in aqueous solution, Catalysis Letters, 92 (2004) 41-47.

[20] M. Haruta, Size- and support-dependency in the catalysis of gold, Catalysis Today, 36 (1997) 153-166.

[21] L. Cao, H.C. Dong, L. Huang, K. Matyjaszewski, M. Kruk, Synthesis of large-pore SBA-15 silica using poly(ethylene oxide)-poly(methyl acrylate) diblock copolymers, Adsorption, 15 (2009) 156-166.

[22] C.L. Peza-Ledesma, L. Escamilla-Perea, R. Nava, B. Pawelec, J.L.G. Fierro, Supported gold catalysts in SBA-15 modified with TiO2 for oxidation of carbon

monoxide, Appl Catal a-Gen, 375 (2010) 37-48.

[23] M.F. Bertino, Z.M. Sun, R. Zhang, L.S. Wang, Facile syntheses of monodisperse ultrasmall Au clusters, Journal of Physical Chemistry B, 110 (2006) 21416-21418.

[24] M.V. Landau, L. Vradman, X.G. Wang, L. Titelman, High loading TiO2 and ZrO2 nanocrystals ensembles inside the mesopores of SBA-15: preparation, texture and stability, Micropor Mesopor Mat, 78 (2005) 117-129.

[25] M. Alvaro, C. Aprile, M. Benitez, E. Carbonell, H. Garcia, Photocatalytic activity of structured mesoporous TiO2 materials, J Phys Chem B, 110 (2006) 6661-6665.

Chapter 8. Photonic Crystal Fabrication and Characterization

8.1 Introduction

As mentioned before, the photocatalysis utilizes semiconductor materials, which can be activated by UV or visible light. One of the most interesting developments in this area is utilization of photonic crystals to increase the light collection efficiency of the catalysts [1, 2]. Photonic crystal has a periodic optical structure that is designed to affect the propagation of photons in a similar way that periodicity of a semiconductor crystal controls the motion of electrons [3, 4].

The study of photonic crystals in general, has a lot of analogy with the study of solid-state physics and semiconductor materials. The periodicity of the dielectric lattice of photonic crystals can form the photonic bandgap (PBG) which can also be interpreted as the forbidden energy bands for photons. The existence of the photonic bandgap can results in altering the wavelength of the semiconductor absorption band and the bandgap energy. It can potentially make large bandgap photocatalysts (Eg > 2.8 eV) active under visible range. Also the increased light path due to the photonic crystal morphology of the film promotes the photocatalytic activities. Trapping light inside the film can potentially hinder the possibility of photons escaping outside the film by transmission and reflection pathways, which leads to increasing the effective light path and the probability of photon absorption.

In the recent years, utilization of photonic crystal TiO_2 films with inverse opal structure for facilitating photocatalytic reactions has been an area of a significant interest. [5-8]

Many methods for synthesis of three-dimensional photonic crystals for the visible or the near infrared have been proposed. For example, 3-D inverse opal titania or Photonic Crystals (PC) are fabricated by various methods including nano-machining (Fleming et al, 1999) [9], lithography ([10] et al, 2003), chemical vapor deposition (CVD) [11] and 3-D holography [12] (Miklyaev et al, 2003; et al,

2000). However, most commonly used methods having the disadvantages of being overly complex and expensive.

The most popular method is the sol-gel method [13]. It uses microporous polymers, such as polystyrene (PS) as templates. There are many methods to arrange the spheres in close-packed structures, including gravity sedimentation, centrifugation, vertical deposition, template deposition, electrophoresis, patterning, and controlled drying. In this research, the polystyrene (PS) latex spheres were used as templates to fabricate 3D photonic crystals. The fabrication of the inverse opal structure of titania and experimental results to examine the photocatalytic efficiency of these structures for NO_2 degradation are introduced in this chapter.

8.2 Fabrication of the photonic crystals

8.2.1 Latex sphere deposition

In this study, a liquid phase chemical reaction method was used. Before the deposition, the microscope slide was washed several times with deionized water and Acetone. Then it was wiped with a soft cloth to remove any attached particles. Polystrene (PS) latex spheres suspension (different diameter,) was diluted in DI water to 0.1%. The slide was vertically dipped in the diluted PS solution and put into an oven at 50-60 °C until all the solution evaporated.

8.2.2 TiO_2 deposition

Chemical vapor deposition (CVD) methods were used in this experiment. 10ml of titanium butoxide was transferred into a flask under the inert atmosphere. The temperature was increased to 50 °C to facilitate titanium butoxide

evaporation and was kept at that temperature for 10 min. The microscope slide was vertically lowered into the flask, and was kept above the liquid level for 5 min and dried in an oven at 50-60 °C for about 10 min. The process was repeated three times. Then the substrates were placed into an oven for calcination. The temperature was increased from the room temperature to 450 °C at the rate of 2 °C/h and maintained at 450 °C for 12 h.

8.3 Characterization of the photonic crystals

8.3.1 SEM characterization

The samples were mounted on a glass slide using carbon tape and coated with gold by sputtering. The coated samples were examined under SEM to obtain secondary electron images. Scanning electron microscopy (SEM) is a valuable tool for probing the structure and morphology of material at the nanometer to micron length scale. Here we used the SEM to determine the type and orientation of the porous titania.

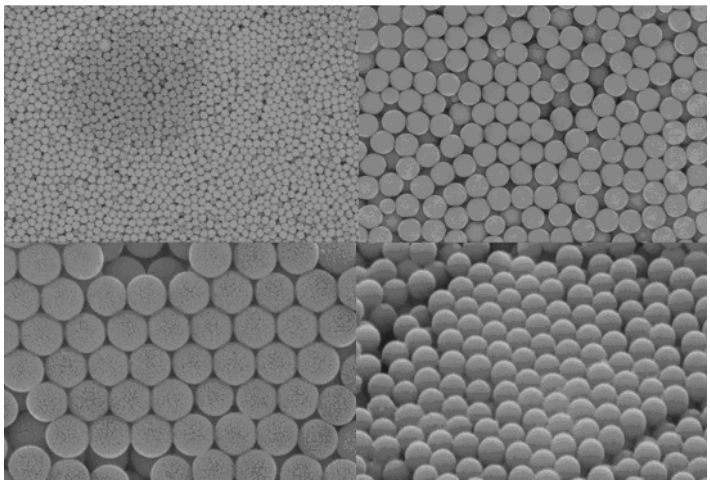

Fig. 8.1 Scanning electron microscope images of coated PS. (A) x10K magnification of coated polystyrene template on the glass, (B) x30K magnification, (C) x150K magnification, (D) polystyrene template on the glass with tilted angle.

Figure 8.1 and 8.2 show SEM images from the PS latex spheres and the resulting macroporous titania generated on glass slide. The image of the PS latex spheres shows that the PS spheres are highly ordered on the surface, although there are some observable defects. It is clear from the image that a highly ordered macroporous structure has been obtained with pore diameter s of about 300 - 400 nm.

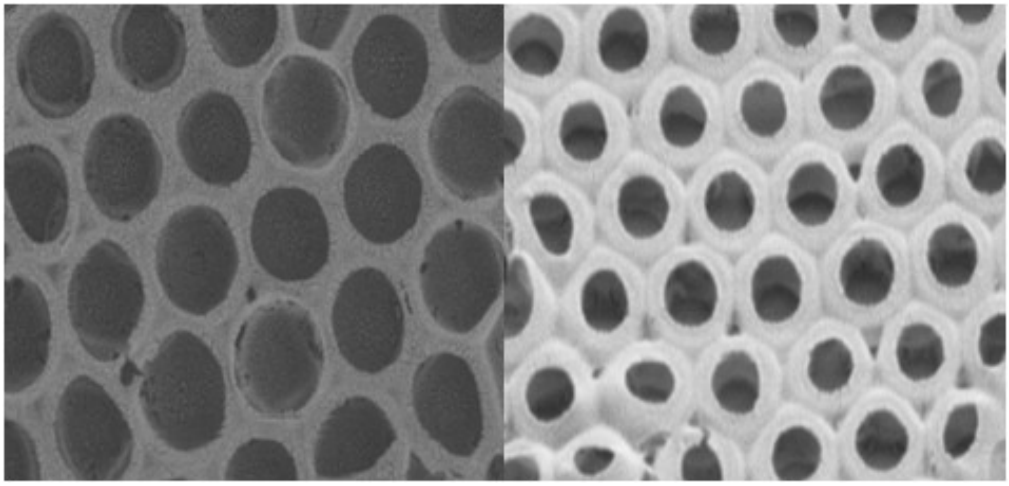

Fig. 8.2 SEM images: the inverse opal titania on the glass slide

Figure 8.2 shows the ordered photonic crystal structure templated with titania after the latex spheres were removed by heat treatment (400 ^{o}C for 2 hrs). It can be concluded that the photonic structures have certain concentration of defects and distortions after the treatment. This is possibly due to difficulty of controlling removal rate of the template, which makes the crystal structure templated with titania somewhat less ordered than the original template. In general, it is clear from the image that a highly ordered macroporous structure is obtained with pore diameter of about 300-400 nm, which can provide the photonic crystal titania with PBG which can potentially cover part of the visible range based on our preliminary calculations. This was confirmed experimentally

by the UV-Vis absorbance spectra of the sample.

8.3.2 X-ray Diffraction

The refractive index of the titania is dependent on the particular crystalline phase. Titania has several polymorphic forms. Two phases relevant to the photonic materials are the anatase (n~2.52) and rutile (n~2.72) forms of titania, both having high refractive index [14]. The rutile phase of the titania is normally formed at high temperatures (T>1000 °C), whereas anatase is formed at lower temperatures (T<550 °C). It is important to mention that high temperature will have a negative effect on the porous structure of the titania film, so normally anatase titania is used in photonic crystals.

The particular phase was experimentally determined by X-ray diffraction (XRD). The XRD spectrum of titania obtained by the templating procedure mentioned above indicated that crystalline anatase phase was the only phase present with the most prominent peak (2Θ = 25.2°) indicating the presence of (101) reflection planes.

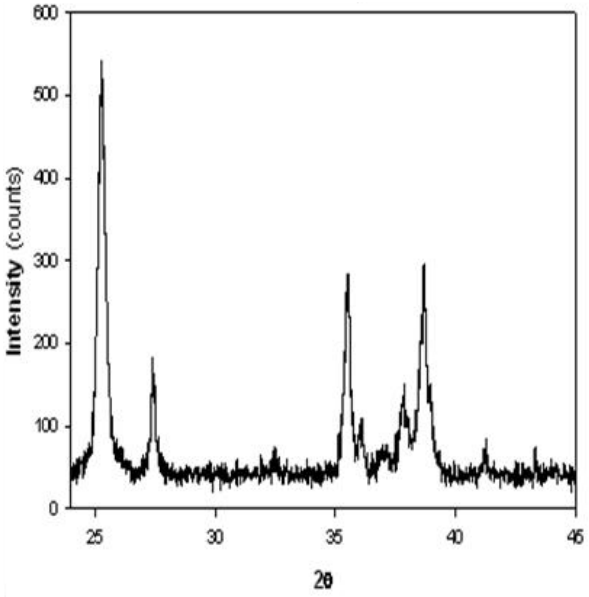

Fig. 8.3 XRD diffraction pattern of the photonic crystal titania thin film

8.3.3 UV-Vis spectroscopy

Figure 8.4 shows the UV absorption spectra of photonic bandgap TiO_2 and TiO_2 titania on a silicon wafer slide. The figure illustrates the differences between the optical spectra of the photonic crystal titania and anatase titania. The spectra from the photonic crystal titania clearly shows a drop in absorption at around 350 nm. In contrast, the spectra of TiO_2 anatase sample obtained by dip-coating in TiO_2 anatase powder solution shows the absorption band of TiO_2 at wavelengths below 350 nm and significantly lesser absorption at longer wavelengths. The absorbance for photonic crystal titania grows when moving towards longer wavelengths which indicate the effect of light entrapment by the photonic sponge [15].

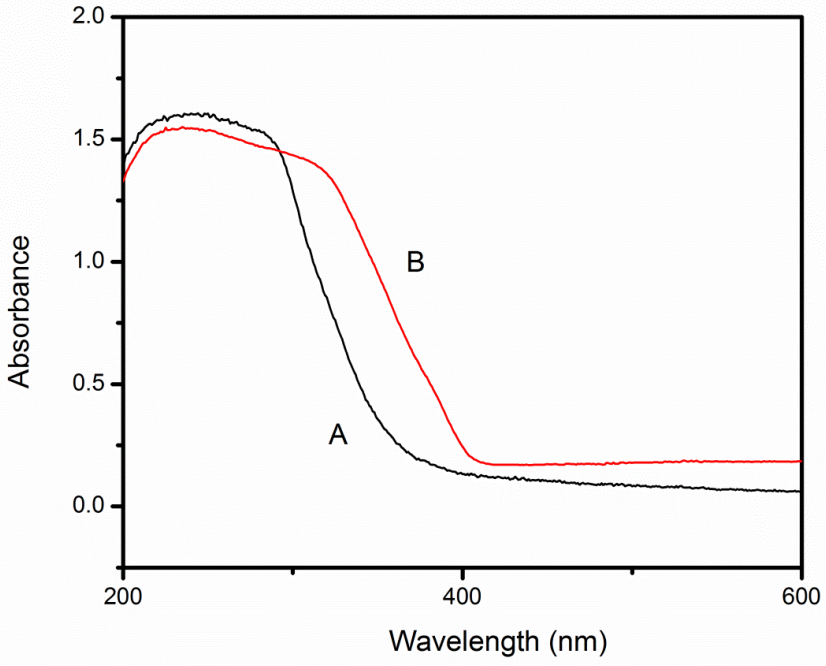

Fig. 8.4 UV absorption spectra of: A) anatase titania and B) photonic band gap titania

8.4 Conclusions

We have demonstrated an improved and facile polystyrene template route to synthesize highly organized nanostructured TiO_2 supports. The TiO_2 support has an organized porous structure with pore diameter distribution in sub um range (~300 nm). Even though our photonic crystals have a relatively low specific surface area, they still have the potential to exhibit an improved catalytic activity as compared to commercial catalysts as indicated by improved absorbance. We attribute this to the increase the light collection efficiency due to formation of photonic bandgap. It can also lead to better catalytic activity due to higher number of available active sites on the catalyst due to the well-organized and interconnected pore structure.

Reference:

[1] A. Blanco, E. Chomski, S. Grabtchak, M. Ibisate, S. John, S.W. Leonard, C. Lopez, F. Meseguer, H. Miguez, J.P. Mondia, G.A. Ozin, O. Toader, H.M. van Driel, Large-scale synthesis of a silicon photonic crystal with a complete three-dimensional bandgap near 1.5 micrometres, Nature, 405 (2000) 437-440.

[2] C. Lopez, Materials aspects of photonic crystals, Adv Mater, 15 (2003) 1679-1704.

[3] P. Lodahl, A.F. van Driel, I.S. Nikolaev, A. Irman, K. Overgaag, D. Vanmaekelbergh, W.L. Vos, Controlling the dynamics of spontaneous emission from quantum dots by photonic crystals, Nature, 430 (2004) 654-657.

[4] K. Yoshinaga, Functionalization of inorganic colloidal particles by polymer modification, B Chem Soc Jpn, 75 (2002) 2349-2358.

[5] J.I.L. Chen, G. von Freymann, V. Kitaev, G.A. Ozin, Effect of disorder on the optically amplified photocatalytic efficiency of titania inverse opals, J Am Chem Soc, 129 (2007) 1196-1202.

[6] I.G. Yu, Y.J. Kim, H.J. Kim, C. Lee, W.I. Lee, Size-dependent light-scattering effects of nanoporous TiO2 spheres in dye-sensitized solar cells, J Mater Chem, 21 (2011) 532-538.

[7] Q. Yang, M.Z. Li, J. Liu, W.Z. Shen, C.Q. Ye, X.D. Shi, L. Jiang, Y.L. Song, Hierarchical TiO2 photonic crystal spheres prepared by spray drying for highly efficient photocatalysis, J Mater Chem A, 1 (2013) 541-547.

[8] J.L. Blin, M.J. Stebe, T. Roques-Carmes, Use of ordered mesoporous titania with semi-crystalline framework as photocatalyst, Colloid Surface A, 407 (2012) 177-185.

[9] J.G. Fleming, S.Y. Lin, Three-dimensional photonic crystal with a stop band from 1.35 to 1.95 mu m, Opt Lett, 24 (1999) 49-51.

[10] I. Divliansky, T.S. Mayer, K.S. Holliday, V.H. Crespi, Fabrication of three-dimensional polymer photonic crystal structures using single diffraction element interference lithography, Appl Phys Lett, 82 (2003) 1667-1669.

[11] Y.V. Miklyaev, D.C. Meisel, A. Blanco, G. von Freymann, K. Busch, W. Koch, C. Enkrich, M. Deubel, M. Wegener, Three-dimensional face-centered-cubic photonic crystal templates by laser holography: fabrication, optical characterization, and band-structure calculations, Appl Phys Lett, 82 (2003) 1284-1286.

[12] M. Campbell, D.N. Sharp, M.T. Harrison, R.G. Denning, A.J. Turberfield, Fabrication of photonic crystals for the visible spectrum by holographic lithography, Nature, 404 (2000) 53-56.

[13] H. Miguez, F. Meseguer, C. Lopez, F. Lopez-Tejeira, J. Sanchez-Dehesa, Synthesis and photonic bandgap characterization of polymer inverse opals, Adv Mater, 13 (2001) 393-396.

[14] H.A. Chen, S. Chen, X. Quan, Y.B. Zhang, Structuring a TiO2-Based Photonic Crystal Photocatalyst with Schottky Junction for Efficient Photocatalysis, Environ Sci Technol, 44 (2010) 451-455.

[15] E. Carbonell, F. Ramiro-Manzano, I. Rodriguez, A. Corma, F. Meseguer, H. Garcia, Enhancement of TiO(2) photocatalytic activity by structuring the photocatalyst film as photonic sponge, Photoch Photobio Sci, 7 (2008) 931-935.

Chapter 9 Novel catalysts development for sustainable energy application: synthetic approaches and work done in collaboration

9.1 Introduction

A snapshot of the energy mix for any given year shows that our progress towards less carbon-intensive fuels is rather limited the trends in various components of energy basket is as following:

- 1980: oil (42%), natural gas (26%), coal (21%), renewable (7%), nuclear (4%) and liquid biofuels (0%).
- 2010: oil (37%), natural gas (25%), coal (21%), nuclear (9%), renewable (7%), and liquid biofuels (1%).
- 2035 (projections): oil (32%), natural gas (25%), coal (20%), renewable (11%), nuclear (9%) and liquid biofuels (4%).

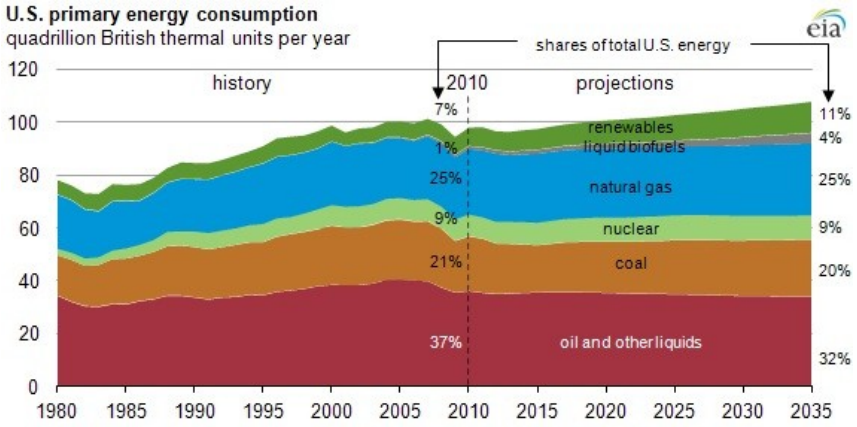

Fig. 9.1 U.S. primary energy consumption by energy source from 1980 to 2010, with projection to 2035

While the consumption of liquid biofuels was shown to grow by a factor of 587, biofuels are projected to remain a negligible part of U.S. energy inventory until 2035. Similarly, while the consumption of renewables is projected to double by 2035, total renewable energy consumption will be vastly overshadowed by

fossil fuels consumption

U.S. Energy Consumption in 2011 by energy Source is shown below. In contrast to the previous figure, this chart shows a detailed contribution of various energy sources to the overall renewable energy consumption.

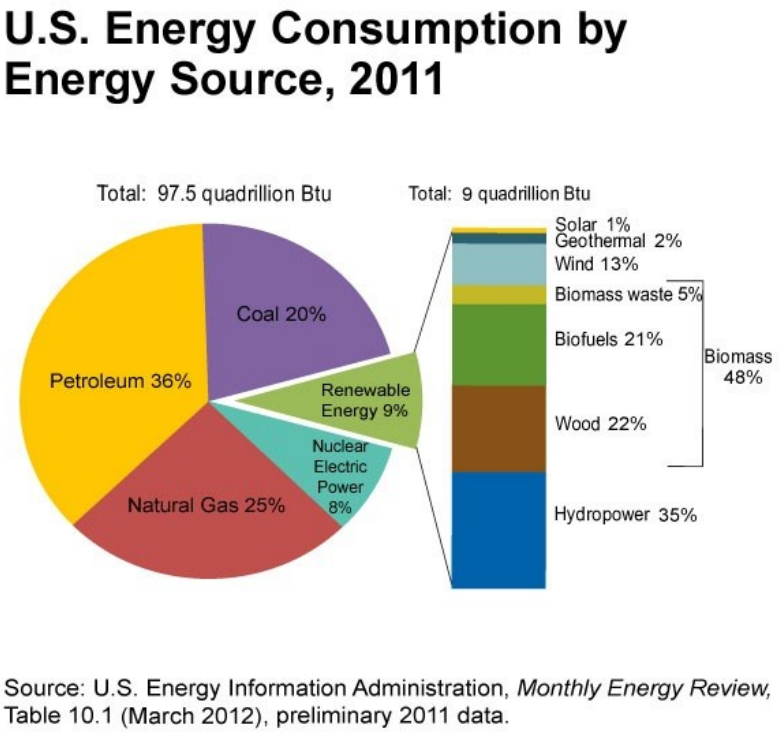

Fig. 9.2 U.S. energy consumption chart by Energy Source in 2011

Figure 9.2 indicates that only 0.1 % of the solar energy is used in the total energy consumption and it only constitutes 1% of all the renewable energy utilized. This negligible use of solar energy is in sharp contrast to the total solar energy available. The surface of the earth absorbs about 3.85×10^6 EJ solar radiation per year, which is almost 10^4 times of the yearly consumption of energy on earth [1]. The potential benefit of better exploitation of solar energy is enormous. Therefore, in order to solve the global energy crisis a better use of this energy source should be made a priority.

9.2 Photocatalysis for energy related application

9.2.1 Water splitting

During the 1970s, a very significant progress has been made on solar energy conversion to fuels by semiconductor photocatalysis. [2]. One possibility to produce fuel is to achieve water splitting to H_2 and O_2 under UV or visible light. Hydrogen (H_2) production by water splitting using semiconductor photocatalysts has attracted considerable interest. The origin of this process is based on pioneering work of Fujishima and Honda, who discovered that water can be photo-electrochemically decomposed into hydrogen and oxygen under UV radiation using a semiconductor (TiO_2) electrode.

$$H_2O + 2h\nu \rightarrow H_2 + \frac{1}{2} O_2$$

A large number of metal oxides and sulfides (e.g. TiO_2, WO_3, $SrTiO_3$, ZnO, CdS, and ZnS) have been tested for as photocatalytic hydrogen production. The photon energy is converted to chemical energy during the water splitting reaction, it is accompanied by a largely positive change in the Gibbs free energy (ΔG^0=+237KJ/mol). [3] Photocatalytic water splitting is often call an “artificial photosynthesis”. Although many reviews on the topic have been published in the previous years, the majority of photocatalysts are show activity for H_2 production only under UV irradiation (λ < 385 nm or $E_g \geqslant$3.0 eV). This chapter illustrates applications of heterogeneous photocatalysis described in previous chapters for H_2 production (half reaction in water splitting) under visible light irradiation.

For example, the most popular semiconductor, TiO_2, has the bandgap of

3.2 eV and therefore can only utilize the UV light. In contrast, CdS has bandgap energy of 2.4 eV and in recent studies has been shown a good photocatalytic activity for H_2 production under visible light irradiation. It has to be mentioned that sacrificial electron donors such as C_2H_5OH, HS^- or SO_3 needs to be used to obtain measurable rates of H_2 production and to avoid the photocorrosion of CdS in the presence of O_2. Moreover, in order to achieve better photocatalytic activities the electronic levels of CdS can be tuned by changing particle size.

This project primarily focused on synthesis of co-catalysts while photocatalytic testing for H_2 production has been done by Peichuan Shen. An example of this collaboration, showing greatly enhanced rates of H_2 production on sub-nm Au modified CdS is shown in Figure 9.3.

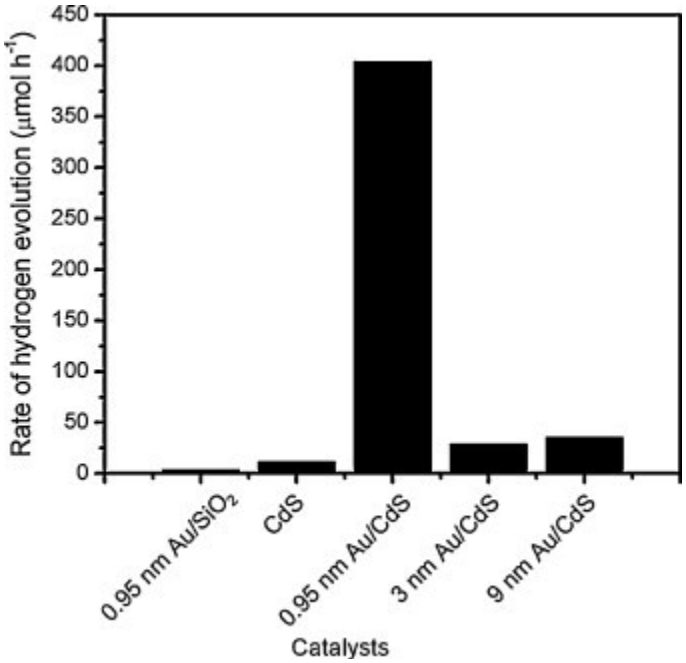

Fig. 9.3 Hydrogen evolution rates for Au/CdS with different sizes of Au nanoparticles.

9.2.2 CO_2 reduction

The efficient conversion of CO_2, a greenhouse gas, into hydrocarbons and oxygenates has an enormous potential to address environmental issues and sustainable energy challenges. Photocatalytic method can convert CO_2 into hydrocarbons and alcohols, which can be recycled either for energy production or for chemical synthesis. If successful, this approach can significantly impact energy and environmental areas by using green routes for producing valuable chemicals. It will reduce CO_2 emissions by utilizing sustainable sources of energy, such as sunlight. More specifically, this project is consistent with these program components: (a) discovery and design of novel nanomaterials for CO_2 photoreduction; and (b) production of hydrocarbons and alcohols from renewable sources. Given the importance of the topic, the results arising from this project are expected to make a significant and lasting impact on sustainable energy generation.

Although photocatalysis is a well-known method for environmental applications, utilizing photocatalysis towards selective organic/inorganic reactions is much less studied. Selective photocatalytic conversions can offer an alternative green route for producing valuable chemicals, utilizing generally mild reaction conditions and organic-free solvents. More specifically, using photocatalysis for capturing and converting carbon dioxide emissions into useful organic compounds can address the issues of global warming and shrinking oil resources. The photocatalytic method utilizes catalyst and UV light for reduction of CO_2 in the presence of H_2O into hydrocarbons and alcohols [4]. Both of those products can be used as valuable chemicals. It was demonstrated that the products of photocatalytic reduction of CO_2 with H_2O at 323 K include CH_4 and CH_3OH with trace amounts of CO, C_2H_2 and O_2. Using alcohols as sacrificial

electron donors can increase the reaction yield. Alternatively, using nitrate can facilitate production of hydrogen, formate, CO, ammonia and urea. Another promising method is to utilize copper-doped commercial TiO_2, which can increase both the overall yield of the reaction and the selectivity to methanol [5].

Analysis of the available literature reveals the major obstacle for this approach becoming viable is very low quantum efficiency. As a result, this potentially revolutionary strategy of addressing energy and environmental challenges has not yet been translated into a viable technology. It is important to mention that the rates of CO_2 photoreduction depend not only on the catalyst type but also on several other parameters, such as CO_2:H_2O ratios, light intensity and others.

There are many challenges, which need to be addressed to achieve higher quantum efficiencies. CO_2 is one of the most stable compounds of carbon. In order to achieve the CO_2 conversion, the first step required is 'activation' of CO_2. Initial steps of CO_2 activation involve Lewis acid and base centers and (C-O) π orbital [6, 7]. The simplest products, which can be produced from the reduction processes, are CO and $HCOO^-$. It shows that single electron transfer to CO is highly endergonic process. It also clear that photoreduction is not a single-step reaction with the first step of activation involving formation of $CO_2^{\bullet-}$ species.

There are also very stringent requirements for semiconductor photocatalysts mediating CO_2 reduction and water oxidation. It needs to absorb light energy, generate electron-hole pairs, minimize their recombination and transfer them to redox active species. Additionally, it requires the conduction band electrons to have higher energy as compared to CO_2 reduction potential while holes in the valence band have the appropriate energy level to be able to oxidize water to O_2 [6, 7].

Currently several tests are underway to use noble metal modified catalysts to reduce CO_2 into valuable chemicals and fuels. It is expected that similarly to H_2 production project nanometer and sub-nanometer particles can increase the rates of these reactions.

9.3 Catalysts development for other energy related applications

9.3.1 Water Gas Shift for hydrogen production

The water-gas shift (WGS) reaction plays an important role in the areas of hydrogen generation and CO purification.

$$CO + H_2O \rightarrow CO_2 + H_2$$

It has been of great interest in fuel cell research in recent years due to the possible application of fuel cell in mobile or domestic power generation. The area of hydrogen production has attracted much interest. Water-gas shift (WGS) reaction plays an important role for not only generating clean, renewable hydrogen but also removing the carbon monoxide gas. Commercially available catalysts for example, $Cu/ZnO/Al_2O_3$, are in general very active but suffer from poor stability under high temperatures. Therefore, attention has been given to semiconductor supported noble metal catalysts. These catalysts are more robust but exhibit lower turnover rates (TOR) than that exhibited by the industrial $Cu/ZnO/Al_2O_3$ catalyst.

In this project, sub-nm Pt modified TiO_2 samples were developed and subsequently tested at Tufts University for WGS applications. During the WGS reaction, the samples developed in this project exhibited improved catalytic H_2 production. The results are presented on Figure 9.4. The catalyst undergoes several cycles of the WGS reaction testing to confirm the stability of the catalysts. The results shown on Figure 9.4 indicate that our catalysts remain active after several cycles of the tests.

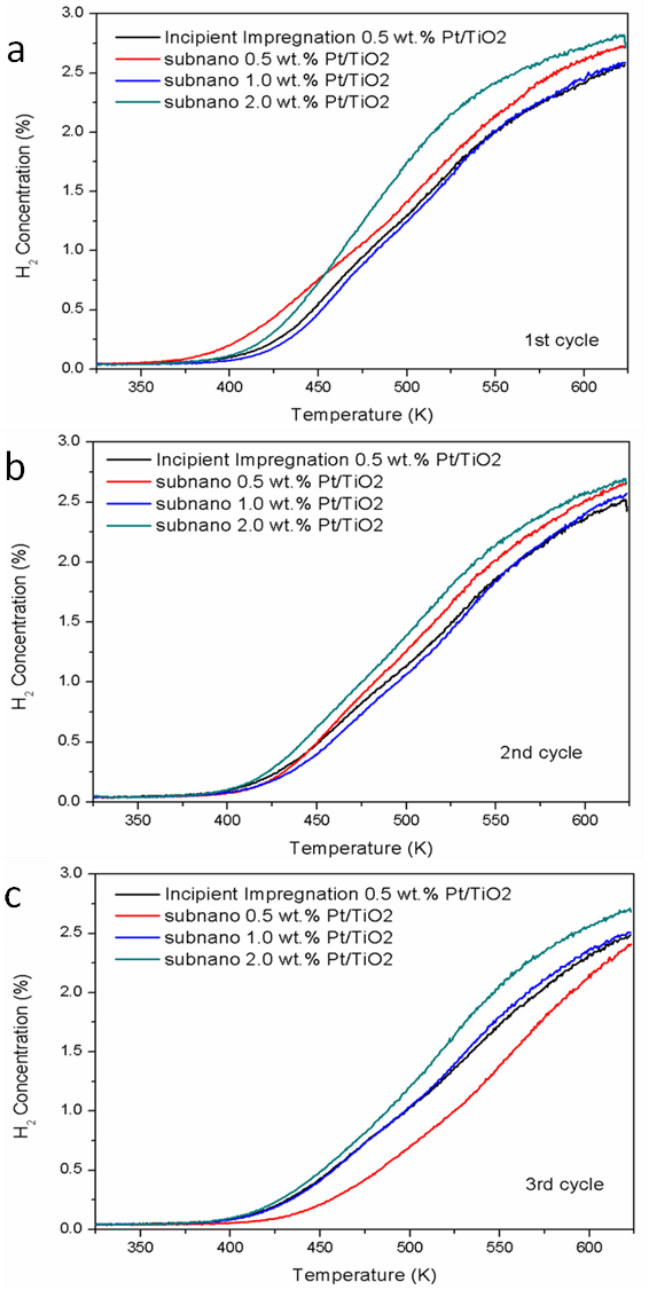

Fig. 9.4 hydrogen production rate on Pt modified TiO_2 for WGS reaction under different temperatures.

9.3.2 Catalysis of oxygen reduction reaction in proton exchange membrane fuel cell

A growing demand for renewable energy has attracted great interest in commercial fuel cells development as a replacement for traditional combustion-based energy sources. Proton exchange membrane fuel cell (PEMFC), where hydrogen is dissociated over a platinum catalyst at the anode into protons and electrons, is considered to be one of the most studied fuel cells in recent years. In PEMFC cell the electrons proceed through an external circuit where their energy can be harnessed in the form of electricity. The protons diffuse through the proton exchange membrane and arrive at the cathode where they combine with oxygen and the electrons arriving through the external circuit to form water.

$$\tfrac{1}{2}O_2 + 2H^+ + 2e^- \rightarrow H_2O$$

In terms of the choice of the catalysts, options unfortunately there are only few options. According to theoretical work done by Norskov et al by using density functional theory calculations, and to significant experimental data, Pt is considered the most active catalysts for oxygen reduction reaction (ORR) and therefore it is the most commonly used cathode catalyst in fuel cell research [8, 9]. However, there are a few disadvantages for using Pt, such as the cost of platinum, its stability over time and other considerations. The idea of alloying of platinum with other metals can be used to improve the fuel cell performance and there is already an experimental evidence research that it leads to increases in rate of ORR reactions.

Based on catalysts developed in this project, the electrochemical characterization of Pt catalysts was done in collaboration with Chemistry department at the Brookhaven National Laboratory. The measurements were obtained in 0.1 M of hydrochloric acid in DI water. Cyclic voltammetry was

performed in 0.1 M $HClO_4$ and run circularly from 0 to 1.0 V at the speed of 30 mV/s.

Based on the cyclic voltammogram, it can be concluded that sub-nm Pt catalyst was not as good as the regular size (2-4 nm) Pt. The reason for such decrease in activity might be related to on-set of metallic/nonmetallic properties of such small Pt particles, although this needs to be verified by further experiments. This result is also consistent with some reports stating optimal size of Pt catalysts is in 2 - 4 nm range [10, 11]. There is another crucial fact, which might be related to Pt synthesis, as cleanness of the metal particle surfaces. It is a crucial factor in electrochemical measurements. Given our synthetic procedures, better cleaning procedures might need to be developed as otherwise any surface contamination might have negative effect on catalytic performances in ORR reactions.

Reference:

[1] O. Morton, Solar energy: A new day dawning?: Silicon Valley sunrise, Nature, 443 (2006) 19-22.

[2] A.J. Nozik, R. Memming, Physical chemistry of semiconductor-liquid interfaces, J Phys Chem-Us, 100 (1996) 13061-13078.

[3] A. Kudo, Y. Miseki, Heterogeneous photocatalyst materials for water splitting, Chem Soc Rev, 38 (2009) 253-278.

[4] V. Subramani, C.S. Song, M. Anpo, Recent advances in catalytic production of hydrogen from renewable sources, Catal Today, 129 (2007) 263-264.

[5] M. Bellardita, M. Addamo, A. Di Paola, L. Palmisano, Photocatalytic behaviour of metal-loaded TiO2 aqueous dispersions and films, Chem Phys, 339 (2007) 94-103.

[6] V.P. Indrakanti, H.H. Schobert, J.D. Kubicki, Quantum Mechanical Modeling of CO2 Interactions with Irradiated Stoichiometric and Oxygen-Deficient Anatase TiO2 Surfaces: Implications for the Photocatalytic Reduction of CO2, Energ Fuel, 23 (2009) 5247-5256.

[7] V.P. Indrakanti, J.D. Kubicki, H.H. Schobert, Photoinduced activation of CO2 on Ti-based heterogeneous catalysts: Current state, chemical physics-based insights and outlook, Energ Environ Sci, 2 (2009) 745-758.

[8] D. Friebel, V. Viswanathan, D.J. Miller, T. Anniyev, H. Ogasawara, A.H. Larsen, C.P. O'Grady, J.K. Norskov, A. Nilsson, Balance of Nanostructure and Bimetallic Interactions in Pt Model Fuel Cell Catalysts: In Situ XAS and DFT Study, J Am Chem Soc, 134 (2012) 9664-9671.

[9] J.K. Norskov, J. Rossmeisl, A. Logadottir, L. Lindqvist, J.R. Kitchin, T. Bligaard, H. Jonsson, Origin of the overpotential for oxygen reduction at a fuel-cell cathode, J Phys Chem B, 108 (2004) 17886-17892.

[10] M.H. Shao, A. Peles, K. Shoemaker, Electrocatalysis on Platinum Nanoparticles: Particle Size Effect on Oxygen Reduction Reaction Activity, Nano Lett, 11 (2011) 3714-3719.

[11] K. Yamamoto, T. Imaoka, W.J. Chun, O. Enoki, H. Katoh, M. Takenaga, A. Sonoi, Size-specific catalytic activity of platinum clusters enhances oxygen reduction reactions (vol 1, pg 397, 2009), Nat Chem, 2 (2010) 790-790.

Chapter 10: Concluding remarks and future challenges

10.1 Concluding remarks

Sub-nm gold and platinum nanoparticles were synthesized using different methods and deposited on various semiconductor supports. The catalytic results indicated that supported Au and Pt exhibit very promising activities for several catalytic oxidation reactions including phenol degradation, NO_2 oxidation, visible light water splitting, and water gas shift reaction. This activity was substantially higher than that observed on regular size supported metal particles. The presence of the sub-nm clusters was confirmed by electron microscopy. Moreover, we also found that sub-nm Pt promotes a very different mechanism as compared to that of sub-nm Au particles. This work is the first ever demonstration of applications of such small precious metal clusters for both liquid and gas phase photocatalytic oxidation and reduction reactions.

This dissertation has described promising applications of newly developed experimental techniques for monitoring the photocatalytic reactions. For example, the new generation of UV source modified DRIFTS was used to monitor NO_2 reactions with illuminated photocatalysts. The results revealed a significant presence of nitrate, nitrite and nitrosyl species on the surface after turning on the UV light, which was consistent with the gas phase analysis of NO_2 removal. These observations also indicated the ability of Pt to affect both oxidation and reduction pathways of NO_2 removal from gas the phase. However, only the oxidation pathway was discovered for Au nanoparticles.

We have employed a novel mesoporous SBA-15 sieves with highly ordered porous structure and relatively short channels. These nanostructured materials were modified with TiO_2 and tested for liquid phase oxidation reactions. Our results show that TiO_2 modified mesoporous silica samples exhibit a significant photocatalytic activity for phenol degradation reactions. We have also

introduced a new strategy of further increasing the TiO_2/SBA-15 activity by modifying it with novel sub-nm precious metal clusters (Au, Pt).

10.2 Future challenges

One of the major challenges of utilizing these sub-nm metal particles is precisely controlling the size and shape of these clusters. There is a correlation between the size, shape and catalytic efficiency. In one route of synthetic approach utilized in this work we use organic ligands, such as thiols to protect Au clusters from agglomeration. In another route we used micelles to confine nanoparticles into a particular size range. However, one of the major challenges is to produce clean metal nanoparticles, where organic groups are removed from the surface without affecting the particle size distribution. We found that this can be crucial for achieving the best performance of nanoparticles, especially for oxygen reduction reactions conducted in an electrochemical setup.

An additional venue for future research is to understand the catalytic reaction mechanisms of sub-nanometer nanoparticles as compared to that of larger particles. The interactions of these particles with semiconductor substrates are crucial in optimizing the photocatalytic performance, and very little is known about such composite systems.